1986

Study of Mixed Mode stress intensity factors by two- and three-dimensional photoelasticity

Tae Hyun Baek
Iowa State University

Baek, Tae Hyun

STUDY OF MIXED MODE STRESS INTENSITY FACTORS BY TWO- AND THREE-DIMENSIONAL PHOTOELASTICITY

Iowa State University PH.D. 1986

PLEASE NOTE:

In all cases this material has been filmed in the best possible way from the available copy. Problems encountered with this document have been identified here with a check mark ✓.

1. Glossy photographs or pages ✓
2. Colored illustrations, paper or print ✓
3. Photographs with dark background ✓
4. Illustrations are poor copy _____
5. Pages with black marks, not original copy _____
6. Print shows through as there is text on both sides of page _____
7. Indistinct, broken or small print on several pages ✓
8. Print exceeds margin requirements _____
9. Tightly bound copy with print lost in spine _____
10. Computer printout pages with indistinct print _____
11. Page(s) _____ lacking when material received, and not available from school or author.
12. Page(s) _____ seem to be missing in numbering only as text follows.
13. Two pages numbered _____. Text follows.
14. Curling and wrinkled pages _____
15. Dissertation contains pages with print at a slant, filmed as received _____
16. Other _____

_____

_____

Study of Mixed Mode stress intensity factors by two- and three-dimensional photoelasticity

by

Tae Hyun Baek

A Dissertation Submitted to the
Graduate Faculty in Partial Fulfillment of the
Requirements for the Degree of
DOCTOR OF PHILOSOPHY

Department: Engineering Science and Mechanics
Major: Engineering Mechanics

Approved:

Signature was redacted for privacy.

In Charge of Major Work

Signature was redacted for privacy.

For the Major Department

Signature was redacted for privacy.

For the Graduate College

Iowa State University
Ames, Iowa

1986

TABLE OF CONTENTS

LIST OF TABLES

LIST OF FIGURES

I. INTRODUCTION

Structural elements frequently fail at stress levels well below the ultimate strength of the material specifications when they are loaded. Investigation of the fracture surfaces usually reveal that there were defects such as cracks and/or discontinuities in the material which initiated "**brittle fracture**" due to the sharp notches or cracks. Such brittle fractures are related to a fracture parameter, called the **Stress Intensity Factor** (SIF). To avoid fracture, it is necessary to know the magnitude of this fracture parameter for the particular crack geometries and loading conditions that apply to a specific design or structure. Towards this end, many analytical, numerical and experimental methods used for extracting SIFs have been developed. In the experimental approaches, photoelasticity is often used because it can show the whole field state of stress in the model.

In photoelastic experiments, however, there are some difficulties in extracting SIFs from the isochromatic data. These are:

1. The broad bands of the isochromatic fringes which make it difficult to accurately record a precise fringe value and the coordinates, with respect to the crack tip, where that value occurs. Care should be taken to minimize the location error.
2. By the definition of K-factors or SIFs, one should measure the parameters associated with the $1/\sqrt{r}$ terms, where r is the radial distance from the crack tip to the data point. The SIF is defined when r goes to zero, but it is almost impossible in an experiment to obtain reliable data that close to a crack tip. So, one usually has to use information near the crack tip to

extract K-factors.

3. In two-dimensional photoelastic models, the crack tip is often obscured by the lens effect, the so called caustic effect, caused by the sharp gradient of the stress near the crack tip. Inaccurate arrangement of the optical system also contributes to this problem.

The main effort in this dissertation has been to solve some of these difficulties. The goal was to improve the experimental accuracy through digital image processing of the photoelastic fields in "cracked" models. Such an approach makes it possible to read the birefringence precisely without the need for any compensation method.

Digital image processing is playing an increasingly important role in photoelastic stress analysis. The rapid and accurate data reduction made possible by digital image processing systems was exploited by Burger and Voloshin [1, 2] to read relatively small amounts of birefringence which conventional photoelasticity finds difficult to resolve. This technique, so called Half Fringe Photoelasticity, has been applied to a wide range of stress analysis problems including SIF analysis in glass plates [3] or in thin slices taken from three-dimensional frozen-stress models [4] whose birefringence does not have enough information for the conventional photoelastic analysis. Another application of digital image processing can make a contribution to the conventional photoelastic data analysis by sharpening the broad band full- and half-order isochromatic fringes to sharp lines that minimize the data location error [5]. This fringe sharpening technique was used in the SIF analyses for the research reported in this

dissertation.

Since one of the most important factors in any experiment is the accuracy or validity of the results, an evaluation of accuracy should be performed. In this study, data collection was made from sharpened isochromatic fringes. To extract the SIFs from fringe patterns near the crack tip, a mathematical model, which describes the stress field around a crack tip, was used. The accuracy of the results can be evaluated by comparing the observed fringes to back-plots of fringes computed from the theoretical equations and parameters. In this dissertation, the exact origin of the crack tip, together with the fracture coefficients, was extracted from data sets that produced an overdeterministic system of equations solved by an iterative least squares technique proposed by Sanford [6]. Regenerated fringes were plotted by using fracture equations with coefficients estimated from the data sets, and the accuracy of the results were evaluated quantitatively by introducing statistical parameters, such as standard deviation, and error distribution between theoretical and experimental fringes.

To prove the validity of the experimental procedure, two-dimensional cracked models were chosen. Some models were cast, others were machined from sheets, and in both cases the analysis was repeated for live models with different loads, and for frozen-stress models after stress-freezing. The technique for data analysis is shown to be accurate. Finally, the developed procedure was used to find the Stress Intensity Factors in the three-dimensional problems posed by inclined semi-circular surface cracks that penetrate part-way through a thick plate.

II. BACKGROUND

The diversity of methods used to obtain stress intensity factors are well documented by Tada et al. [7], Sih [8], Rooke and Cartwright [9], and Smith and Mullinix [10]. These include analytical solutions and numerical approximations. For more complicated conditions, the SIFs have been estimated by any one of several numerical methods. These are approximate in nature and their accuracies need verification. For this purpose, experimental techniques which obtain physical phenomena directly from a prototype or a model have been used to verify analytical and numerical solutions as well as explore problems with unknown solutions. Hence, the history of fracture mechanics shows development along both theoretical and experimental lines.

Experiments, such as those conducted for this dissertation, that use the photoelastic method for the study of K-factors should be based on the concept of an analytical singularity. Consequently, a brief history of the theoretical formulation of singularity solutions together with photoelastic techniques for SIF analysis are reviewed below.

A. Two-dimensional Crack Theory

The first attempt at a mathematical approach to fracture mechanics was made by Inglis in 1913 [11]. By analyzing the case of an elliptical hole in a plate under uniform tensile stress, he showed that the maximum stress occurs at the apex of the major axis of the ellipse, where the radius of curvature is a minimum. In the limit, as the minor axis tends towards zero we approximate a true crack and the stress at the crack tip

becomes infinitely large.

Since real materials can support only a finite stress, the above result would seem to indicate that a cracked component cannot sustain any load. In the early 1920s, Griffith [12] became interested in this problem. According to Boyd [13], Griffith questioned why the theoretical tensile strength of glass should be about 100-10,000 times greater than is actually found in tests. He explained this phenomenon by assuming that there exits some crack-like flaw in the glass and showed that a crack would become unstable when the elastic strain energy release rate, due to crack extension, exceeded the rate of increase in surface energy associated with the newly formed crack surfaces when the crack extends.

It should be noted that Griffith's energy criterion is a global approach, which does not involve the distribution of stress around the crack tip. Hence, his approach cannot be conveniently used to characterize different types of fracture.

Based on the analysis of Westergaard [14], Irwin [15] suggested that the strain energy release rate of an elastic body containing cracks could be related to the crack tip stresses by a single parameter which he called the "Stress Intensity Factor(SIF)". The advantage of the SIF criterion is that it is a local criterion, which allows different modes of crack tip deformations to be characterized separately. As a consequence, the Westergaard equations have been employed extensively to obtain crack tip stress and displacement fields. It is instructive to examine these equations.

In an infinite plate with a central through-thickness crack (Figure

2-1), Westergaard made use of the properties of complex variable functions to show that the normal stresses and the shearing stress in the directions x and y can be stated in the form of

$$\sigma_x = \mathrm{Re}Z(z) - y\mathrm{Im}Z'(z)$$
$$\sigma_y = \mathrm{Re}Z(z) + y\mathrm{Im}Z'(z) \qquad (2\text{-}1)$$
$$\tau_{xy} = -y\mathrm{Re}Z'(z)$$

where $z = x + iy$, $Z(z)$ is a stress function in complex form and $Z' = \partial Z/\partial z$. Re and Im indicate the Real and Imaginary components.

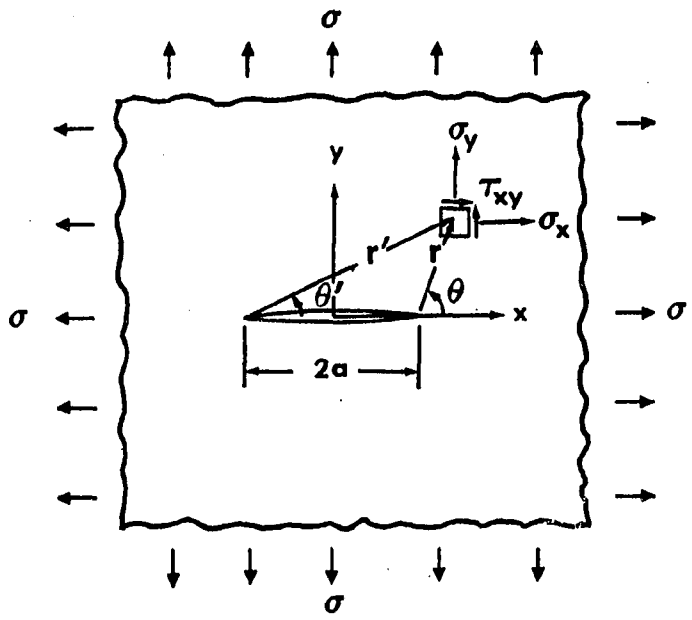

Figure 2-1. Coordinate system used in the Westergaard analysis

For a crack subjected to biaxial loadings at infinity as shown in Figure 2-1, Westergaard proposed the following complex form for the stress function

$$Z(z) = \frac{\sigma z}{\sqrt{z^2-a^2}} \qquad (2\text{-}2)$$

Use the notation in Figure 2-1 and substitute equation (2-2) and its derivative into equations (2-1). Consider only a limited region at the crack tip, with the conditions $r<<1$, $r' \to 2a$ and $\theta' \to 0$, to get:

$$\sigma_x = \frac{K_I}{\sqrt{2\pi r}}\cos\frac{\theta}{2}\left(1-\sin\frac{\theta}{2}\sin\frac{3}{2}\theta\right) + O(\sqrt{r})$$

$$\sigma_y = \frac{K_I}{\sqrt{2\pi r}}\cos\frac{\theta}{2}\left(1+\sin\frac{\theta}{2}\sin\frac{3}{2}\theta\right) + O(\sqrt{r}) \qquad (2\text{-}3)$$

$$\tau_{xy} = \frac{K_I}{\sqrt{2\pi r}}\sin\frac{\theta}{2}\cos\frac{\theta}{2}\cos\frac{3}{2}\theta + O(\sqrt{r})$$

Where $O(\sqrt{r})$ implies a truncated higher term; K_I is the opening mode stress intensity factor (Mode I); and r and θ are polar coordinates with the origin located at the crack tip.

When the singular terms of these equations are retained for $r \to 0$, the results is the well known Westergaard equations. There are a few severe restrictions inherent in the assumptions that underlie Westergaard's development. These restrictions have practical importance in most experimental studies of SIFs where the loading conditions are often not equibiaxial and the models are not infinitely large.

In the practical use of the Westergaard equations, the stress function of equation (2-2) is therefore not sufficient for accurate experimental analysis. In a discussion [16] of the photoelastic work

done by Wells and Post [17], Irwin points out that according to the Westergaard equations, the characteristic loops of the isochromatic fringes at a crack tip, will have their maximum radii normal to the crack line, thus Θ_{max} in Figure 2-2 will be 90^{o}. However, in actual tests on a large plate with a central through-thickness crack loaded in uniaxial tension ($\sigma_x>0$; $\sigma_y=0$), the isochromatic fringes lean forward as in Figure 2-2 and $\Theta max<90^{o}$.

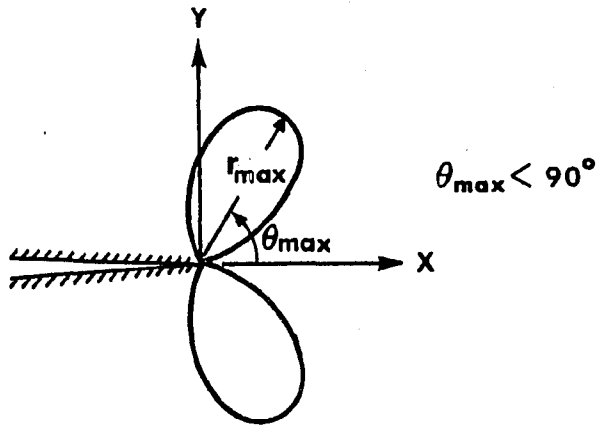

Figure 2-2. Tilting of isochromatic fringe loops under uniaxial tension load

To account for this leaning of the fringe loops, Irwin suggested the addition of a constant term, a so called nonsingular term σ_{ox}, to the σ_x expression in equations (2-3). The resultant equations, which are often called the modified Westergaard equations, are widely used in photoelastic analysis. For Mixed Mode loading, they are [16]:

$$\sigma_x = \frac{K_I}{\sqrt{2\pi r}}\cos\frac{\theta}{2}\left(1-\sin\frac{\theta}{2}\sin\frac{3\theta}{2}\right) - \frac{K_{II}}{\sqrt{2\pi r}}\sin\frac{\theta}{2}\left(2+\cos\frac{\theta}{2}\cos\frac{3\theta}{2}\right) - \sigma_{ox} \quad (2\text{-}4a)$$

$$\sigma_y = \frac{K_I}{\sqrt{2\pi r}}\cos\frac{\theta}{2}\left(1+\sin\frac{\theta}{2}\sin\frac{3\theta}{2}\right) + \frac{K_{II}}{\sqrt{2\pi r}}\sin\frac{\theta}{2}\left(2+\sin\frac{\theta}{2}\cos\frac{3\theta}{2}\right) \quad (2\text{-}4b)$$

$$\tau_{xy} = \frac{K_I}{\sqrt{2\pi r}}\sin\frac{\theta}{2}\cos\frac{\theta}{2}\cos\frac{3\theta}{2} + \frac{K_{II}}{\sqrt{2\pi r}}\cos\frac{\theta}{2}\left(1-\sin\frac{\theta}{2}\sin\frac{3\theta}{2}\right) \quad (2\text{-}4c)$$

where K_{II} is the shearing mode stress intensity factor (Mode II). Notice that equations (2-4) retain only the first terms in equations (2-3). The region of validity of these equations is therefore restricted to $r/a \ll 1$.

It was soon found [18, 19, 20, 21, 22] that the modified Westergaard equations are inadequate for accurate photoelastic analysis in a problem where the boundary conditions ahead of the crack can be expected to play a significant role on the stress field. Eventually, a series type of complex stress function was introduced to account for the effect of general boundary and loading conditions. Discussions of series type stress functions and applications to practical problems are given in the references [23, 24, 25].

Before the recent introductions of the series type of complex stress function, Williams [26] and Karal and Karp [27] proposed eigen-solutions for the displacement and stress distributions at angular corners in an elastic medium (Figure 2-3). Both studies were limited to the localized displacement or stress field in the vicinity of sharp corners.

The boundary conditions assumed by Williams [26] considered two radial edges of a sector including a variable vertex angle "α". The boundary conditions along the circumferential edge were unspecified inasmuch as the stresses near the vertex would be locally determined solely by the boundary conditions along the radial edge ("h" in Figure 2-3). This is a reasonable assumption if the circumferential boundary is greater than several plate thickness away from the vertex ($h>>t$). There is not any distinguishable difference from the Westergaard approach except that these solutions for angular sharp corners make it possible to calculate different singularity terms depending on vertex angle "α". Williams subsequently extended this work with angular sharp corners to study the stress distribution of a stationary crack in stretching and bending load [28, 29].

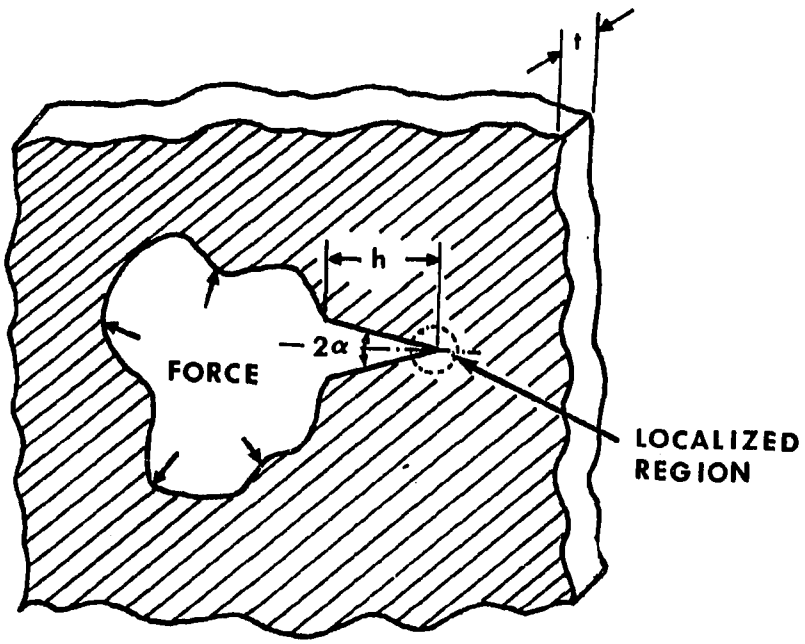

Figure 2-3. Model for the study of localized stress behavior in the neighborhood on angular sharp corners [27]

This brief review of the development of stress functions will be useful in explaining the wide range for physical behavior of stresses observed in some experiments. The common feature in studying the stress distributions around crack tips is a series type of stress function that takes account of the near and far field characteristics of the stresses observed in experiments.

The main studies included in this dissertation are for two-dimensional through-thickness edge cracked models and for three-dimensional surface cracked models in tension. The analytical approach used to interpret the photoelastic fields was the Williams stress function [28]. These equations are more adaptable to the geometries concerned. This will be explained in detail in Chapter III-A.

B. Three-dimensional Surface Crack Problems

In most engineering structures, failures due to cyclic loading, fatigue and/or stress corrosion occur from defects or flaws that are either embedded in the material, or occur on the surface or at a corner. A common example is a flaw that originate from a weld defect in a joint or in a pressure vessel shell. Whether the flaws are embedded or on the surface, they require a three-dimensional analysis.

A semi-circular surface crack, that penetrates only part-way through a plate loaded in tension normal to the plane of the crack, represents the simple case of a surface flaw. Several attempts, both analytical and experimental, have been made to estimate the stress intensity factors for such cracks in a finite or semi-infinite body.

These are reviewed below.

Early in 1950, Green and Sneddon [30] proposed an analytical solution of the stress analysis problem of an isolated flat elliptical crack in an infinite elastic solid under uniform tensile stress at infinity in a direction that is normal to the plane of the crack. This analysis was used by Irwin [31] as the basis for obtaining the elastic SIF solution for a buried elliptical crack and also to approximate the SIF for a semi-elliptical surface crack. The solution for the SIF around the perimeter of a buried elliptical crack under uniform tensile stress, σ, applied normal to the plane of the crack (Figure 2-4) is the reference condition for most three-dimensional analyses of cracks. It forms the basis for calculations of "magnification factors" that extends usefulness of this solution to a number of surface crack geometries in plates of finite thickness.

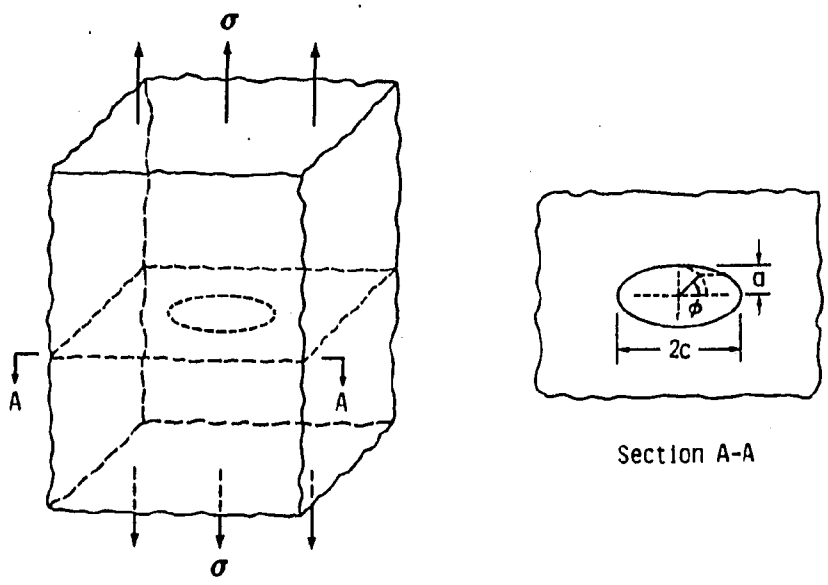

Figure 2-4. Embedded elliptical flaw in an infinite solid under remote tension normal to the crack plane

For the geometry of Figure 2-4, the SIFs are:

$$K_I = \frac{\sigma\sqrt{\pi a}}{\Phi} \left[\left(\frac{a}{c^2}\right)^2 \sin^2\phi + \cos^2\phi \right]^{1/4} \qquad (2\text{-}5)$$

where

$$\Phi = \int_0^{\pi/2} \left[\left(\frac{a}{c^2}\right)^2 \sin^2\phi + \cos^2\phi \right]^{1/2} d\phi$$

For geometries other than the ideal one of Figure 2-4, a correction factor or "magnification factor" (F_m), as shown in equation (2-6), is used.

$$F_m = \frac{K_I(\phi)}{\frac{\sigma\sqrt{\pi a}}{\Phi} \left[\left(\frac{a}{c^2}\right)^2 \sin^2\phi + \cos^2\phi \right]^{1/4}} \qquad (2\text{-}6)$$

Where $K_I(\phi)$ is the SIF value of a surface flaw at the same angle ϕ in a finite body.

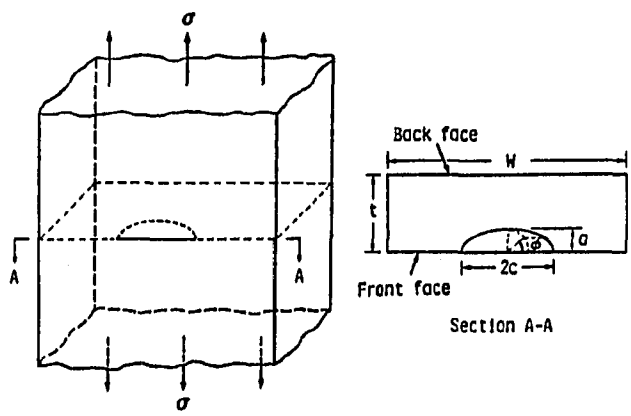

Figure 2-5. Surface crack in a finite plate subjected to uniform tensile stress

Exact solutions are not, as yet, available for surface flaws in finite or semi-infinite bodies (Figure 2-5). Numerous solutions have been obtained by approximate analytical methods but, due to the complexities of the three-dimensional analyses, the solutions differ considerably.

In 1973, Merkle [32] presented a review of the earlier SIF solutions for the surface crack. In 1978, Newman [33] published a similar review in which he assessed the accuracy of the various solutions by correlating fracture data on surface cracked tension specimens made of a brittle epoxy material.

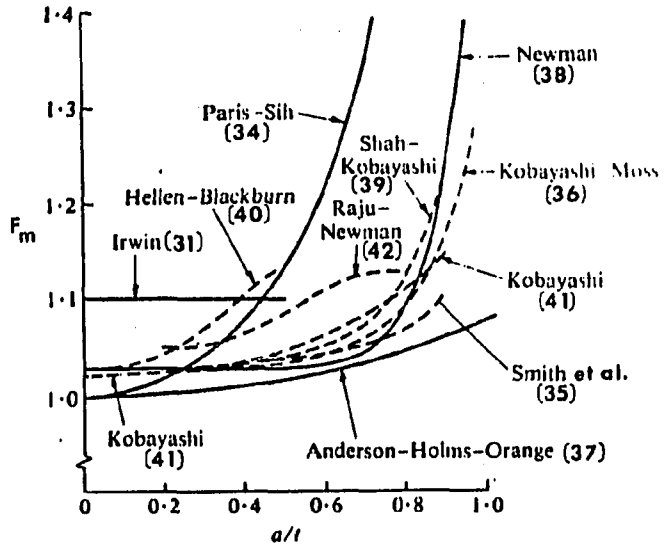

F_m = magnification factor defined by equation (2-6)
t^m = plate thickness
a = maximum depth of a semi-circular surface crack

Figure 2-6. Stress intensity magnification factor at maximum depth point ($\phi=\pi/2$) for a semi-circular surface crack under Mode I loads [33]

Because the fracture of the epoxy material can be characterized by a constant value of stress intensity factor at failure, the correctness of the various solutions could be judged by the variations in the stress intensity factors at failure. Figure 2-6 compares the results for the magnification factors (F_m) from different sources.

At the maximum crack depth ($\phi = \pi/2$ as shown in Figure 2-5), most solutions (except the estimate from Irwin [31]) agree within about 5 percent when a/t ratios are less than 0.4. For larger a/t ratios, however, the disparity in the values of F_m becomes large. In some cases, the difference is as much as 50 percent.

The data for Figure 2-6 were drawn from various sources. The approximation methods used included the alternating method [35, 36, 39], the finite element method [40, 42], and engineering estimates [31, 37] based on the analytical solutions. For semi-elliptical surface cracks, other solutions not shown on Figure 2-6 include the line spring method [43], the boundary integral equation method [44, 45] and the body force method [46, 47]. These latter solutions are all numerical methods and have not yet been compared to each other.

Experimental methods for the three-dimensional analysis of surface crack problems require special techniques, which are complex and expensive. As a result, very few experimental results for three-dimensional cracked bodies are available in the literature. Smith and his associates [48, 49] conducted a number of photoelastic experiments on surface cracks which were either naturally grown or which were machined to part-circular shapes. Comparison between these experimental studies and the previous theoretical solution is difficult

because Smith's [48, 49] crack geometries were different from the pure semi-circular or semi-elliptical shapes used in the analyses.

Recently, Phang and Ruiz [50] performed photoelastic experiments for SIF determination of both single and multiple semi-circular and circular cracks. According to them, the SIF varies along the crack front in a way that is quite different from that predicted by the analytical solutions (Figure 2-7).

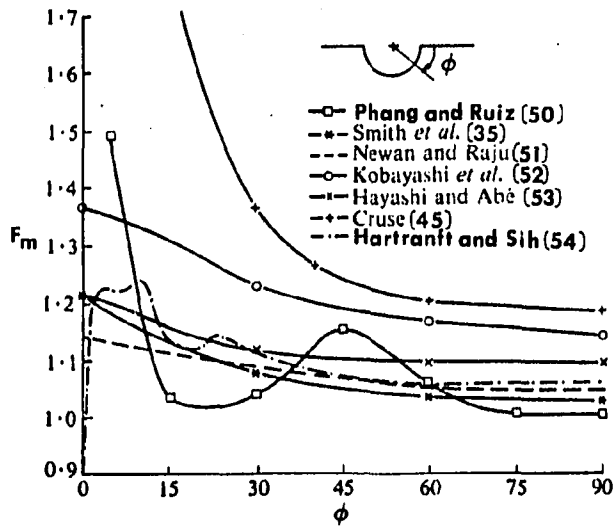

Figure 2-7. A comparison of stress intensity distribution along the semi-circular crack front according to Phang and Ruiz in a half space and under Mode I loads [50]

The disagreement between the results from different methods and authors (Figures 2-6 and 2-7) led McGowan et al. [55] to establish a "benchmark" surface flaw problem that would arrive at a "best estimate" of the pure Mode I SIF variation along the flaw border for fixed semi-elliptical surface cracks. The derived best estimate curve for the

SIF was believed to be within $\pm$ 3 percent of the actual value along the crack front. This curve compared well within $\pm$ 10 percent with the experimental data that was available at the time. The difference between the "best estimate" curve and experiment was thought to be largely due to the differences in geometry and Poisson's ratio [55].

The very important problem of a surface flaw in a finite body under Mixed Mode loading has received much less attention [56]. Absence of information on this subject is not unexpected since this problem is substantially more complex than the pure Mode I problem discussed above. Also, it is very difficult to find experimental results for Mixed Mode surface crack problems. Only Smith et al. [57] have published Mixed Mode SIF distributions for part-circular surface flaws. They used the three-dimensional stress-freezing method to obtain their results. So far, no analytical solutions for these geometries and loading condition are available. Their results showed that maximum SIF values did not necessarily occur at maximum flaw depth, and the effect of inclining the crack with respect to the boundary was to reverse the magnitude of K_I and K_{II} in going from a 30^o to a 60^o angle between the crack surface and the boundary. Since the part-circular geometries employed by them does not match either a naturally grown shape nor any one of the analytical geometries (semi-circular or semi-elliptical), the validation of their results by other analyses may be difficult. Their results may not contribute much to solve controversial three-dimensional crack problems.

The study in this dissertation is concerned with the application of the frozen stress technique to pure Mode I as well as Mixed Mode loading of surface flaws of semi-circular shape in plates of finite thickness.

C. Methods for the Determination of K-factors from Photoelastic Experiments

Since the first use of the photoelastic method to study the stress field in the vicinity of an edge crack by Post [58], many different techniques have been tried to extract fracture parameters from the isochromatic fringes near the crack tip. Every one of these methods has its own strength and weakness, and there is no agreement on which method is the most suitable for the determination of SIFs for cracks in the general case. Even for pure Mode I loading, there are differences in the results from different experimental schemes [59].

To calculate SIFs from the isochromatic fringes near a crack tip, a basic theory which can describe the stress field around the crack tip is necessary. Depending on the equations selected, the methods for interpreting the photoelastic data can be classified into three groups; two-parameter methods, three-parameter methods and multiple-parameter methods.

The two-parameter methods use the "modified Westergaard equations" (Equations 2-4a,b,c). The two parameters are: Stress intensity factors, K_I and K_{II}, i.e., the singular terms in equations (2-4) and the far field stress term in the same equations. These methods include a nonsingular term, σ_{ox}, together with the singularity terms. This approach was first suggested by Irwin [16] for determining the opening mode SIF (pure Mode I) from the isochromatic fringe patterns. It is, however, sensitive to data location because measurements are taken at the extreme positions, $r=r_m$ and $\theta=\theta_m$, on a given fringe loop (Figure

2-8). The method calculates K_I and σ_{ox} and is, strictly speaking, not applicable to Mixed Mode problems, i.e., it cannot determine K_{II}.

Several other techniques have been proposed to improve the experimental accuracy of the two-parameter method and avoid the sensitivity to data location. These include the Bradley-Kobayashi maximum shear stress difference method [60, 61], the Schroedl-Smith's selected line approach using statistical iteration procedures [62, 63], Smith's extrapolation technique [64, 65], the Theocaris-Gdoutos extrapolation method [66, 67], the Smith-Olaosebikan "quadratic method" [68], Redner's method using the measurement of maximum width (W_m in Figure 2-8) of fringe loops [69], the Ruiz-Phang linear slope method [70, 71, 72] and Sanford and Dally's iterative least squares method [73, 74]. Most of these authors sought to extract both K_I and K_{II} from the photoelastic data.

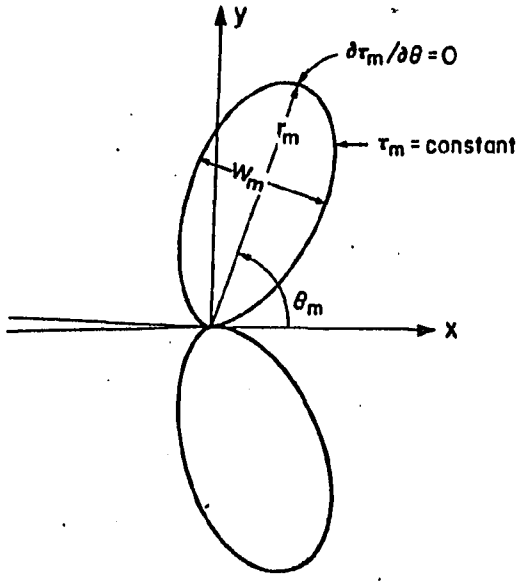

Figure 2-8. Fringe-loop tilt angle θ_m and maximum radial position r_m for a crack-tip isochromatic fringe loops

Practically, in the application of all these two-parameter methods, one should find the zone in which the singular equations (2-4a,b,c) are valid. Hence, the accuracies of all these methods depend on the data collection region. Unfortunately the collection region usually varies with the particular method of analysis while the valid zone changes as the crack geometries and loading conditions change.

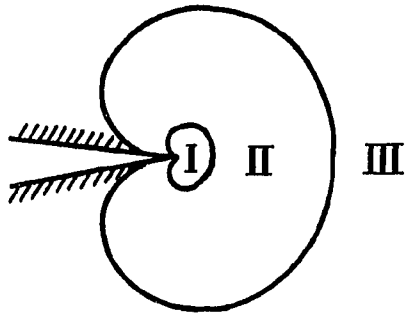

Figure 2-9. Schematic illustration of three regions associated with crack tip stress field

Several authors [62-72] noticed that the stress field can be divided into three regions as shown in Figure 2-9: A small area at the crack tip (**Region I**) where the effects of crack tip geometry (blunt, cast to shape, machined slit or natural crack), material and optical nonlinearity, "caustic effect", and plastic yielding cause departure from the assumptions of linear elasticity. A singular zone (**Region II**) where the singular equations (2-4a,b,c) are valid and the effect of crack tip shape is small. A far field area (**Region III**) where the influence of the presence of boundaries, interactions with other stress raisers, the effects of nonuniform far field stresses and loading conditions cause the higher order terms of the series type of stress

function, that was truncated to yield equations (2-4a,b,c), to have a major influence on the shape of the stress field.

Several authors, e.g., Smith and his associates [64, 65, 68], Ruiz and Phang [70], Phang and Ruiz [71], and Morton and Ruiz [72], have attempted to distinguish the singular zone from the other zones by graphical methods. These methods work in particular cases but it remains difficult to define this zone for the general case. This is particular true for problems where the photoelastic data is not well defined or where the boundary conditions are complex.

To extend the data collection region into the far field (Region III) and thus improve the accuracies of the measurement of K-factors from isochromatic fringe loops, Etheridge and Dally [75] proposed a three-parameter method. Further, improvements in data collection and interpretation have been proposed by Sanford [21], Irwin et al. [23], Cottron and Lagarde [24], Rossmanith [76, 77], Banks-Sills and Arcan [78], and Ramulu et al. [79]. These are multiple-parameter methods using complex or power series types of stress functions applied to the photoelastic fields for various crack geometries and boundary conditions. A major feature of Sanford and Dally's work [74] is the formulation of regenerated back plot fringes which are compared to the observed fringes in order to assess the acceptability of the experimentally determined SIFs.

In spite of all this work, there is still no consensus on which method is the most desirable and accurate for the determination of SIF values.

A general tendency in the development of photoelastic techniques

for the extraction of K-factors shows that the global methods [6, 23, 24, 73] which can take advantage of the full field characteristics of the fringe pattern are preferable to either the selected line approaches [48-50, 62-72] or the point matching techniques [16, 60]. Also, with the rapid adoption of electronic computers and digital image processing techniques [1, 2, 5, 80] in optical stress analysis, the potential of global methods can be more readily utilized [3, 4, 24, 78, 81-83].

For these reasons, it was decided to use a full field method which incorporates Sanford's [6] iterative least squares method coupled with Williams' power series type of equations [28] for the studies of inclined edge crack and semi-circular surface crack problems presented in this dissertation.

III. THEORETICAL MODEL AND EXPERIMENTAL TECHNIQUES

As discussed in Chapter II, numerous photoelastic techniques for the interpretation of K-factors have been developed and applied to various crack geometries and complex boundary conditions. The study presented in this dissertation takes advantage of the whole field capabilities of the photoelastic field near the crack tip. It avoids the ambiguity of the outer limit of the singularity zone (**Region II** in Figure 2-8), by using a classical theory for the study of localized elastic fields in the vicinity of crack tips.

In this chapter, Williams' local coordinate representation of elastic fields surrounding a static crack tip [28] is reviewed. This method is an extension of eigen-solutions for sharp edges and/or notches. The experimental techniques, that were used to overcome some of the earlier difficulties occurring in the photoelastic analysis of crack problems, are described. The procedure for evaluating the accuracy of the experimentally obtained SIFs is discussed.

A. Theoretical Model used in the Crack Analysis

1. Derivation of Williams equations [26,28,84,85]

For a homogeneous and isotropic solid in a state of plane stress or strain and with zero body forces, a valid stress function must satisfy the biharmonic equation (3-1) derived from the considerations of equilibrium and compatibility in linear elasticity.

$$\nabla^2(\nabla^2\chi)=0 \qquad (3\text{-}1)$$

where χ is the Airy stress function, and the operator ∇^2 in polar

coordinates is

$$\nabla^2 = \frac{\partial^2}{\partial r^2} + \frac{1}{r}\frac{\partial}{\partial r} + \frac{1}{r^2}\frac{\partial^2}{\partial \theta^2} \tag{3-2}$$

where r and θ are the polar coordinate components of radial and angular location, respectively.

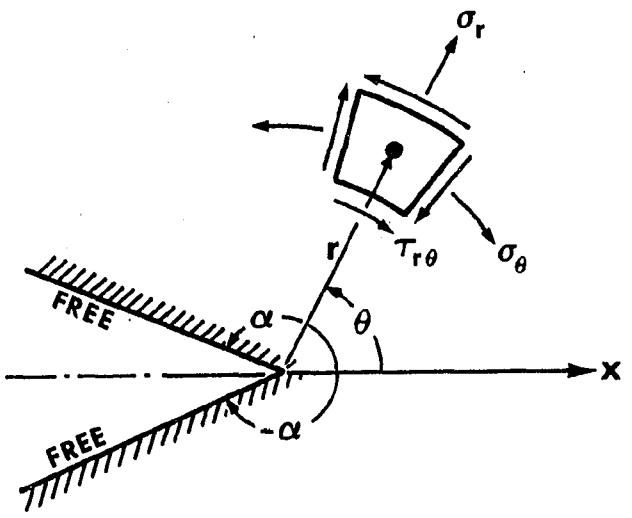

Figure 3-1. Polar stress components in a sharp angular corner

The stress components are then represented in terms of the stress function, χ, as

$$\sigma_r = \frac{1}{r^2}\frac{\partial^2 \chi}{\partial \theta^2} + \frac{1}{r}\frac{\partial \chi}{\partial r} \tag{3-3a}$$

$$\sigma_\theta = \frac{\partial^2 \chi}{\partial r^2} \tag{3-3b}$$

$$\tau_{r\theta} = -\frac{1}{r}\frac{\partial^2 \chi}{\partial r \partial \theta} + \frac{1}{r^2}\frac{\partial \chi}{\partial \theta} \qquad (3\text{-}3c)$$

where σ_r, σ_θ and $\tau_{r\theta}$ are the radial, tangential and shear stress components, respectively, in polar coordinates (Figure 3-1).

The boundary conditions on each of the free edges are:

$$\sigma_\theta = 0 \quad \text{and} \quad \tau_{r\theta} = 0 \qquad \text{at } \theta = \pm \alpha \qquad (3\text{-}4)$$

The stress function assumed by Williams has the product form

$$\chi = r^{\lambda+1} f(\theta) \qquad (3\text{-}5)$$

Then, the differential equation with the boundary conditions can be setup through equations (3-1), (3-3) and (3-4) to determine the constant λ and the unknown function $f(\theta)$ in equation (3-5).

$$\frac{d^4 f(\theta)}{d\theta^4} + 2(\lambda^2+1)\frac{d^2 f(\theta)}{d\theta^2} + (\lambda^2-1)^2 f(\theta) = 0 \qquad (3\text{-}6)$$

$$f(\theta) = \frac{df(\theta)}{d\theta} = 0 \qquad \text{at } \theta = \pm \alpha \qquad (3\text{-}7)$$

Where α is defined in Figure 3-1. The general solution of the differential equation (3-6) is

$$f(\theta) = C_1\cos(\lambda-1)\theta + C_2\sin(\lambda-1)\theta + C_3\cos(\lambda+1) + C_4\sin(\lambda+1)\theta \qquad (3\text{-}8)$$

where $C_1, \ldots, C_4$ are constants which need to be determined. To find these constants, substitute equation (3-8) into (3-7) to satisfy the boundary conditions. Arranging the sets of equation by simple additions

and subtractions, each pair of homogeneous equations can be written as

$$\begin{bmatrix} \cos(\lambda-1)\alpha & \cos(\lambda+1)\alpha \\ (\lambda-1)\sin(\lambda-1)\alpha & (\lambda+1)\sin(\lambda+1)\alpha \end{bmatrix} \begin{bmatrix} C_1 \\ C_3 \end{bmatrix} = \begin{bmatrix} 0 \\ 0 \end{bmatrix} \tag{3-9a}$$

$$\begin{bmatrix} \sin(\lambda-1)\alpha & \sin(\lambda+1)\alpha \\ (\lambda-1)\cos(\lambda-1)\alpha & (\lambda+1)\cos(\lambda+1)\alpha \end{bmatrix} \begin{bmatrix} C_2 \\ C_4 \end{bmatrix} = \begin{bmatrix} 0 \\ 0 \end{bmatrix} \tag{3-9b}$$

A nontrivial solution requires that the determinants of equations (3-9) be zero. This leads to the respective characteristic equations for the eigenvalue λ's

$$\lambda \sin 2\alpha = \pm \sin 2\lambda\alpha \tag{3-10}$$

When α approaches π, the notch simulates a crack, and equation (3-10) reduces to

$$\sin(2\pi\lambda) = 0 \tag{3-11}$$

which has only real roots for

$$\lambda = \frac{1}{2} n \qquad n=\text{integer} \tag{3-12}$$

Each of the eigenvalues of λ for n=1,2,3,..., will correspond to a relationship between the constants through equations (3-9) as below:

$$\text{For } n=1,3,5,\ldots, \quad C_{3n} = -\left(\frac{n-2}{n+2}\right)C_{1n} \quad C_{4n} = -C_{2n} \tag{3-13a}$$

$$\text{For } n=2,4,6,\ldots, \quad C_{3n} = -C_{1n} \quad C_{4n} = -\left(\frac{n-2}{n+2}\right)C_{2n} \tag{3-13b}$$

By substituting equations (3-13) into (3-8) and (3-5) successively and changing C_{1n} to A_n and C_{2n} to B_n to avoid the complexity of double subscript notation, the stress function can be written as

$$\chi = \sum_{n=1,3,5\cdots} r^{n/2+1}\left[A_n\left\{\cos\left(\frac{n}{2}-1\right)\theta - \left(\frac{n-2}{n+2}\right)\cos\left(\frac{n}{2}+1\right)\theta\right\} + B_n\left\{\sin\left(\frac{n}{2}-1\right)\theta - \sin\left(\frac{n}{2}+1\right)\theta\right\}\right] +$$

$$\sum_{n=2,4,6\cdots} r^{n/2+1}\left[A_n\left\{\cos\left(\frac{n}{2}-1\right)\theta - \cos\left(\frac{n}{2}+1\right)\theta\right\} + B_n\left\{\sin\left(\frac{n}{2}-1\right)\theta - \left(\frac{n-2}{n+2}\right)\sin\left(\frac{n}{2}+1\right)\theta\right\}\right] \qquad (3\text{-}14)$$

Note that the terms multiplied by A_n are symmetric (Mode I) and the terms with B_n are anti-symmetric (Mode II) with respect to $\theta=0$.

Finally, the expressions for stress components can be derived by putting equation (3-14) into (3-3).

$$\sigma_r = \sum_{n=1,3,5\cdots} r^{n/2-1}\left[A_n\left\{\left(\frac{-n^2+6n}{4}\right)\cos\left(\frac{n-2}{2}\right)\theta + \left(\frac{n^2-2n}{4}\right)\cos\left(\frac{n+2}{2}\right)\theta\right\} + B_n\left\{\left(\frac{-n^2+6n}{4}\right)\sin\left(\frac{n-2}{2}\right)\theta + \left(\frac{n^2+2n}{4}\right)\sin\left(\frac{n+2}{2}\right)\theta\right\}\right] +$$

$$\sum_{n=2,4,6\cdots} r^{n/2-1}\left[A_n\left\{\left(\frac{-n^2+6n}{4}\right)\cos\left(\frac{n-2}{2}\right)\theta + \left(\frac{n^2+2n}{4}\right)\cos\left(\frac{n+2}{2}\right)\theta\right\} + B_n\left\{\left(\frac{-n^2+6n}{4}\right)\sin\left(\frac{n-2}{2}\right)\theta + \left(\frac{n^2-2n}{4}\right)\sin\left(\frac{n+2}{2}\right)\theta\right\}\right] \qquad (3\text{-}15a)$$

$$\sigma_\theta = \sum_{n=1,3,5\cdots} r^{n/2-1}\left[A_n\left\{\left(\frac{n^2+2n}{4}\right)\cos\left(\frac{n-2}{2}\right)\theta - \left(\frac{n^2-2n}{4}\right)\cos\left(\frac{n+2}{2}\right)\theta\right\}\right.$$
$$\left. + B_n\left\{\left(\frac{n^2+2n}{4}\right)\sin\left(\frac{n-2}{2}\right)\theta - \left(\frac{n^2+2n}{4}\right)\sin\left(\frac{n+2}{2}\right)\theta\right\}\right] +$$
$$\sum_{n=2,4,6\cdots} r^{n/2-1}\left[A_n\left\{\left(\frac{n^2+2n}{4}\right)\cos\left(\frac{n-2}{2}\right)\theta - \left(\frac{n^2+2n}{4}\right)\cos\left(\frac{n+2}{2}\right)\theta\right\}\right.$$
$$\left. + B_n\left\{\left(\frac{n^2+2n}{4}\right)\sin\left(\frac{n-2}{2}\right)\theta - \left(\frac{n^2-2n}{4}\right)\sin\left(\frac{n+2}{2}\right)\theta\right\}\right] \qquad (3\text{-}15b)$$

$$\tau_{r\theta} = \sum_{n=1,3,5\cdots} r^{n/2-1}\left[A_n\left\{\left(\frac{n^2-2n}{4}\right)\sin\left(\frac{n-2}{2}\right)\theta - \left(\frac{n^2-2n}{4}\right)\sin\left(\frac{n+2}{2}\right)\theta\right\}\right.$$
$$\left. + B_n\left\{\left(\frac{-n^2+2n}{4}\right)\cos\left(\frac{n-2}{2}\right)\theta + \left(\frac{n^2+2n}{4}\right)\cos\left(\frac{n+2}{2}\right)\theta\right\}\right] +$$
$$\sum_{n=2,4,6\cdots} r^{n/2-1}\left[A_n\left\{\left(\frac{n^2-2n}{4}\right)\sin\left(\frac{n-2}{2}\right)\theta - \left(\frac{n^2+2n}{4}\right)\sin\left(\frac{n+2}{2}\right)\theta\right\}\right.$$
$$\left. + B_n\left\{\left(\frac{-n^2+2n}{4}\right)\cos\left(\frac{n-2}{2}\right)\theta + \left(\frac{n^2-2n}{4}\right)\cos\left(\frac{n+2}{2}\right)\theta\right\}\right] \qquad (3\text{-}15c)$$

Equations (3-15) were expanded up to six terms (n=1,2,...,6) in the photoelastic analysis to investigate whether or not the constants of the $1/\sqrt{r}$ terms (n=1) converge. For the convenience of understanding the arrangement of the higher order terms, the stress components for n=1,2,...,6 are written below.

$$\sigma_r = r^{-1/2}\left[A_1\left\{\frac{5}{4}\cos\left(\frac{1}{2}\theta\right) - \frac{1}{4}\cos\left(\frac{3}{2}\theta\right)\right\} + B_1\left\{-\frac{5}{4}\sin\left(\frac{1}{2}\theta\right) + \frac{3}{4}\sin\left(\frac{3}{2}\theta\right)\right\}\right]$$
$$+ \quad A_2\left\{2 + 2\cos(2\theta)\right\}$$

$$+ r^{1/2}\left[A_3\left\{\frac{9}{4}\cos\left(\frac{1}{2}\theta\right)+\frac{3}{4}\cos\left(\frac{5}{2}\theta\right)\right\}+B_3\left\{\frac{9}{4}\sin\left(\frac{1}{2}\theta\right)+\frac{15}{4}\sin\left(\frac{5}{2}\theta\right)\right\}\right]$$

$$+ r\left[A_4\left\{2\cos\theta + 6\cos(3\theta)\right\}+B_4\left\{2\sin\theta + 2\sin(3\theta)\right\}\right]$$

$$+ r^{3/2}\left[A_5\left\{\frac{5}{4}\cos\left(\frac{3}{2}\theta\right)+\frac{15}{4}\cos\left(\frac{7}{2}\theta\right)\right\}+B_5\left\{\frac{5}{4}\sin\left(\frac{3}{2}\theta\right)+\frac{35}{4}\sin\left(\frac{7}{2}\theta\right)\right\}\right]$$

$$+ r^{2}\left[A_6\left\{12\cos(4\theta)\right\} +B_6\left\{6\sin(4\theta)\right\}\right] \qquad (3\text{-}16a)$$

$$\sigma_\theta = r^{-1/2}\left[A_1\left\{\frac{3}{4}\cos\left(\frac{1}{2}\theta\right)+\frac{1}{4}\cos\left(\frac{3}{2}\theta\right)\right\}+B_1\left\{-\frac{3}{4}\sin\left(\frac{1}{2}\theta\right)-\frac{3}{4}\sin\left(\frac{3}{2}\theta\right)\right\}\right]$$

$$+ A_2\left\{2 - 2\cos(2\theta)\right\}$$

$$+ r^{1/2}\left[A_3\left\{\frac{15}{4}\cos\left(\frac{1}{2}\theta\right)-\frac{3}{4}\cos\left(\frac{5}{2}\theta\right)\right\}+B_3\left\{\frac{15}{4}\sin\left(\frac{1}{2}\theta\right)-\frac{15}{4}\sin\left(\frac{5}{2}\theta\right)\right\}\right]$$

$$+ r\left[A_4\left\{6\cos(\theta) - 6\cos(3\theta)\right\}+B_4\left\{6\sin(\theta) - 2\sin(3\theta)\right\}\right]$$

$$+ r^{3/2}\left[A_5\left\{\frac{35}{4}\cos\left(\frac{3}{2}\theta\right)-\frac{15}{4}\cos\left(\frac{7}{2}\theta\right)\right\}+B_5\left\{\frac{35}{4}\sin\left(\frac{3}{2}\theta\right)-\frac{35}{4}\sin\left(\frac{7}{2}\theta\right)\right\}\right]$$

$$+ r^{2}\left[A_6\left\{12\cos(2\theta)-12\cos(4\theta)\right\}+B_6\left\{12\sin(2\theta)-6\sin(4\theta)\right\}\right] \qquad (3\text{-}16b)$$

$$\tau_{r\theta} = r^{-1/2}\left[A_1\left\{\frac{1}{4}\sin\left(\frac{1}{2}\theta\right)+\frac{1}{4}\sin\left(\frac{3}{2}\theta\right)\right\}+B_1\left\{\frac{1}{4}\cos\left(\frac{1}{2}\theta\right)+\frac{3}{4}\cos\left(\frac{3}{2}\theta\right)\right\}\right]$$

$$+ A_2\left\{-2\sin(2\theta)\right\}$$

$$+ r^{1/2}\left[A_3\left\{\frac{3}{4}\sin\left(\frac{1}{2}\theta\right)-\frac{3}{4}\sin\left(\frac{5}{2}\theta\right)\right\}+B_3\left\{-\frac{3}{4}\cos\left(\frac{1}{2}\theta\right)+\frac{15}{4}\cos\left(\frac{5}{2}\theta\right)\right\}\right]$$

$$+ r\left[A_4\left\{2\sin(\theta)-6\sin(3\theta)\right\}+B_4\left\{-2\cos(\theta)+2\cos(3\theta)\right\}\right]$$

$$+ r^{3/2}\left[A_5\left\{\frac{15}{4}\sin\left(\frac{3}{2}\theta\right)-\frac{15}{4}\sin\left(\frac{7}{2}\theta\right)\right\}+B_5\left\{-\frac{15}{4}\cos\left(\frac{3}{2}\theta\right)+\frac{35}{4}\cos\left(\frac{7}{2}\theta\right)\right\}\right]$$

$$+ r^{2}\left[A_6\left\{6\sin(2\theta)-12\sin(4\theta)\right\}+B_6\left\{-6\cos(2\theta)+6\cos(4\theta)\right\}\right] \qquad (3\text{-}16c)$$

2. Discussions of Williams equations

From the definition of K-factors and equations (3-15), Mode I and Mode II fracture parameters can be defined by

$$K_I = \lim_{\substack{r\to 0\\ \theta\to 0}} \sqrt{2\pi r}\ \sigma_\theta = \sqrt{2\pi}\, A_1 \qquad (3\text{-}17a)$$

$$K_{II} = \lim_{\substack{r\to 0\\ \theta\to 0}} \sqrt{2\pi r}\ \tau_{r\theta} = \sqrt{2\pi}\, B_1 \qquad (3\text{-}17b)$$

The equations provide the needed theory which can describe the stress field in the vicinity of the crack tip. They were used to extract K-factors by fitting the expressions for the stress components to the physical fringe loops in a photoelastic model by the iterative least squares method.

If only the first term (n=1) is considered in equations (3-15), they reduce to "Westergaard equations" which have only singular terms of $1/\sqrt{r}$ [14]. If the first two terms (n=1,2) are included, equations (3-15) turn out to be the same as the "modified Westergaard equations"

(equations 2-3a,b,c) [16].

In equation (2-3a), the nonsingular term, σ_{ox}, in the expression of σ_x, can be related to the coefficient in Williams equations (3-15a) through the coordinate transformation from polar coordinates to Cartesian ones.

$$\sigma_{ox} = - 4A_2 \tag{3-18}$$

Also, it can be observed that the stress components of σ_y and τ_{xy} of the Williams equations in Cartesian coordinates do not have any constant terms similar to the σ_{ox} that appears in the expression for σ_x, even though σ_r, σ_θ and $\tau_{r\theta}$ in polar coordinates have the constant terms as shown in equations (3-16a,b,c). This suggests that Williams' elastic singular solutions for a sharp notch problem [26] were well established in 1952 before the introduction of σ_{ox} to Westergaard singular terms by Irwin in 1958 [16]. An alternate explanation of the nonsingular term is that σ_{ox} is one of the coefficients of higher order terms which can be determined from other remote boundary conditions together with those in crack itself. Hence, it may not have been a chance occurrence when Irwin proposed the insertion of σ_{ox} into the Westergaard equations when loads are not equibiaxial.

Only a few people have applied the Williams equations to the photoelastic analysis of crack problems. Bradley and Kobayashi [61] used only the symmetric terms of Williams stress function in equation (3-14) to extract K_I from dynamic photoelastic photographs of fracture. Quite recently, Zhang and Burger [86] used those equations for the study of Mixed Mode fracture parameters for edge cracks under transient

thermal stresses by photoelastic experiment. The research reported in this dissertation uses the expanded version of Williams equations with n=1 to 6.

B. Experimental Techniques

1. Experimental considerations in crack tip analysis

According to the definition of K-factors specified in equations (3-17a,b), SIFs can be calculated through the expressions of stress components when radial coordinate (r) goes to zero. Practically, however, it is not possible to measure SIFs directly from photoelastic images when $r \to 0$. Several factors cause errors in the photoelastic determination of fracture parameters.

The major sources of errors are nonlinearities that arise very near a crack tip in a photoelastic model under high local stresses. These nonlinearties may be caused by localized yielding of the material, crack tip blunting, dimpling at the crack tip due to transverse contractions caused by Poisson's ratio and optical nonlinearity because two polarized components do not follow the same paths in high stressed region.

In addition to the above fundamental sources of error, there are the realities associated with the artificial notches and slits that are, of necessity, used in fracture models. In photoelastic analysis, it is often necessary to simulate the crack tip with an artificial notch to get the desired crack geometry. These notches may be produced by saw cutting or they can be cast into the model. In either case, they will have rounded tips and the assumption of an infinitely sharp crack cannot be justified.

Schroedl and Smith [62] investigated the influence of the finite root radius on the stress distribution by comparing the Kolosoff-Inglis solution for an oblong elliptical hole to a solution of a line crack. They found that the stress distribution very near to the notch tip depends on its root radius. However, away from the notch tip, the influence decreases rapidly and the stress distribution approaches that of a line crack. Figure 3-2 presents their results. For $\rho<0.01a$, the error from crack tip blunting is negligible when $r>0.06a$. These are limits that can be achieved in photoelastic models.

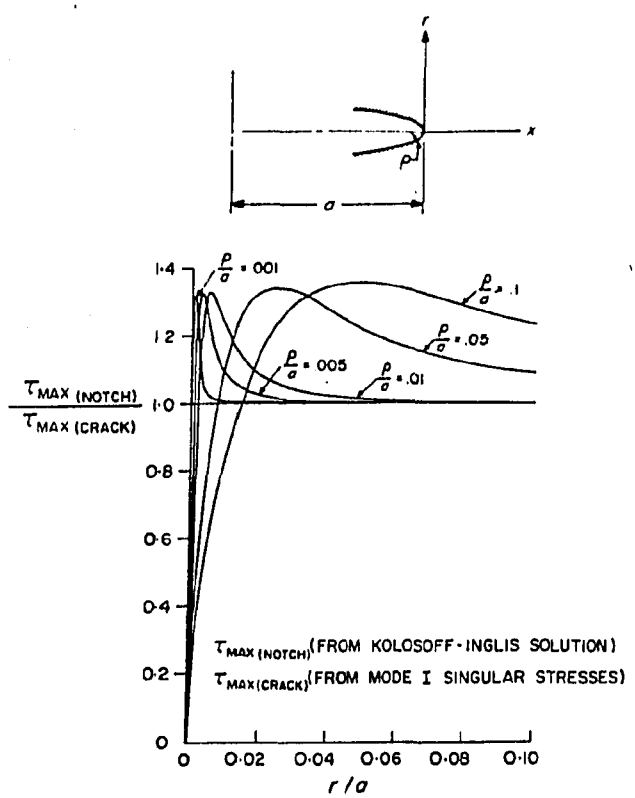

Figure 3-2. Effect of finite root radius on in-plane maximum shearing stress along a line perpendicular to crack surface passing through the crack tip [62]

In an experimental study for crack tip simulation, Smith et al. [87] showed that saw cut slits 1/16 inch (1.59 mm) wide terminating in a 30-degree vee notch of approximately 0.001 inch (0.025 mm) root radius yielded essentially the same SIF values as natural cracks.

It is therefore clear that, in order to estimate fracture parameters accurately, methods to manufacture models with very narrow slits and sharp tips are needed.

Also, as discussed in Chapter II-C, several experimentalists [48-50, 57, 62-72] have found a singular zone (**Region II** in Figure 2-9) from which K-factors can be extrapolated and/or interpolated by any one of the two-parameter methods based on the modified Westergaard equations (2-4). Care should be taken to define the boundaries of the singular zone before applying equations (2-4).

For the convenience of data acquisition and K-factor calculation, some authors [16, 62-72] prefer to use a selected line approach, i.e., they take data along a line such as $\theta=\pm 90^{o}$ or at θ_{max} (Figure 2-2). In contrast, the overdeterministic least squares fitting method [6, 73, 74] uses data from the whole singular zone portion of the fringe field where equations (2-4) are valid for all data points.

In many practically important cases, the effect of a boundary ahead of the crack tip may affect the stress field. Then, the ambiguity of the singular zone increases and K-factors need to be estimated by using the definitions of equations (3-17a,b). These expressions for stress components incorporate several of the higher order terms in the expansion to relax the need to accurately define the singularity zone. Data can then be gathered from selected fringe loops along which the

quality is good rather than just from a vaguely defined "singular" zone.

Another difficulty in photoelastic determination of SIFs is that the exact position of a "crack tip" is hard to define. It may be obscured by the caustic effect and inaccurate arrangement of the optical system. The exact location of crack tip is important for experimental accuracy because the distances of data points from the crack tip (r) are so small that even a little deviation in the placement of the crack tip may introduce large errors within the small and limited data collection region. Particularly, the difficulty in locating the crack tip becomes pronounced when the crack is a one that does not have a real physically defined "tip".

The broad band nature of most isochromatic fringes also tends to increase the uncertainty in the exact location of the data points. Some compensation techniques can be used to read the fractional fringe orders exactly, but compensation itself may introduce measurement errors. Any procedure that minimize the location error will improve the reliability of the K-factor determination.

In this study, data collection for the extraction of fracture parameters was done within the limited zone $0.05<r/a<0.35$. This is in agreement with the limits set by previous experimentalists [62-72]. It eliminates the non-linear zone while, at the same time, it reduces the importance of so called "far field" effects.

To decrease the experimental location error, the fringe patterns generated by the EyeCom II digital image processing system [88] were sharpened with a related program "TRACE" [89]. In this way the contour lines of the minimum and maximum light intensities are clearly drawn so

that the locations of the half- and full-order fringes can be accurate.

The ambiguity of the origin of a crack tip was solved by including the origin of the tip as two more unknowns (x_o and y_o) in the overdeterministic iterative least squares method [6, 73, 74], by which the coefficients for the specified equations are calculated to fit the equations to the observed fringe loops.

The quality of the experimental results was evaluated with a back-plot scheme by which the actual isochromatic fringe pattern was overlaid onto a simulated fringe pattern computed from the experimentally determined coefficients. This provided a visual comparison. A quantitative measure of the accuracy of the results was obtained by using simple statistical parameters, such as mean of percentage error, standard deviation and correlation coefficient between the regenerated fringe values at the location of the original data points with the observed values at these points.

The mathematical formulation of the above mentioned considerations will be discussed in detail in the following sections.

2. Numerical procedure of photoelastic data analysis

The expressions of stress components used in the crack analysis were equations (3-15a,b,c) from Williams stress function [28]. The numerical procedure for extracting fracture parameters and crack tip location was an extension of the iterative least squares method proposed by Sanford [6].

The stress optic law in photoelasticity relates the isochromatic fringe order (N) to in-plane maximum shear stress (τ_{max}).

$$\tau_{max} = \frac{Nf_\sigma}{2h} \tag{3-19}$$

Where f_σ is the stress-optical coefficient of the material, and h is the length of the light path in the model.

The maximum in-plane shear stress can be expressed in terms of polar components as

$$(\tau_{max})^2 = (\frac{\sigma_r - \sigma_\theta}{2})^2 + (\tau_{r\theta})^2 \tag{3-20}$$

where σ_r, σ_θ and $\tau_{r\theta}$ are the radial, tangential and shear stress components, respectively, as shown in Figure 3-1. Equations (3-15) were used for these stress components.

By substituting equation (3-19) into (3-20), one can obtain an arbitrary function G, whose value should be zero in the ideal case.

$$G(A_n,B_n) = (\frac{\sigma_r - \sigma_\theta}{2})^2 + (\tau_{r\theta})^2 - (\frac{Nf_\sigma}{2h})^2 = 0 \tag{3-21}$$

Where A_n and B_n, n=1,2,...,j, are the unknown coefficients in equations (3-15a,b,c) to be extracted by the least squares method.

The least squares fitting technique to calculate the unknown location of the crack tip started with the initial measured location of crack tip. This was considered as a first estimation which is assumed to deviate from the unknown origin. The deviation x_o, y_o is shown on Figure 3-3. Here, O_m is the initial estimated origin of a crack tip and O_c is the corrected one. Radius r_m and angle θ_m are the measured

coordinates of a data point P at which fringe order is N. The corrected coordinates for point P are r_c and θ_c, where

$$r_c = \sqrt{(x_o+r_m\cos\theta_m)^2 + (y_o+r_m\sin\theta_m)^2} \tag{3-22}$$

$$\theta_c = \tan^{-1}\left(\frac{y_o+r_m\sin\theta_m}{x_o+r_m\cos\theta_m}\right) \tag{3-23}$$

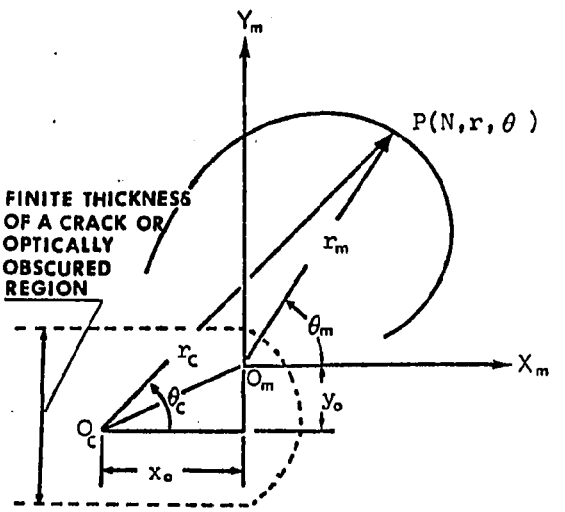

Figure 3-3. Relationship between measured and corrected coordinates with consideration of crack tip deviation from the initial estimated crack tip origin

The unknown parameters, x_o and y_o, are added to the fracture coefficients of A_n and B_n, n=1,2,...,j, and equation (3-21) can be rewritten as

$$G_k(A_n,B_n,x_o,y_o) = 0 \tag{3-24}$$

where the subscript k refers to the number of arbitrary data points

whose number should be more than that of the unknown parameters. In this experiment, 40 data points were chosen to estimate up to 11 coefficients A_n and B_n (n=1,...,6) and x_o, y_o for a total of 13 unknowns.

Obviously, equations (3-22), (3-23) and (3-24) are nonlinear with respect to unknown parameters A_n, B_n, x_o and y_o. A truncated Taylor series expansion about the unknown parameters can linearize equation (3-24) and an iterative procedure is developed with

$$(G_k)_{i+1} = (G_k)_i + \sum_{n=1}^{j} \left(\frac{\partial G_k}{\partial A_n}\right)_i \Delta A_n + \sum_{n=1}^{j} \left(\frac{\partial G_k}{\partial B_n}\right)_i \Delta B_n + \left(\frac{\partial G_k}{\partial x_o}\right)_i \Delta x_o + \left(\frac{\partial G_k}{\partial y_o}\right)_i \Delta y_o \tag{3-25}$$

Where the subscript i denotes the iteration step, and ΔA_n, ΔB_n, Δx_o and Δy_o are corrections to the previous estimates of A_n, B_n, x_o and y_o, respectively. The corrections are incorporated and the procedure is repeated until the desired result, $(G_k)_{i+1} = 0$, is attained. Thus, equation (3-25) gives

$$\sum_{n=1}^{j} \left(\frac{\partial G_k}{\partial A_n}\right)_i \Delta A_n + \sum_{n=1}^{j} \left(\frac{\partial G_k}{\partial B_n}\right)_i \Delta B_n + \left(\frac{\partial G_k}{\partial x_o}\right)_i \Delta x_o + \left(\frac{\partial G_k}{\partial y_o}\right)_i \Delta y_o = -(G_k)_i \tag{3-26}$$

Applying the iteration scheme suggested in equation (3-26) to k equations of the form given in equation (3-24) results in an overdetermined set of linear equations in terms of unknown corrections ΔA_n, ΔB_n, Δx_o and Δy_o given in matrix notation as

$$\{G\}_i = [B]_i \{\Delta C\}_i \tag{3-27}$$

where

$$\{G\} = \begin{Bmatrix} G_1 \\ G_2 \\ \cdot \\ \cdot \\ G_k \end{Bmatrix} \tag{3-27a}$$

$$[B] = - \begin{bmatrix} \frac{\partial G_1}{\partial A_n} & \frac{\partial G_1}{\partial B_n} & \frac{\partial G_1}{\partial x_o} & \frac{\partial G_1}{\partial y_o} \\ \frac{\partial G_2}{\partial A_n} & \frac{\partial G_2}{\partial B_n} & \frac{\partial G_2}{\partial x_o} & \frac{\partial G_2}{\partial y_o} \\ \cdot & \cdot & \cdot & \cdot \\ \cdot & \cdot & \cdot & \cdot \\ \frac{\partial G_k}{\partial A_n} & \frac{\partial G_k}{\partial B_n} & \frac{\partial G_k}{\partial x_o} & \frac{\partial G_k}{\partial y_o} \end{bmatrix} \tag{3-27b}$$

$$\{\Delta C\} = \begin{Bmatrix} \Delta A_n \\ \Delta B_n \\ \Delta x_o \\ \Delta y_o \end{Bmatrix} \tag{3-27c}$$

It can be shown that $\{\Delta C\}$ in equation (3-27) can be determined in a least squares sense by multiplying both sides from the left by $[B]^T$, where $[B]^T$ is the transpose of $[B]$.

$$[B]^T\{G\} = [B]^T[B]\{\Delta C\} \tag{3-28}$$

or

$$\{D\} = [A]\{\Delta C\} \tag{3-29}$$

where

$$\{D\} = [B]^T\{G\} \tag{3-29a}$$

$$[A] = [B]^T[B] \tag{3-29b}$$

Finally,

$$\{\Delta C\} = [A]^{-1}\{D\} \tag{3-30}$$

where $[A]^{-1}$ is the inverse of [A]. The solution of equation (3-30) gives ΔA_n, ΔB_n, Δx_o and Δy_o which are used to correct the initial estimates of A_n, B_n, x_o and y_o by

$$(A_n)_{i+1} = (A_n)_i + \Delta A_n \tag{3-31a}$$

$$(B_n)_{i+1} = (B_n)_i + \Delta B_n \tag{3-31b}$$

$$(x_o)_{i+1} = (x_o)_i + \Delta x_o \tag{3-31c}$$

$$(y_o)_{i+1} = (y_o)_i + \Delta y_o \tag{3-31d}$$

where the subscript i is the iteration step, and n is the number of terms in equations (3-15a,b,c). Up to 6 terms were considered to see whether or not the fracture parameters (coefficients of $1/\sqrt{r}$) converge. The iteration continues until the delta quantities (ΔA_n, ΔB_n, Δx_o and Δy_o), as shown in equations (3-31a,b,c,d), become acceptably small. This procedure fits the function $G_k(A_n,B_n,x_o,y_o)$ to the k data points, i.e., k=40 in our case.

The convergence of the method is rapid and usually five to ten iterations are sufficient for obtaining a small number of coefficients. The minimum number of terms used was for n=2. There are then 5 coefficients in all: 2 coefficients A_1, A_2, one coefficient B_1 (B_2=0) plus xo, yo, which locate the crack tip. As the number of coefficients increases, the convergence of the solution becomes more sensitive to the

values of the initial guess of the coefficients. To overcome this sensitivity, the coefficients determined in the 5-coefficient fit, which always converged, were used as the initial guess for the 7-coefficient fit (n=3) and the coefficients determined in this fit used as the initial guess in the 9-coefficient fit (n=4) and so on in order to obtain an initial guess as close to the final values as possible. In this manner, convergence to the final values of several coefficients in higher order terms of equations (3-15) was usually achieved in less than 20 iterations.

This fitting technique cannot ensure the validity of data analysis. Because, by the nature of a least squares fit, data points can be fitted to any given equations. Hence, the accuracy should be evaluated by comparing analytically determined isochromatic fringe pattern with the input data. This will be discussed in the following section.

3. Accuracy evaluation by back-plot

From the given stress field in the vicinity of the crack tip, photoelastic data are collected from manually selected points where the fringe order is well defined. These data are used to calculate the coefficients of equations (3-15a,b,c) by an iterative least squares method. The results for the coefficients are then used to compute what the equivalent fringe field would have looked like, if those coefficients represented the stress field. This regenerated fringe pattern is called the back-plot. When it is compared to the actually observed fringes over the whole field, the validity of the experimental results can be easily shown qualitatively. A quantitative check for the

quality of fit between real and regenerated fringes is then made by a statistical comparison for a predetermined number of points in the field.

From equations (3-19) and (3-20), the basic relation between isochromatic fringe order (N) and in-plane stress components can be expressed as

$$\left(\frac{Nf_\sigma}{2h}\right)^2 = \left(\frac{\sigma_r - \sigma_\theta}{2}\right)^2 + (\tau_{r\theta})^2 \qquad (3\text{-}32)$$

Substituting equations (3-15a,b,c) into (3-22) with the calculated values for coefficients A_n and B_n in place (n is the number of terms) yields a polynomial type of equation in terms of $\sqrt{r}$. For a chosen angle θ and a chosen fringe order N, the coordinate r along the line θ, where the fringe order will occur, can be calculated. With θ and N fixed in equations (3-15) and (3-32), the substitution yields a polynomial equation in $\sqrt{r}$ only. If only the first terms in equations (3-15) are used, i.e., only the first terms for n=1, then the polynomial equation will be of the form:

$$C_1(\sqrt{r})^2 + C_2(\sqrt{r}) + C_3 = 0 \quad (C_2=0 \text{ for this case})$$

If two terms are used in equations (3-15), the polynomial will be

$$C_1(\sqrt{r})^2 + C_2(\sqrt{r}) + C_3 = 0$$

Three terms in equations (3-15) yield

$$C_1(\sqrt{r})^4 + C_2(\sqrt{r})^3 + C_3(\sqrt{r})^2 + C_4(\sqrt{r}) + C_5 = 0$$

where C_1, C_2,..., are different constants in each of the equations above. So, generally,

$$C_1(\sqrt{r})^m + C_2(\sqrt{r})^{m-1} + \ldots + C_{m+1} = 0 \qquad (3\text{-}33)$$

where m is the order of $\sqrt{r}$ and C_1, C_2, ..., C_{m+1} are constants of the polynomial. It is not easy to solve equation (3-33) for all the roots of $\sqrt{r}$ which exist in the polynomial. So, a searching technique, which scans all the points in a specified limited area, is used. Unfortunately, this technique often requires longer computation time than the direct solving of equation (3-33). When Newton's method is used with a synthetic division, known as Horner's method, all real roots can be found more efficiently, especially over large areas. This algorithm is described in detail in the references [90,91], and the computer code for this polynomial root finder (PLROOT) is attached in the Appendix (Library Subroutines "BLIB").

The results are used to generate fringe loops. When these back-plots are visually compared to the actual fringe field, we obtain a qualitative assesment of the accuracies of the values of SIFs. We need an index which can make a quantitative comparison between the back-plot and physical fringes observed from a model. For this purpose, simple types of statistical parameters, such as mean and standard deviation of percentage error, and correlation coefficient between the calculated and measured fringes, were used. Figure 3-4 illustrates how this is done.

For any point P, the experimentally measured photoelastic data (N_{exp}, r_m, θ_m) are known. The analysis then computes the coefficients A_n, B_n, x_o and y_o. The corrected coordinates r_c and θ_c are then

available. They are substituted into equation (3-32) together with the coefficients A_n and B_n to yield an analytically regenerated fringe value, N_{reg}, at the original point P.

$$N_{reg} = f(r_c, \theta_c, A_n, B_n) \tag{3-34}$$

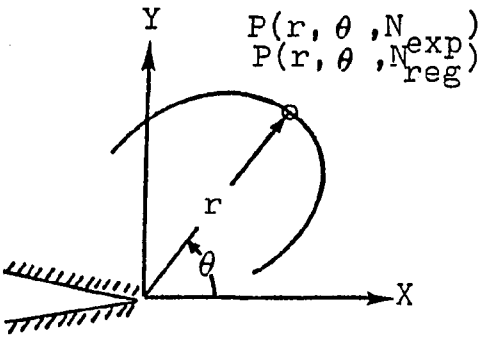

Figure 3-4. Illustration for the comparison between experimentally observed fringe value and regenerated one at a point P

The percentage error (E) between the regenerated and experimentally observed fringe value at any point is then

$$E = \frac{N_{reg} - N_{exp}}{N_{exp}} \times 100 \ (\%) \tag{3-35}$$

The mean of the percentage errors for k data points can be written as

$$\bar{E} = \frac{1}{k} \sum_{i=1}^{k} E_k \tag{3-36}$$

Then, standard deviation, SD, of the percentage errors can be calculated from

$$SD = \sqrt{\frac{1}{k-1}\left[\sum_{i=1}^{k} E_k^2 - \frac{1}{k}\left(\sum_{i=1}^{k} E_k\right)^2\right]} \qquad (3\text{-}37)$$

Another statistical index may be derived from the relations between N_{reg} and N_{exp}. We have k numbers for N_{exp} and for N_{reg} at θ_i and r_i, where i=1,2,...,k. In the ideal case, N_{reg} should have the same value N_{exp}. However, there will be a scatter band due to experimental error and the accuracy with which the coefficients A_n and B_n were determined. This accuracy or level of fit varies with the number of terms, n, used in equations (3-15). The scatter band is shown in Figure 3-5.

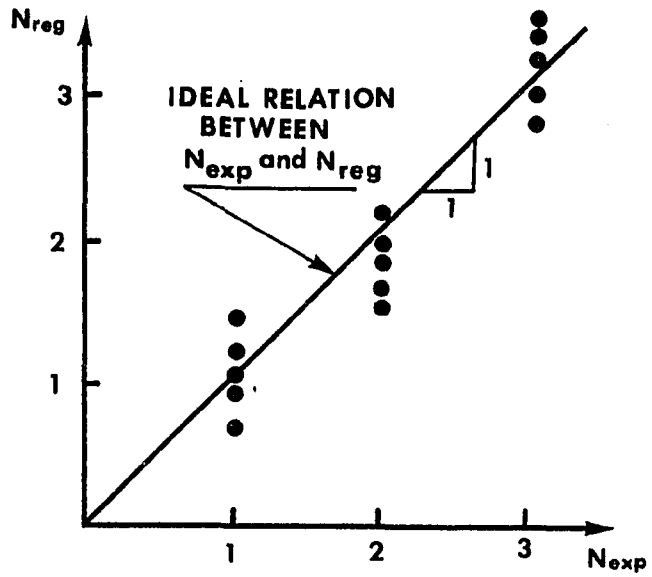

Figure 3-5. Illustration of the relation between analytically determined fringe value (N_{reg}) and experimentally observed fringe value (N_{exp})

The goodness of fit of N_{reg} to N_{exp} can be expressed in terms correlation coefficient, ρ, defined by [92] as

$$\rho = \frac{n\Sigma(N_{exp})(N_{reg})-\Sigma(N_{exp})\Sigma(N_{reg})}{\sqrt{[n\Sigma(N_{exp})^2-(\Sigma N_{exp})^2][n\Sigma(N_{reg})^2-(\Sigma N_{reg})^2]}} \qquad (3\text{-}38)$$

This correlation coefficient ranges from 0 to 1, where 1 is the ideal case, that is, the values of N_{reg} are exactly the same as those of N_{exp} for all the data points.

As a consequence, statistical expressions of equations (3-35) through (3-38) can be used for quantitative comparison between the observed physical fringe values and the analytically regenerated fringes. In its present form, the program makes the comparison only at collected data points. These parameters that measure quality are simple to calculate. Thus, quantitative comparisons are possible without the need to make back-plot fringes. Back-plotting usually requires long computation time.

4. Procedure of SIF analysis

To calculate fracture parameters from the given isochromatic fringes in the neighborhood of a crack tip, and evaluate the accuracy of SIF results obtained from the analysis, several computational programs were developed. These include programs for fringe sharpening, data acquisition, calculation of coefficients by the iterative least squares method and accuracy evaluation for the experimental results. All the data acquisition and processing were done on an "EyeCom II" digital image processing manufactured by Loge/Spatial Data Systems, Inc. The

system is shown in Figure 3-6.

The description of the system and brief explanation of the related programs are written below.

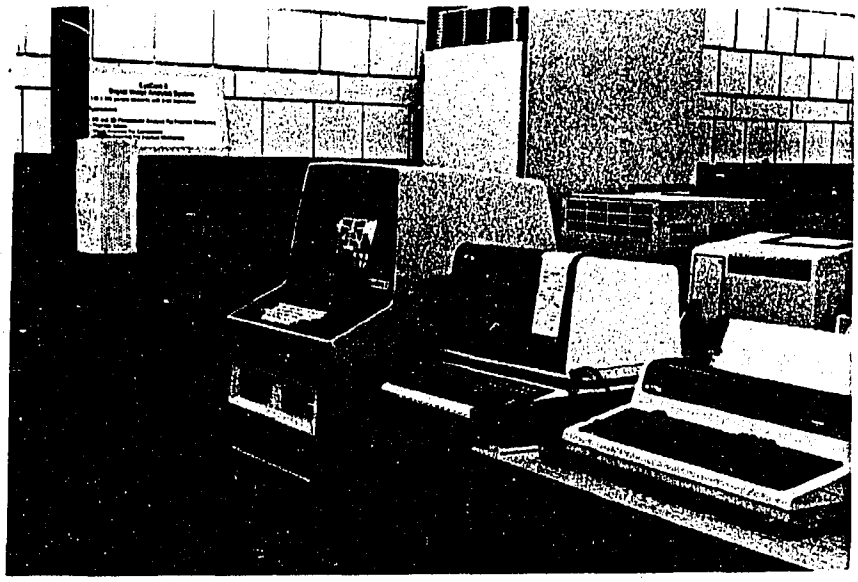

Figure 3-6. The EyeCom system with peripherals

a. Description of the System [1,2,88] The "EyeCom II" system is an digital image processing system that combines three types of man-machine communications, i.e., alphanumeric, graphic and pictorial, into a single unit to provide the tools required for efficient image processing. Figure 3-7 is a schematic diagram of the system.

It consists firstly of a polariscope in which the camera or viewing lens is replaced with a video camera. For the analysis from a negative, the polariscope can be removed. The main function of the system and the accessaries include:

- A scanner which uses a special vidicon television-camera tube to scan the chosen image. The picture is divided 480 lines and each line is divided into 640 parts. The brightness (Z-value) is converted into a video signal with 8-bit resolution. This division represents 307,200 points or picture elements (called "pixels"). The intensity for each pixel is read and digitized on a scale which divides the range from a preselected darkest to a lightest point into 256 different grey levels.
- A real-time digitizer which digitizes the video signal in 1/30 second. This is too fast for direct transfer to the computer, so a special digitizer data bus transfers the data to a refresh memory where it can be accessed later by the computer.
- A display system or monitor which visualizes the information and acts as a graphics/numeric terminal for data processing, program development, and graphical data displays.
- A LSI-11/2 computer and peripherals.

b. Program "TRACE" [5,89] Photoelastic analysis requires that the isochromatic fringe order and location of selected data point be read as accurately as possible. For this purpose, a program "TRACE" was developed [89]. It uses a procedure that uses the rate of change of the slope of the light intensity vector to sharpen the broad bands of isochromatic fringes to sharp lines at each half- and full-order fringe. After digitization of a photoelastic image into the system, TRACE can be used to obtain contour lines of half- and full-order fringes over any specified area of the displayed image.

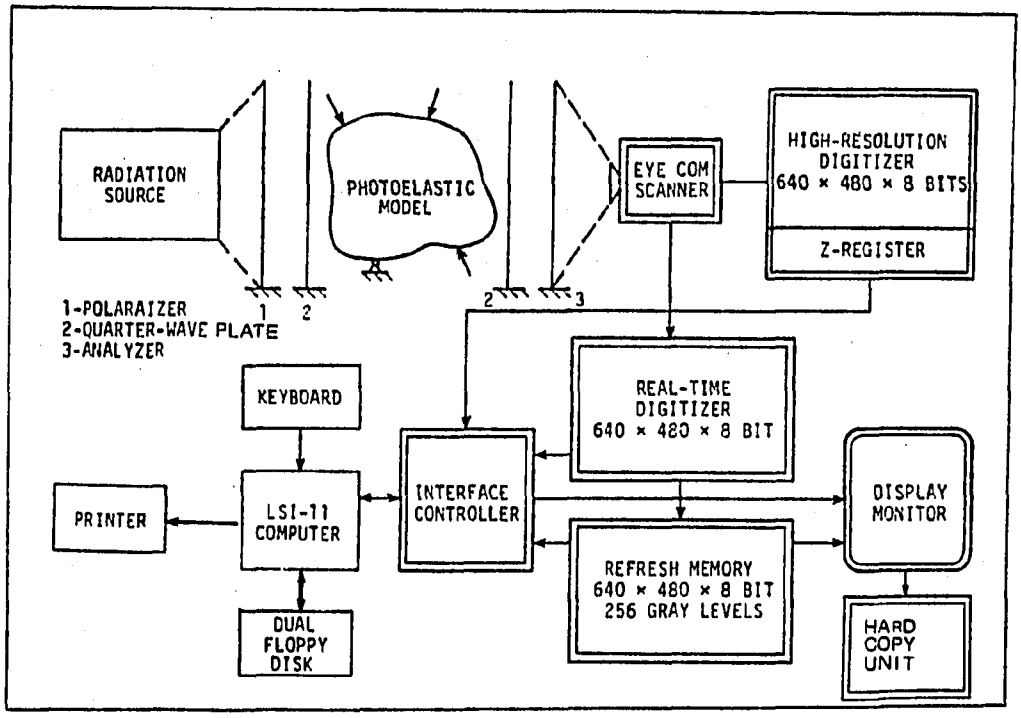

Figure 3-7. Schematic diagram of the EyeCom II system

c. Program "BCOL2" [89] This program acquires the data from the fringe sharpened image and stores it in a data file. The informations required at each selected point are fringe order (N), radial coordinate (r) and angular location (θ). The limits of the data collection region are specified by inner and outer circles centered at the crack tip as illustrated in Figure 3-8. The inner radius (r_i) and outer radius (r_o) are calculated from the values of $(r/a)_{min}$ and $(r/a)_{max}$, where "a" is the crack length for an edge crack or half the crack length for an internal crack. The user therefore inputs "a", $(r/a)_{min}$ and $(r/a)_{max}$. The crack tip and the crack direction are entered by pointing the cursor

first to C_1 and then to C_2. A scaling factor is determined by pointing to S_1 and S_2 and entering the distance between them. The crack tip data (crack position and its direction) together with the geometric scaling factor used in the data collection are stored for later use when the regenerated fringes are compared to the real ones.

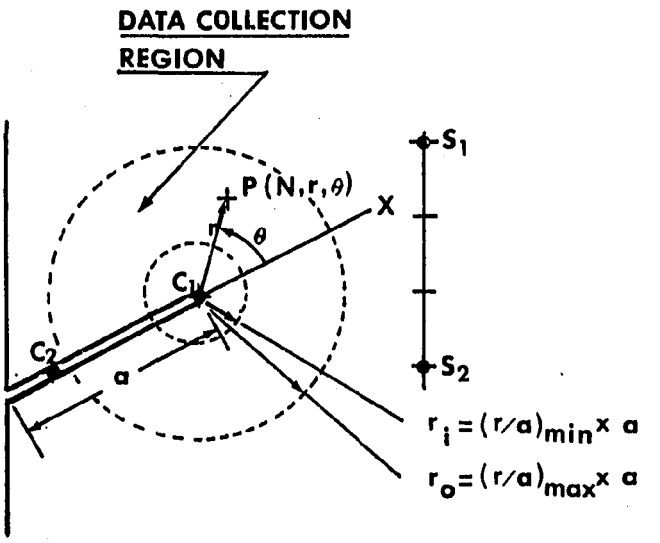

Figure 3-8. Illustration of data collection for crack analysis

d. Programs "WIL1~6" [89] From the collected photoelastic data (N,r,θ), the coefficients of Williams' stress expressions are calculated. The crack tip coordinates x_o, y_o and the coefficients of up to six terms in equations (3-16a,b,c), i.e., n=1,2,...,6, can be calculated with these programs. The procedure is the iterative least squares method described in detail in the section B-2. Program "WIL1" uses one term of Williams equations, "WIL2" two terms, and so on. In each case, the thickness (h) of the model, and its material fringe

value (f_σ), the error limit for the iteration and maximum iteration number ($iter_{max}$) are entered. Thus the program will stop when either the specified conditions are satisfied or the number of iterations exceeds $iter_{max}$.

e. Programs "BPOW1~6" [89] To check the experimental results obtained by programs WIL1~6, these programs generate analytically determined fringe values at the the collected data points by equation (3-34). The percentage errors between the calculated fringe values and observed ones are computed from equation (3-35), the mean of the percentage errors from equation (3-36), the standard deviation of the percentage errors from equation (3-37) and the correlation coefficient from equation (3-38). If the user chooses to do so, he can request that any specified fringe contour be drawn. This is done by solving equation (3-33). The result is an excellent pictorial measure of the quality of the results. Program "BPOW1" will use the results obtained from program "WIL1", while "BPOW2" uses the results from "WIL2", and so on. "WIL4" usually produces good results. It calculates a total of four coefficients A_n and three coefficients B_n plus x_o, y_o form a total of nine unknowns. The input data for all these calculation are 40 data points.

The whole procedure and programs used in the data analysis are summarized in Figure 3-8. The data collection program "BCOL2", the SIF analysis program "WIL4", the accuracy checking program "BPOW4" are attached in the Appendix. All other programs reside in the Program Bank of the Experimental Stress Laboratory, Department of Engineering Science and Mechanics, Iowa State University [89].

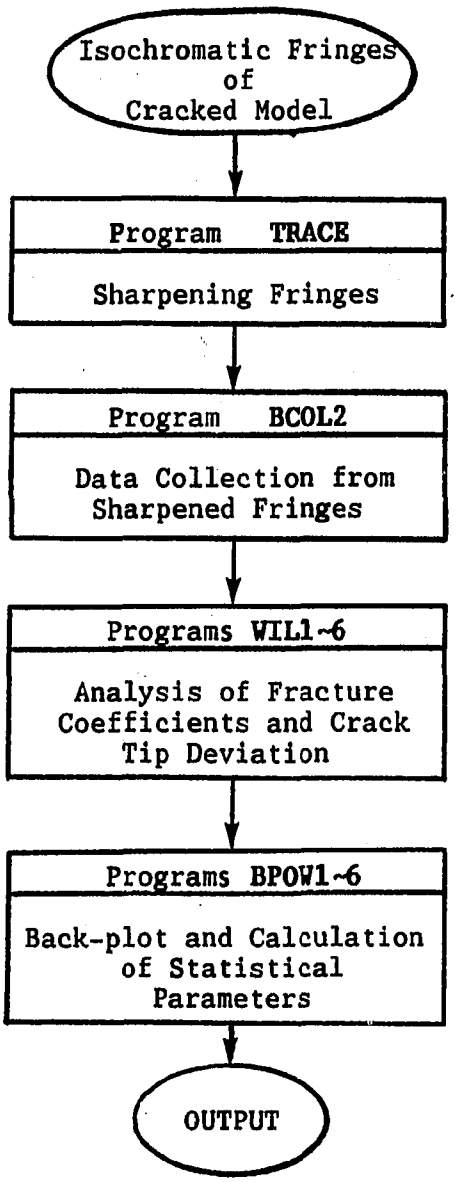

Figure 3-9. Block diagram of SIF analysis procedure

IV. TWO-DIMENSIONAL EXPERIMENTS

Conventional photoelasticity has been extensively used to estimate the stress intensity factors from two-dimensional cracked plates. Murthy and Rao [59] processed identical photoelastic data according to 4 widely used methods. There was as much as 30 percent difference in the estimation for K_I for identical conditions. The wide range of SIF results for a geometry as simple as a straight-edge cracked plates suggests that the jury is still out on which method is the most accurate.

In this chapter, the methods from Chapter III-B for testing and improving the accuracy of photoelastic measurements of Mixed Mode SIFs are applied to plates with inclined edge cracked plates.

For this purpose, plates were cast from three-dimensional photoelastic material so that analyses could be made to see if the results obtained from live and stress frozen models are different and to check the variation of SIF results between them.

Before running these tests, however, several preliminary tests were made. The final test sequence was as follow:

- An analysis to compare the SIFs from tests that manually located the crack tip and those that used the corrected position of the crack tip.
- An analysis that compared the number of terms needed in the Williams equations for pure Mode I and Mixed Mode conditions. The comparisons were on the basis of the match between the back-plots and original fringes.

- Tests at different loads (in live models) to check for variations in the normalized SIFs.
- An analysis from live models and frozen-stress models to compare their results.

The whole two-dimensional test procedures, from the preparation of models to the final results, are described and discussed in this chapter.

A. Model Preparation

1. Materials and mixing and curing procedures

The specimens used in this investigation were cast from "3DMU-050" three-dimensional photoelastic material [93] mixed with 50 percent by weight of phthalic anhydride. This material requires simple procedures in casting, is fast-curing and possess excellent machinability, all features that are important in three-dimensional work. The casting procedures for 3DMU-050 in three-dimensional stress-freezing has been well-developed by Cernosek [94, 95]. Typical properties as specified by him are given in Table 4-1. The detailed procedures for the preparation of this material are described below.

After preheating 3DMU-050 epoxy resin to 220 ^{o}F, 50 percent by weight of phthalic anhydride (PA) is added to the resin. The mixture is heated to 225$\pm$5 ^{o}F while stirring constantly until PA dissolves completely. When PA has dissolved, cool the mixture to 220 ^{o}F and place the container into the oven preheated to 206$\pm$2 ^{o}F. Record time (T) at this stage. Every one hour, take out the container from the oven, and cool it, stirring constantly, to 210 ^{o}F and return it to the oven.

After T+2.5 hours, take out the container from the oven, cool the mixture to 210 ^{o}F and return it into the oven for 5~10 minute period. The mixture is now slowly poured into the mold preheated to 206$\pm$2 ^{o}F. Then proceed to pre-cure the casting according to the time/temperature schedule of Figure 4-1. After being pre-cured, the material is only partially cured, but the casting is strong enough to be handled and is easily machined into the final desired shape.

Table 4-1. Average properties of 3DMU-050 three-dimensional photoelastic material at stress-freezing temperature

Properties	Characteristics
Critical temperature	275 ^{o}F
Modulus of elasticity	2900 ~ 3200 psi
Material fringe value	2.15 ~ 2.20 psi-in/fringe
Tensile strength	205 ~ 225 psi (110 fringes/in-thickness)

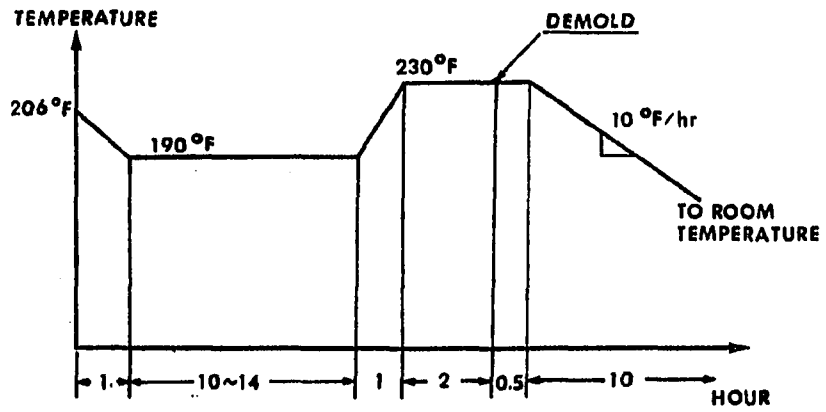

Figure 4-1. Pre-curing procedure of 3DMU-050 photoelastic material

For machining the brittle photoelastic material, sharp cutting tools are essential. Single point fly-cutters are favored for surface cutting, because they apply less pressure to the model and result in less heat generation [96]. After being machined, the pre-cured plate is placed in the oven for post-curing and/or stress-freezing according to the time/temperature schedule described in Figure 4-2. From each batch of resin, a calibration disc is also cast, machined and cured identically to the model. All curing processes were done in the programmable oven whose temperature and time can be controlled by the computer.

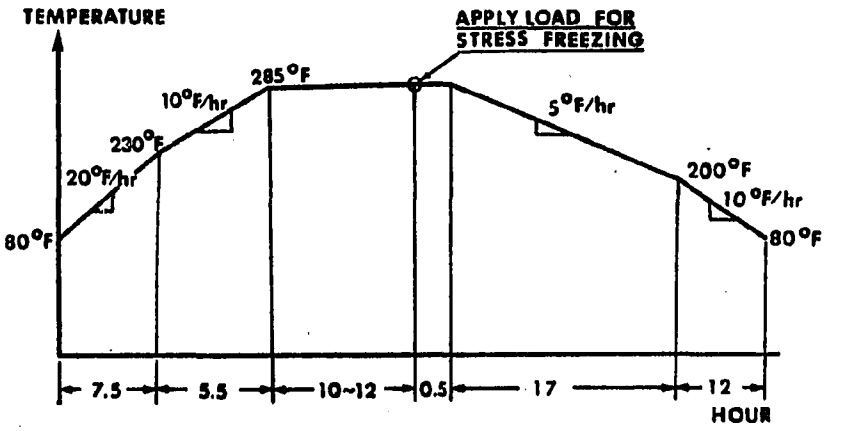

Figure 4-2. Post-curing and/or stress-freezing cycle of 3DMU-050 three-dimensional photoelastic material

2. Model geometries

For the study of Mixed Mode fracture parameters, plates were cast, pre-cured and machined to the shape and size shown in Figure 4-3. Simulated cracks were introduced into the plate with a thin jeweler's

slitting saw whose thickness was 0.006 inch. The nominal crack length, a, is 0.375 inch.

The effect of the far boundary on the crack tip field was kept small by holding a/W=0.2. A uniform far-field tensile stress across the plate width, W, was achieved by choosing H/W=2. These dimensions were based on the previous research on boundary effects [97, 98].

After machining, the plates were post-cured to remove all residual stresses including those caused by machining.

Final dimensions of the three models are given in Table 4-2. Figure 4-4 is a photograph of the three models observed through the light field polariscope setup after post-curing. There are neither appreciable residual stresses nor any noticeable edge effects. Also, mottles, which often occur during the production of three-dimensional photoelastic models due to inhomogenous mixture, cannot be seen.

Table 4-2. Dimensions[a] of inclined through-thickness edge cracked plates after machining

Model No.	β (degree)	a (inch)	W (inch)	t (inch)	2H (inch)	d (inch)
1A	-0.5~1.5[b]	0.3757	1.874	0.1230	8.74	0.0068
2A	22.5	0.3744	1.873	0.1223	8.76	0.0064
3A	44.5	0.3698	1.874	0.1235	8.73	0.0065

[a] See Figure 4-3 for the symbols.
[b] Due to warping of a thin slitting saw when machining the slits, the crack was not straight. One side of the crack angle was -0.5^{o} and the other 1.5^{o} measured as shown in Figure 4-3.

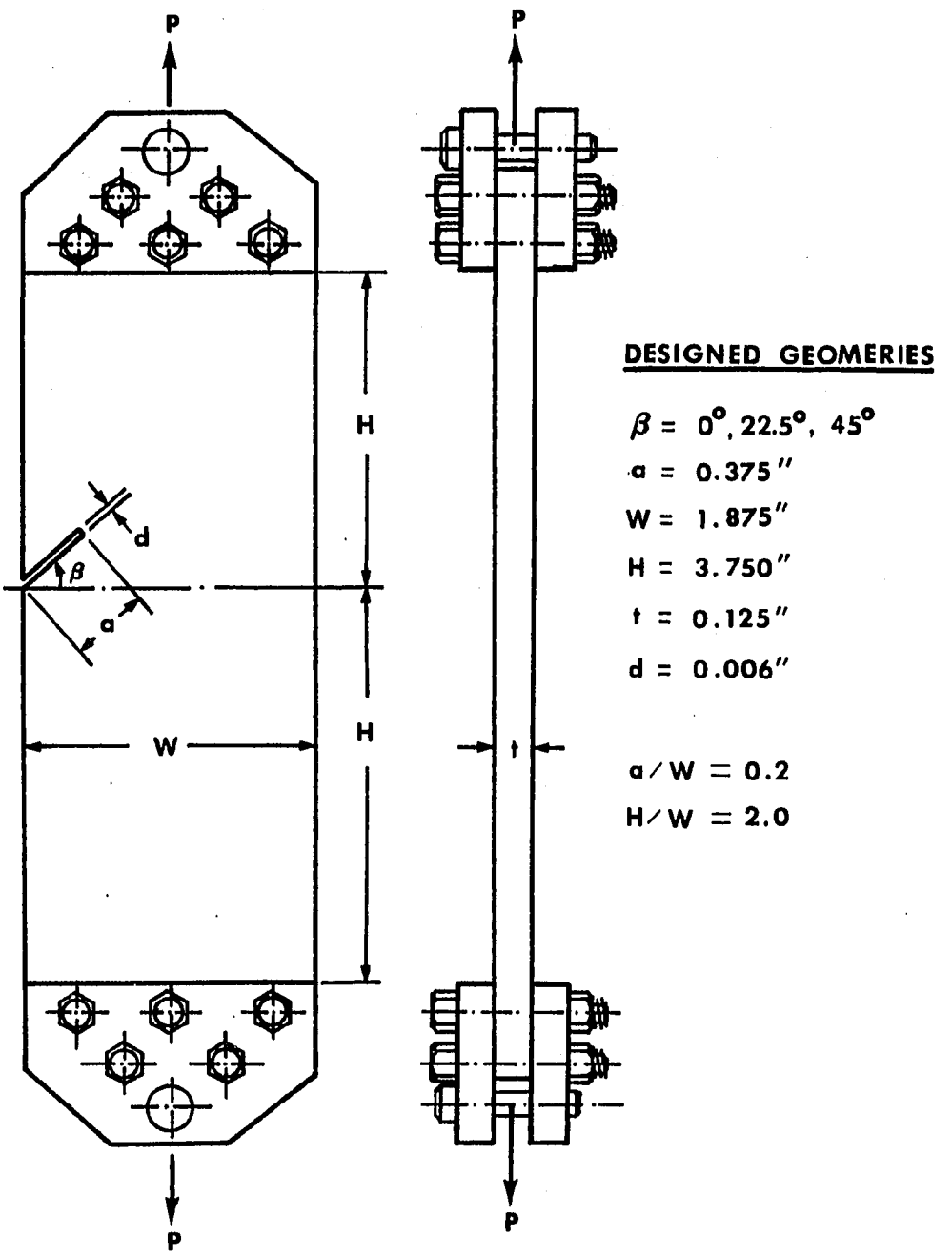

Figure 4-3. Model geometries of inclined through-thickness edge cracked plates

a. Model No. 1A

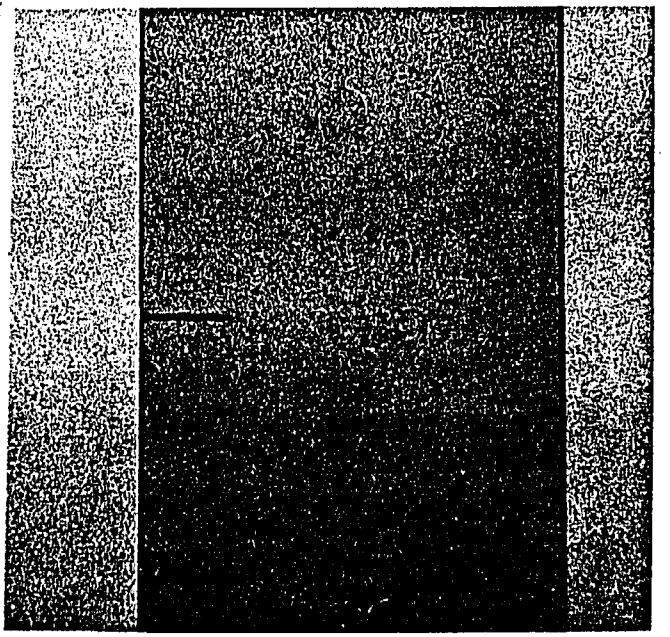

b. Model No. 2A

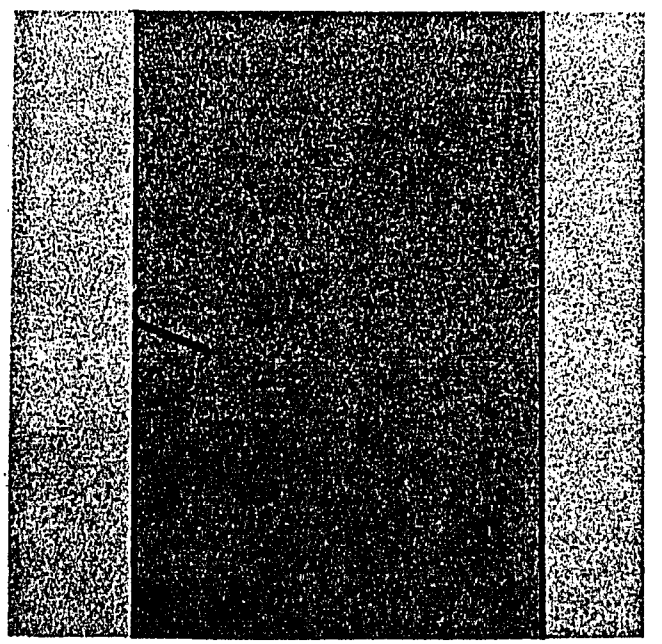

Figure 4-4. Photographs of stress-relieved models observed through the light field polariscope setup after post-curing

c. Model No. 3A

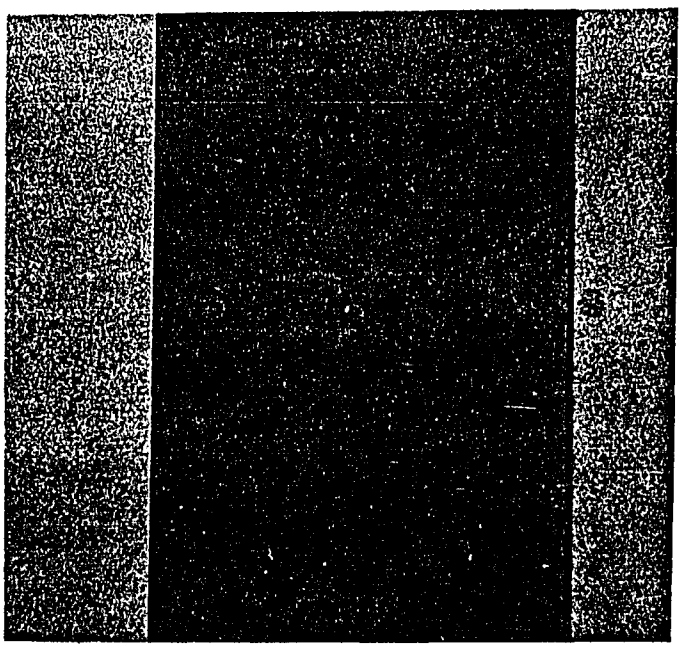

Figure 4-4. Continued.

B. Preliminary Work for Data Analysis

1. Calibration of the material fringe value

The material fringe constant, f_σ, for any particular model depends upon the degree of polymerization of the polymer. It can vary even for materials with the same chemical composition cured as identically as possible. It is, therefore, highly desirable that a calibration specimen accompany the model and undergo the same thermal treatment such as curing, post-curing and stress-freezing.

In this experiment, two calibration methods were used. The first calibration specimen was obtained from a circular disk loaded in diametral compression. For the center of the disk, the relation yielding f_σ is expressed as [99, p. 458]:

$$f_\sigma = \frac{8P}{\pi DN} \tag{4-1}$$

where

f_σ = material fringe value

P = applied load

D = disk diameter

N = fringe order at the center of the disk

For the calibration of the material fringe value from a live model, f_σ can be determined by plotting several points of P versus $(\pi D/8)N$ as shown in Figure 4-5. Since, from equation (4-1),

$$P = f_\sigma \left(\frac{\pi D}{8} N\right) \tag{4-2}$$

The slope of the line in Figure 4-5 is f_σ. By calculating the slope by linear regression using the least squares method, the uncertainty associated with a single value determination of N is removed.

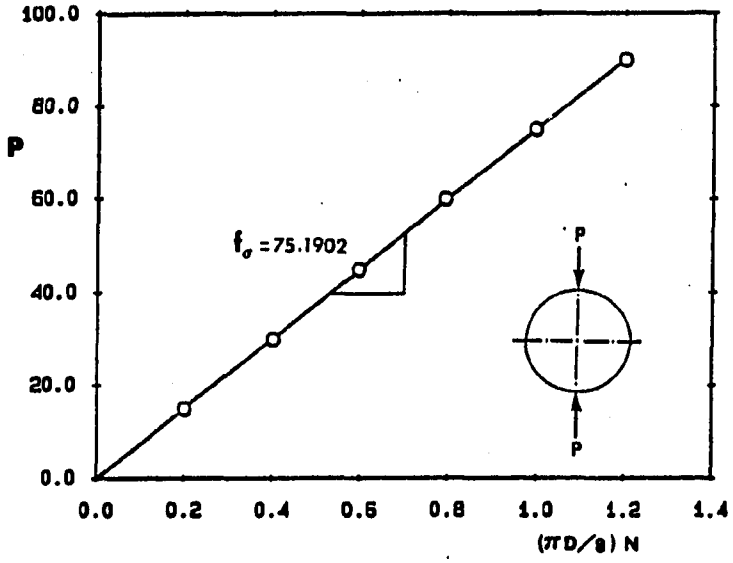

Measured Data

P (lb)	(πD/8)N (in-fringe)
0.	0.
14.967	0.201
29.934	0.400
44.901	0.595
59.868	0.791
74.835	0.994
89.802	1.198

Figure 4-5. Material fringe calculation from the plot of load (P) versus fringe value (N) at the center of the disk for Model No. 1A

The second calibration method uses the relationships for a uniaxial tensile specimen [101, p. 457]. Since a requirement for all the two-dimensional tests was the existence of a uniform stress across the plate in a region removed from the crack, this zone of uniaxial tensile stress could be used to calibrate the model without the need of a separate calibration specimen. The calibration is performed at the same time as the check to assure uniformity of load distribution along the cross section. For a uniaxial tensile load

$$f_\sigma = \frac{P}{W\,N} \qquad (4\text{-}3)$$

where N is the fringe order at the cross section of the uniform stress region.

2. Isochromatic fringes and processed images

Before testing any of the live models, they were loaded and viewed in white light in a circular polariscope. The uniformity of the far-field stress was checked visually to ensure uniform color across the cross section far from the crack tip.

Then the two-dimensional models were viewed live in a dark field circular polariscope. The applied stress at which the SIFs were determined, the material fringe value and the sizes of the circular disk used for calibration are given in Table 4-3. While Figure 4-6 shows the fringe patterns around the crack tip. These images were processed as described in the previous chapter. Figure 4-7 are the photographs of the sharpened images after application of program "TRACE". These photographs include an inner and an outer circle indicating inner and outer limits of the data acquisition zone.

Considering the root radius as half of the slot width, ρ=0.003 inch, a=0.375 inch and ρ/a=0.008. Then from Figure 3-2, $\tau_{max}(notch)/\tau_{max}(crack)$ approaches unity when $r/a>0.05$. This implies that data collection should be done at $r/a\geq 0.05$ to avoid errors from the finite thickness of the slot. As shown in each photograph of Figure 4-7, the range of r/a was specified when data were collected.

Multiplying the crack length (a) of the each model gives the actual data acquisition zone whose inner radius, r_i, and outer radius, r_o. These dimensions are shown in Figure 4-7. The "+" marks on these photographs are the cursor points where data were collected. The cursor was manually moved (with a joystick) to selected points on the sharpened fringes. The computer automatically recorded the coordinates of each point with respect to the crack tip, and the fringe order for the corresponding point was entered manually. Forty points were collected in this way.

The images are slightly distorted. These were caused by a misadjusted of the hard copy unit. There was no distortion in the actual image stored in the memory of the image processing system.

Table 4-3. Applied uniaxial tensile stress (σ) to the models and material fringe value (f_σ) obtained from the circular disk

Model No.[a]	σ[b] (psi)	f_σ (lb/in-fringe)	Disk Dia.(inch)xThick.(inch)
1A	511.150	75.190	1.760 x 0.125
2A	522.714	74.781	1.760 x 0.125
3A	594.990	74.935	1.762 X 0.125

[a]See Table 4-2 for model geometries.
[b]The stress σ=P/A, where P=applied load and A=gross cross section of the model.

a. Model No. 1A

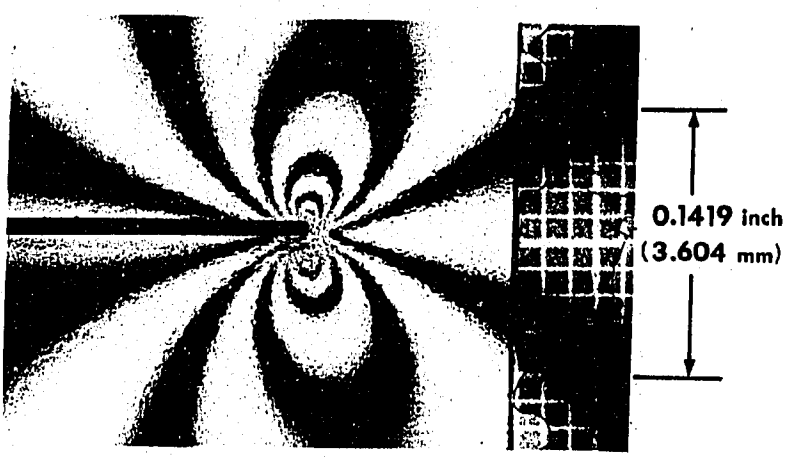

b. Model No. 2A

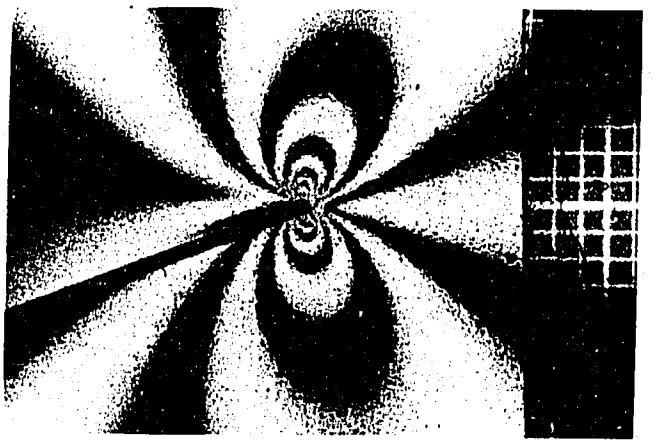

c. Model No. 3A

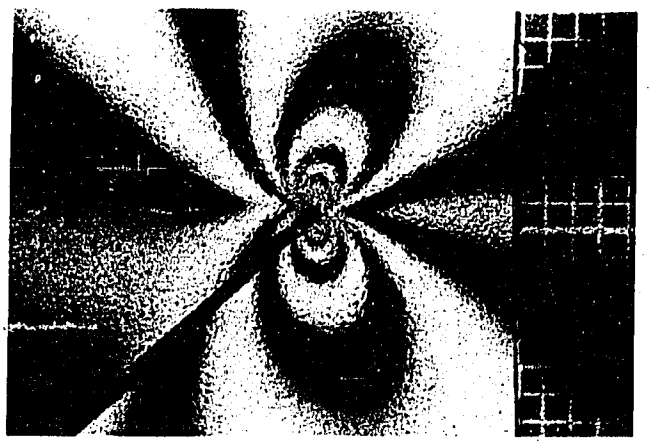

Figure 4-6. Isochromatic fringe loops in the vicinity of the crack tip

a. Model No. 1A

0.07<r/a<0.275

a=0.3757 inch

r_i=0.026 inch (r/a=0.07)

r_o=0.103 inch (r/a=0.275)

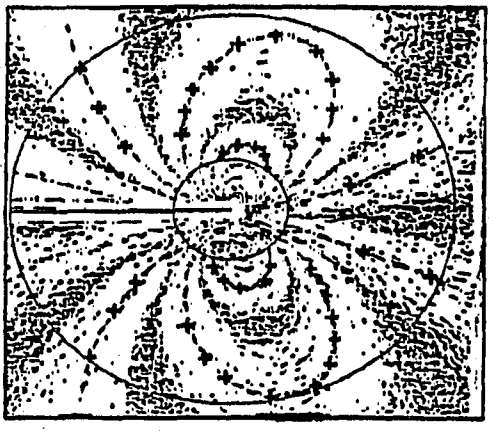

b. Model No. 2A

0.07<r/a<0.314

a=0.3744 inch

r_i=0.026 inch (r/a=0.07)

r_o=0.118 inch (r/a=0.314)

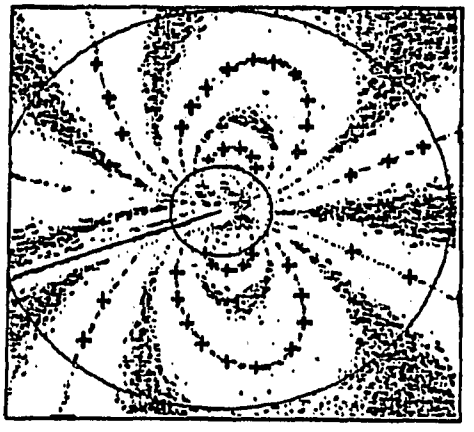

c. Model No. 3A

0.05<r/a<0.255

a=0.3698 inch

r_i=0.018 inch (r/a=0.05)

r_o=0.094 inch (r/a=0.255)

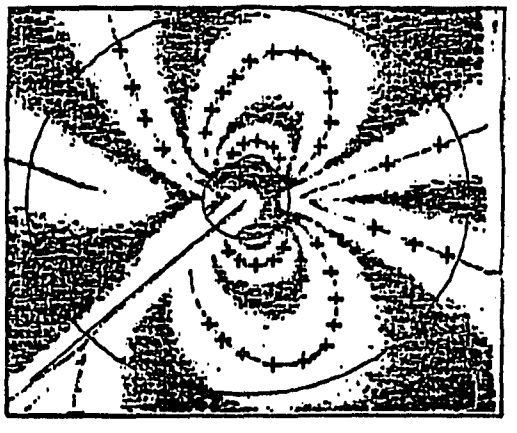

Figure 4-7. Fringe sharpened images and collected data locations from Figure 4-6

C. Data Analysis

1. Comparison between SIF results and statistical parameters obtained from arbitrary located crack tip origin and corrected one

For the SIF analysis from raw data collected on the fringe sharpened images shown in Figure 4-7, two sets of programs were developed. The first set, "TWIL1~6" [89], do not correct the crack tip origin and calculate the coefficients directly by the usual iterative least squares method [73,74]. The second set, "WIL1~6" [89], includes the statistical correction for the crack tip origin. They yield the fracture coefficients for equations (3-16) as well as the deviation of the crack tip from the estimated one.

To test these two sets of programs, Model No. 1A (Figure 4-6a and 4-7a) was chosen. The crack direction on the two faces of this model is slightly different from each other in this model (Table 4-2). This undesirable discrepancy of the crack occurred due to the warping of the thin slitting saw (thickness = 0.006 inch) when machining the slit. It is, therefore, very difficult to locate the crack tip accurately from the photoelastic image and the model is a good test for the effectiveness of the procedure that corrects the origin of the crack tip.

To compare the SIF results estimated by programs TWIL and WIL, the same data file collected from Model No. 1A (Figure 4-7a) was used. The SIF results and the statistical parameters calculated by both program sets are shown in Tables 4-4 and 4-5. For brevity, several symbols in Tables and Figures are used. The definitions of symbols are:

n = number of terms of Williams equations (see equations 3-16a,b,and c). Note that the number of fracture coefficients are 2 for n=1, 3 for n=2, 5 for n=3, and so on.

$K_{Io} = \sigma\sqrt{\pi a}$, normalizing stress intensity factor, where σ is the applied stress as measured from σ=P/A (P=applied load, A=gross cross section of the model, and "a" is the length of the edge crack).

$\bar{E}$ = mean of the percentage error defined by equation (3-36)

SD = standard deviation of the percentage errors defined by equation (3-37)

CC = correlation coefficient (ρ) defined by equation (3-38)

The results from Tables 4-4 and 4-5 are plotted on Figures 4-8a, b and c. It is clear from Figure 4-8a that K_I/K_{Io} obtained by program WIL converges to a value, K_I/K_{Io} =1.40, as the number of terms increases. This conclusion is not entirely supported by the plot of standard deviations (SD) in Figure 4-8b where SD tends to increase above 4 terms. This implies that K_I/K_{Io} starts to diverge when n>4 as shown in the back-plots in Figure 4-9. The variation of K_I/K_{Io} as calculated with TWIL programs, on the other hand, has a different tendency. It diverges when there are more than 4 terms. The statistical parameters are not as good as for the WIL programs. The standard deviations are higher and the correlation coefficient becomes lower. This implies that the iterative least squares procedures used to correct for the position of the crack tip can improve the accuracy of the results. When the crack tip location is ambiguous, any mislocation affects the results adversely and yields uncertain values for the fracture coefficients.

Using up to six terms of Williams equations, complete back-plots from the results obtained by programs TWIL and WIL are shown in Figure 4-9. Note that the inner radius (r_i) and outer radius (r_o) in the back-plots of Figure 4-9 were drawn to see where the collected data are located. These circles do not imply the data collection region. Actual data collection regions were limited to $0.07 \leq r/a \leq 0.30$ as shown in Figure 4-7. In Figure 4-9, back-plots from the results of WIL programs show two crack lines. The first one is drawn from the originally estimated crack tip while the line that has the loops attached to its tip is the corrected one. The best back-plot, whose SD value is also a minimum, was obtained for n=4 terms by the WIL4 program. For this plot, the regenerated fringes match the data points in the near, intermediate and far fields. This pretty well indicates the decision to include higher order terms in $\sqrt{r}$, in addition to the singularity terms ($1/\sqrt{r}$). In fact, the back-plot for n=1, i.e., when only the singularity terms are included in the analysis, is very poor.

For reference, typical computer outputs generated by programs WIL4 are listed in Figure 4-10. Note that the coefficient B_2 is always zero and is therefore not printed in the output. The symbol Sox stands for σ_{ox}, K1 for $K_I=\sqrt{2\pi}\ A(1)$ and K2 for $K_{II}=\sqrt{2\pi}\ B(1)$ according to equations (3-17a,b). The "BACK PLOT" printout is for 40 data points. The first two columns are the coordinates for the points as indicated by the cursor (under joystick control); the third column, the fringe order N entered by the operator for each point; the last two columns are computed by the program BPOW4 with n=4 in equations (3-34) and (3-35).

Table 4-4. Model No. 1A: SIF results and statistical parameters obtained by programs "WIL1-6"

n	K_I psi$\sqrt{in}$	K_{II} psi$\sqrt{in}$	K_I/K_{Io} [a]	K_{II}/K_I	$\bar{E}$ %	SD %	CC
1	889.764	4.408	1.602	0.005	-0.435	15.138	0.9683
2	773.610	3.078	1.393	0.004	0.482	3.382	0.9981
3	831.897	4.525	1.498	0.005	-0.447	4.693	0.9976
4	787.189	5.383	1.418	0.007	0.264	0.903	0.9998
5	787.668	5.059	1.418	0.006	0.091	1.038	0.9998
6	777.814	4.841	1.401	0.006	1.934	2.178	0.9987

[a] $K_{Io}=\sigma\sqrt{\pi a}$ =555.321 psi$\sqrt{in}$ (a=0.3757 inch, σ=511.150 psi).

Table 4-4. Continued.

n	Crack Tip Deviation (inch) [b]	
	x_o	y_o
1	-0.0058	-0.0040
2	-0.0022	-0.0038
3	-0.0022	-0.0037
4	-0.0015	-0.0037
5	-0.0016	-0.0035
6	-0.0013	-0.0035

[b] See Figure 3-3 for the coordinates of crack tip deviation.

Table 4-5. Model No. 1A: SIF results and statistical parameters obtained by programs "TWIL1-6"

n	K_I psi$\sqrt{in}$	K_{II} psi$\sqrt{in}$	K_I/K_{Io} [a]	K_{II}/K_I	$\bar{E}$ %	SD %	CC
1	898.611	3.575	1.618	0.004	-0.189	22.458	0.9194
2	734.262	4.884	1.322	0.007	1.632	5.634	0.9926
3	783.071	-1.094	1.410	-0.001	0.343	6.781	0.9922
4	775.086	10.359	1.396	0.013	0.636	5.703	0.9953
5	748.822	8.102	1.349	0.011	0.783	4.201	0.9976
6	676.481	7.285	1.218	0.002	-0.266	5.113	0.9970

[a] K_{Io}=555.321 psi$\sqrt{in}$ (a=0.3757 inch, σ=511.150 psi).

Results by programs WIL

Results by programs TWIL

a. K_I/K_{Io} Variation

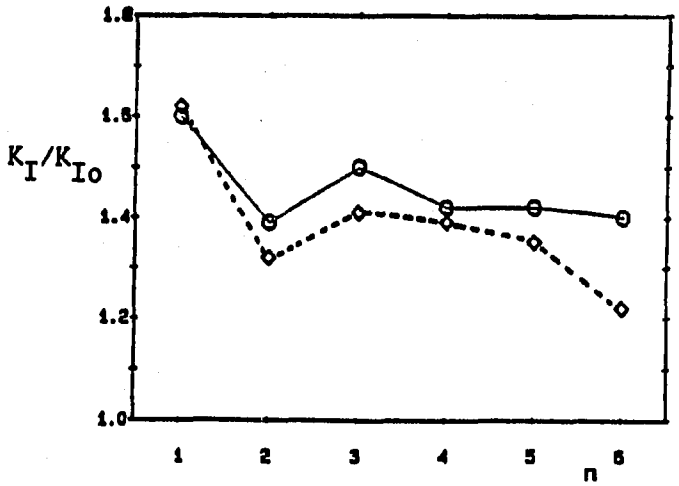

b. Standard Deviation

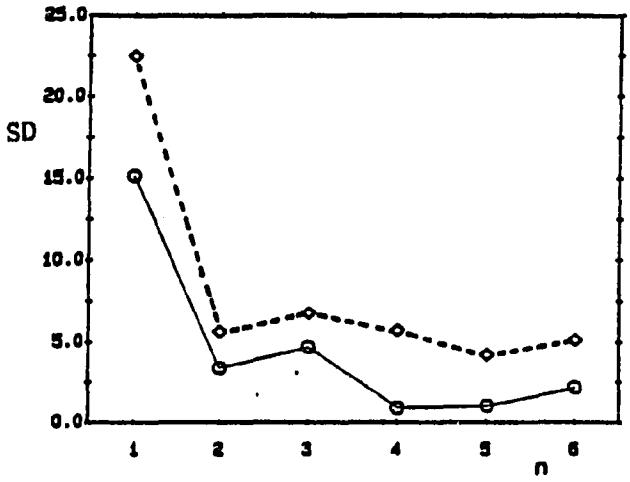

c. Correlation Coefficient

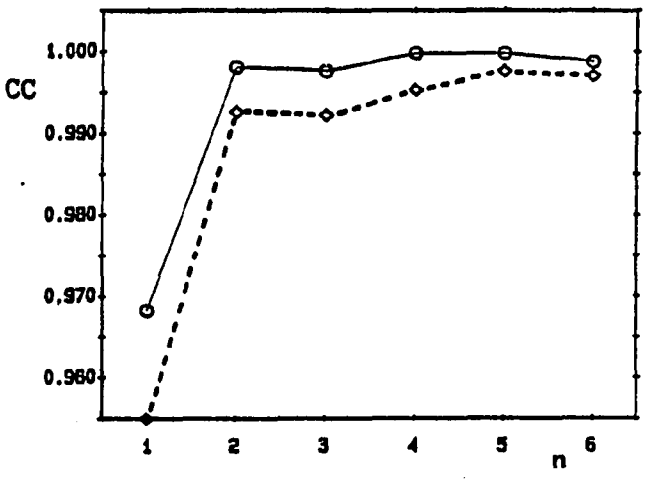

Figure 4-8. Model No. 1A: Comparison between the results obtained by programs TWIL and WIL

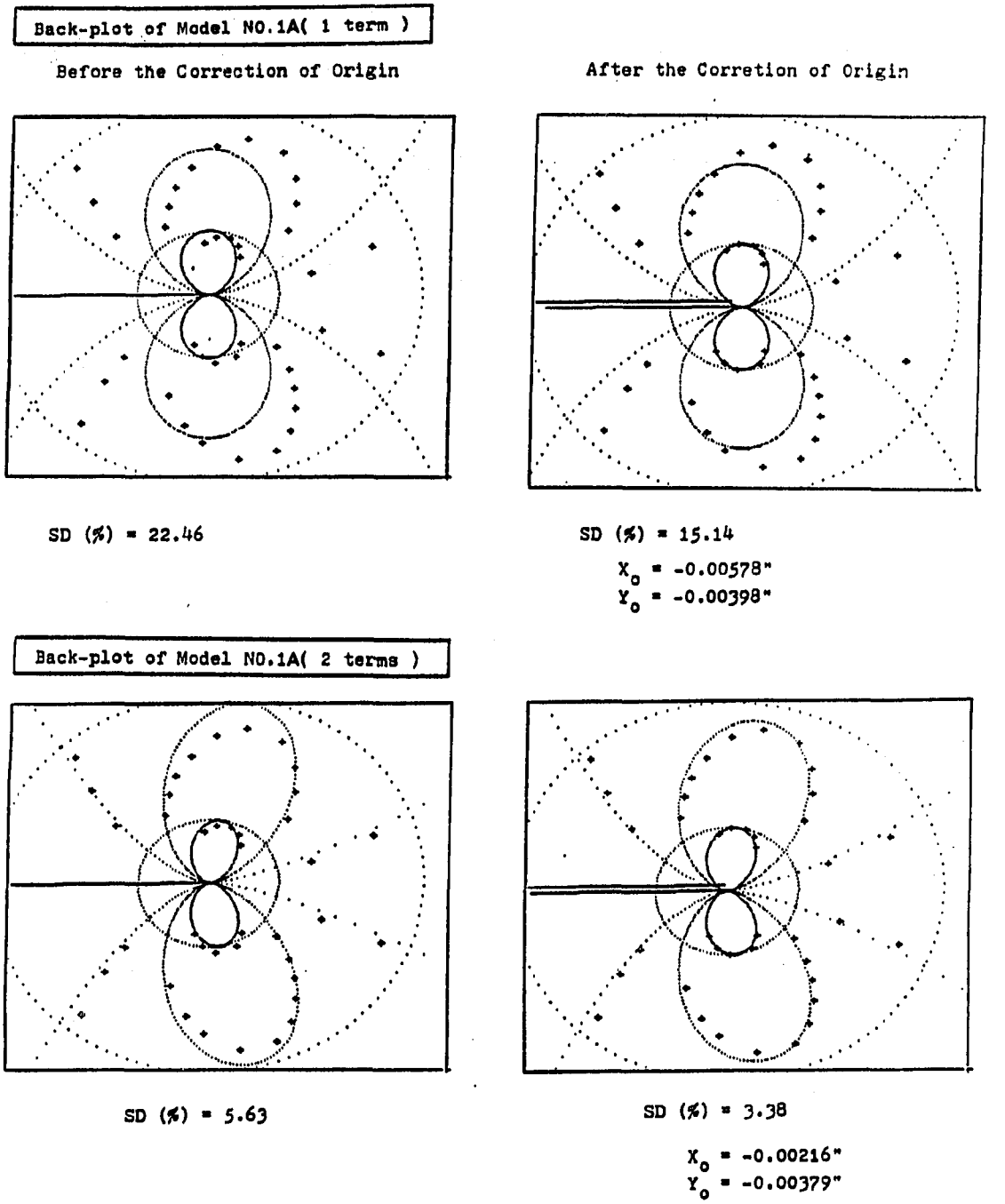

Figure 4-9. Model No. 1A: Comparison between the back-plots drawn by the results calculated by programs TWIL and WIL (r_i=0.0376 inch (0.954 mm) for inner circle and r_o=0.1127 inch (2.863 mm) for outer circle)

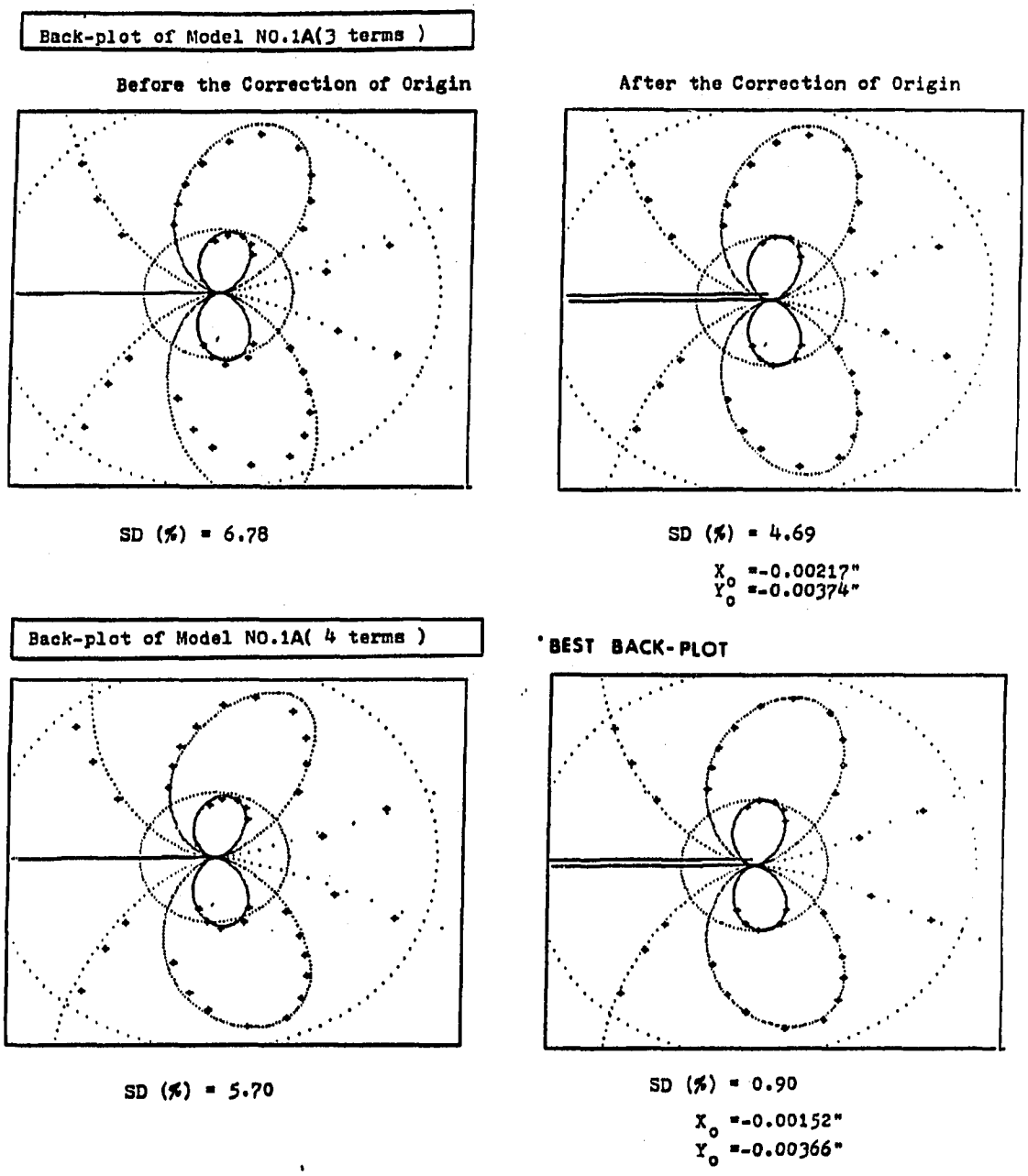

Figure 4-9. Continued

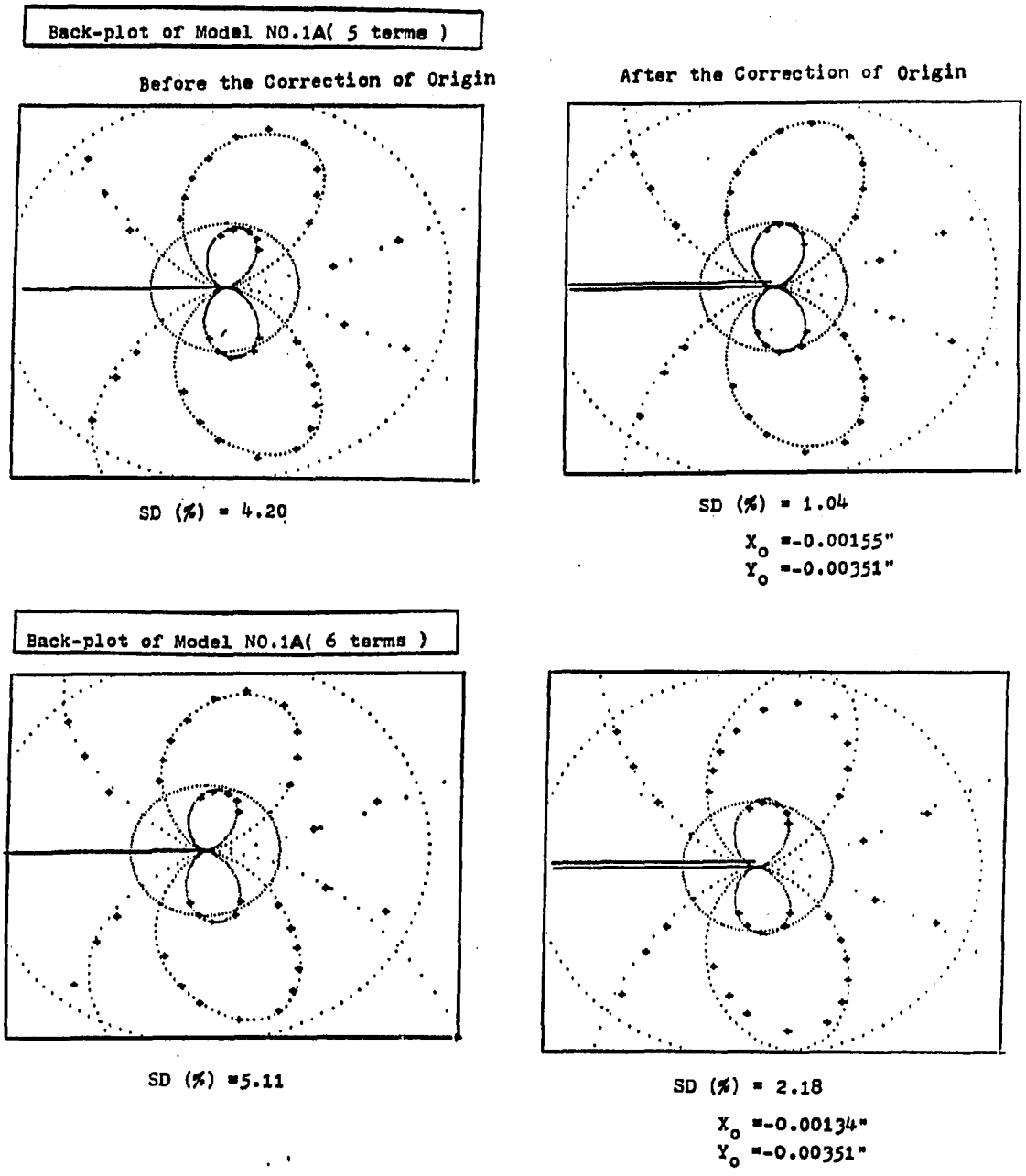

Figure 4-9. Continued

```
SIF ANALYSIS PROGRAM : WIL4
---------------------------

[ MODEL SPECIFICATION      ]

  THICKNESS OF MODEL(inch)----------------------      0.1230
  MATERIAL FRINGE VALUE(lb/Fr-in)---------------     75.1902
  CRACK LENGTH(inch)----------------------------      0.3757

[ CALCULATED COEFFICIENTS  ]

  A( 1) =      314.0430
  B( 1) =        2.1476
  A( 2) =      -75.6140
  A( 3) =       50.2532
  B( 3) =       -1.1892
  A( 4) =      -65.1760
  B( 4) =       12.6222

[ STRESS INTENSITY FACTORS ]

  K 1   =      787.1890
  K 2   =        5.3833
  Sox   =      302.4561

[ DEVIATION OF CRACK TIP   ]

  X o   =       -0.00152
  Y o   =       -0.00356


[ DEVIATION TABLE ]

Number of Data Point--------------------------------   40.0000
Average Deviation between Nexp & Nres in Percent--      0.2639
Variance between Nexp & Nres in Percent-------------    0.8161
Standard Deviation of Percentage error--------------    0.9034

Correlation between Nexp & Nres---------------------    0.9998
```

Figure 4-10. Model No. 1A: Computer outputs of SIF analysis results generated by the program WIL4

BACK PLOT PROGRAM ; BPOW4

[INPUT DATA TABLE]

NO	R-DIST	THETA	N(exp)	N(res)	% ERROR
1	0.03449	-97.70	3.0000	2.9986	-0.05
2	0.03757	-86.66	3.0000	2.9976	-0.08
3	0.03778	-74.78	3.0000	2.9797	-0.68
4	0.03509	-66.06	3.0000	2.9702	-0.99
5	0.02989	-59.55	3.0000	3.0332	1.11
6	0.02796	109.97	3.0000	3.0066	0.22
7	0.03399	98.91	3.0000	2.9921	-0.26
8	0.03757	87.01	3.0000	2.9998	-0.01
9	0.03640	68.04	3.0000	2.9781	-0.73
10	0.03061	58.26	3.0000	3.0061	0.20
11	0.05058	-119.44	2.0000	2.0033	0.17
12	0.06059	-112.11	2.0000	2.0134	0.67
13	0.06995	-106.03	2.0000	2.0006	0.03
14	0.07980	-98.28	2.0000	2.0079	0.40
15	0.09125	-88.61	2.0000	1.9971	-0.15
16	0.09725	-78.91	2.0000	2.0027	0.13
17	0.09476	-66.69	2.0000	2.0061	0.31
18	0.08400	-58.31	2.0000	2.0103	0.51
19	0.07226	-52.01	2.0000	2.0077	0.39
20	0.05762	-45.39	2.0000	2.0036	0.18
21	0.04488	38.84	2.0000	2.0035	0.17
22	0.05896	45.10	2.0000	2.0073	0.36
23	0.06909	50.00	2.0000	2.0149	0.74
24	0.07923	55.16	2.0000	2.0144	0.72
25	0.08943	61.47	2.0000	2.0081	0.41
26	0.09724	68.69	2.0000	1.9939	-0.31
27	0.09697	80.83	2.0000	1.9889	-0.55
28	0.08551	93.21	2.0000	1.9983	-0.08
29	0.07592	100.53	2.0000	2.0082	0.41
30	0.06075	111.17	2.0000	2.0185	0.93
31	0.06326	-143.08	1.0000	1.0132	1.32
32	0.08623	-136.89	1.0000	1.0159	1.59
33	0.10676	-132.38	1.0000	0.9988	-0.12
34	0.05695	143.74	1.0000	1.0211	2.11
35	0.07399	139.45	1.0000	1.0103	1.03
36	0.09894	132.94	1.0000	1.0113	1.13
37	0.05510	-16.59	1.0000	0.9671	-3.29
38	0.09034	-20.01	1.0000	0.9962	-0.38
39	0.06167	17.64	1.0000	1.0209	2.09
40	0.09535	19.95	1.0000	1.0091	0.91

Figure 4-10. Continued.

2. Comparison between back-plots for pure Mode I and Mixed Mode

In order to discuss on differences between pure Mode I and Mixed Mode cases, the data sets shown in Figure 4-7 were used to compute SIFs and the statistical parameters with programs WIL1~6. The results for Model Nos. 2A and 3A are tabulated in Tables 4-6 and 4-7, respectively.

Since standard deviation (SD) is closely related to quality of fit between the data points and regenerated fringes, plots for the variation of SD with respect to number of terms of the Williams equations from Tables 4-4, 4-6 and 4-7 are given in Figure 4-11.

In all cases the standard deviation for n=1 is high. However, for Model No. 1A, which is almost a pure Mode I case, the standard deviation for two terms, n=2, is already below 5 percent, which is an acceptable level. This is not the case for the Mixed Mode models where there is not much difference between the SD values for one term, n=1, and two terms, n=2.

The discussions of the Williams equations in Section 2 of Chapter III-A pointed out that the one term Williams equations (n=1) are identical to the Westergaard equations (2-3). The first two terms of Williams equations are the same as the modified Westergaard equations (2-4). For pure Mode I, the two terms solution is acceptable. That is not so for Mixed Mode Problems. Notice that the data collection region was within r/a=0.07~0.30 for Model Nos. 1A and 2A, and r/a=0.07~0.25 for Model No. 3A as shown in Figure 4-7.

These two sets of the equations, i.e., the Westergaard and the modified Westergaard have been widely used in experimental studies of

fracture parameters for pure Mode I, Mode II and Mixed Mode conditions. The plots in Figure 4-11, however, show that there are significant differences between pure Mode I and Mixed Mode in the number of terms appropriate in the equations. It is clear that the Westergaard equations, which are equivalent to n=1, are inadequate even for pure Mode I. The modified Westergaard equations, which are equivalent to n=2, are barely adequate for pure Mode I (Model No. 1A) but inadequate for Mixed Mode problems (Model Nos. 2A and 3A). Mixed Mode cases require more terms in the equations. In the modified Westergaard equations (2-4), the role of σ_{ox} may be an important factor for improving the accuracy of the results in pure Mode I. Figure 4-11a confirms this conclusion because the standard deviation decreases sharply from n=1 to n=2. The significance of σ_{ox} in the Mixed Mode cases, which require higher order terms, cannot be observed. In Figures 4-11b and c from Mixed Mode conditions, the standard deviation decreases only a little from n=1 to n=2.

The statistical improvement caused by an increase in the number of terms is obvious from Figure 4-11. Standard deviations continuously decrease until 4 terms of the equations are used. For n>4, the SDs increase for all three models (Model Nos. 1A, 2A and 3A). SD values were minimum when 4 terms were used. So, even though data were collected fairly close to the crack tip (r/a<0.3; r<0.12 inch), higher order terms are needed for reliable determination of Mixed Mode SIFs.

To show the physical effect of the number of terms of the equations, and to explain the differences between pure Mode I and Mixed

Mode cases, complete back-plots, using the results of fracture coefficients obtained from the analyses with from one to six terms, were drawn for Model Nos. 1A and 3A in Figure 4-12. As expected, the test with the minimum standard deviation yields the best back-plot. There is excellent agreement between the data points and back-plot fringes over the whole data collection region when four terms of the equations are used. It reinforces the claim n=4 was the optimum number of terms for the analyses performed here.

Table 4-6. Model No. 2A: SIF results and statistical parameters obtained by programs "WIL1~6"

n	K_I psi$\sqrt{in}$	K_{II} psi$\sqrt{in}$	K_I/K_{Io} [a]	K_{II}/K_I	$\bar{E}$ %	SD %	CC
1	795.476	-160.132	1.403	0.203	-1.562	15.088	0.9725
2	748.589	-171.962	1.301	0.230	-0.477	12.369	0.9803
3	749.757	-168.572	1.323	0.225	-0.445	3.026	0.9989
4	730.752	-169.372	1.289	0.232	0.111	1.303	0.9997
5	732.293	-168.064	1.292	0.230	0.705	1.961	0.9994

[a] $K_{Io}=\sigma\sqrt{\pi a}$=566.901 psi$\sqrt{in}$ (a=0.3744 inch, σ=522.714 psi).

Table 4-7. Model No. 3A: SIF results and statistical parameters obtained by programs "WIL1~6"

n	K_I psi$\sqrt{in}$	K_{II} psi$\sqrt{in}$	K_I/K_{Io} [a]	K_{II}/K_I	$\bar{E}$ %	SD %	CC
1	512.595	-289.052	0.799	0.564	-0.545	15.897	0.9659
2	548.822	-276.702	0.856	0.504	-2.355	13.532	0.9764
3	549.255	-271.677	0.857	0.495	-0.333	2.300	0.9993
4	545.860	-269.778	0.851	0.494	0.015	1.447	0.9996
5	551.248	-267.390	0.860	0.485	1.039	2.001	0.9994
6	555.034	-266.054	0.866	0.479	2.574	4.128	0.9979

[a] $K_{Io}=\sigma\sqrt{\pi a}$=641.310 psi$\sqrt{in}$ (a=0.3698 inch, σ=594.990 psi).

a. Model No. 1A
(β=-0.5°~1.5°)

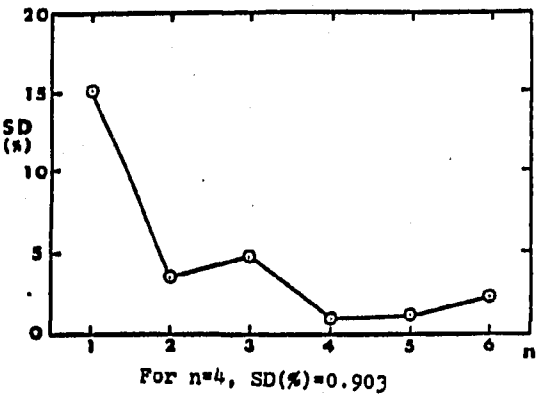

For n=4, SD(%)=0.903

b. Model No. 2A
(β=22.5°)

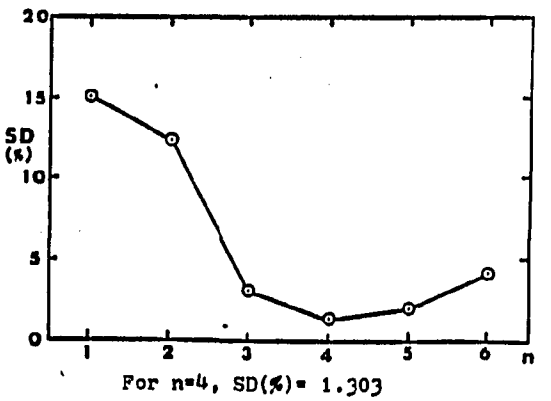

For n=4, SD(%)= 1.303

c. Model No. 3A
(β=44.5°)

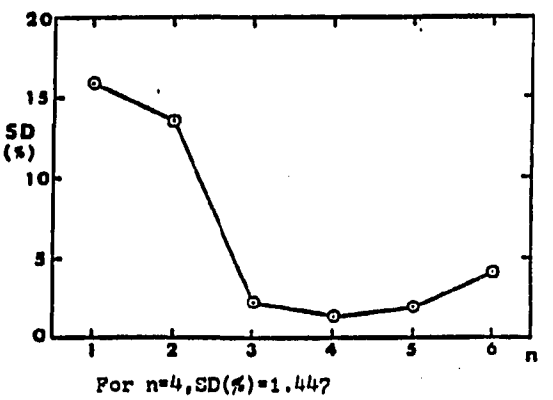

For n=4,SD(%)=1.447

Figure 4-11. Model Nos. 1A, 2A and 3A: Variation of standard deviation with respect to the number of terms of Williams equations

Model No. 1A (β=-0.5°~1.5°)

r_i=0.0376 inch

r_o=0.1127 inch

Model No. 3A (β=44.5°)

r_i=0.0185 inch

r_o=0.0925 inch

a1. 1 term (n=1); SD(%)=15.14

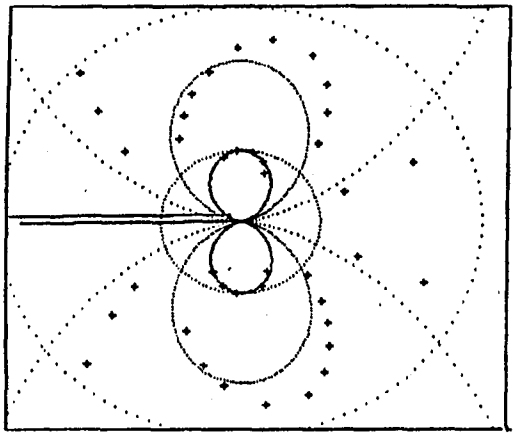

a2. 1 term (n=1); SD(%)=15.90

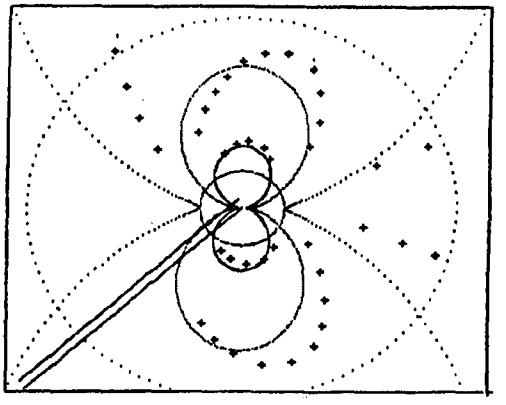

b1. 2 terms (n=2); SD(%)=3.98

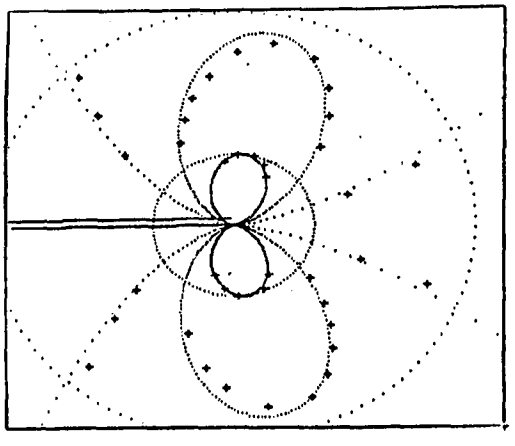

b2. 2 terms (n=2); SD(%)=13.53

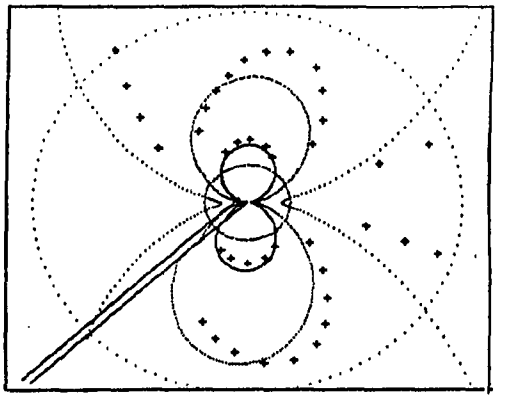

Figure 4-12. Model Nos. 1A and 3A: Comparison between the back-plots for pure Mode I and Mixed Mode

Model No. 1A (β=-0.5°~1.5°)

r_i=0.0376 inch

r_o=0.1127 inch

c1. 3 terms (n=3); SD(%)=4.69

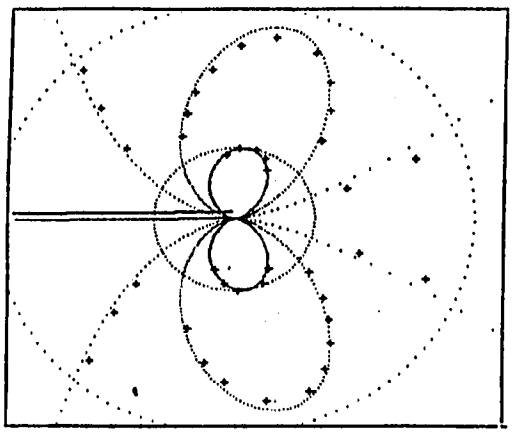

d1. 4 terms (n=4); SD(%)=0.90

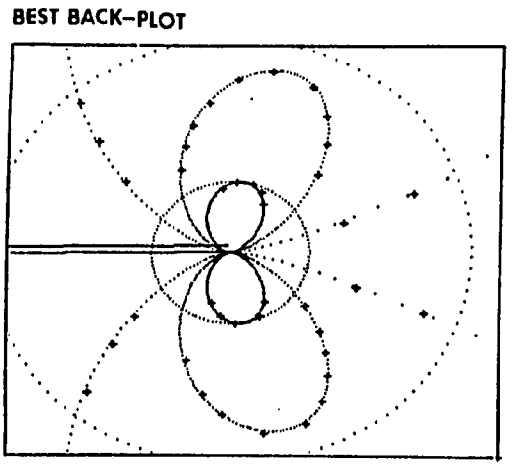

Model No. No. 3A (β=44.5°)

r_i=0.0185 inch

r_o=0.0925 inch

c2. 3 terms (n=3); SD(%)=2.30

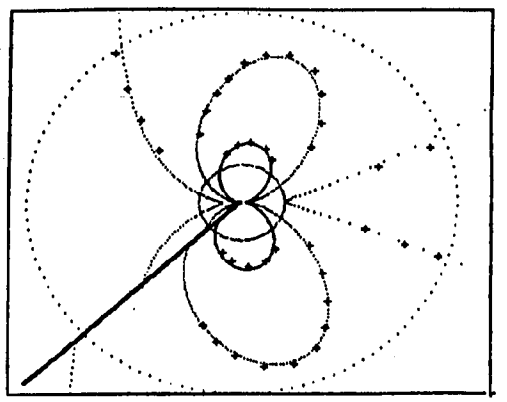

d2. 4 terms (n=4); SD(%)=1.45

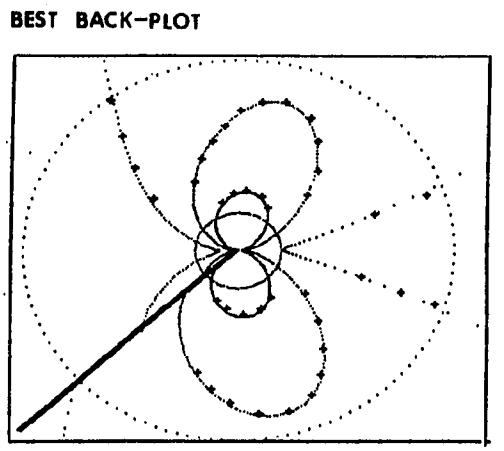

Figure 4-12. Continued

Model No. 1A (β=-0.5°~1.5°)

r_i=0.0376 inch

r_o=0.1127 inch

e1. 5 terms (n=5); SD(%)=1.04

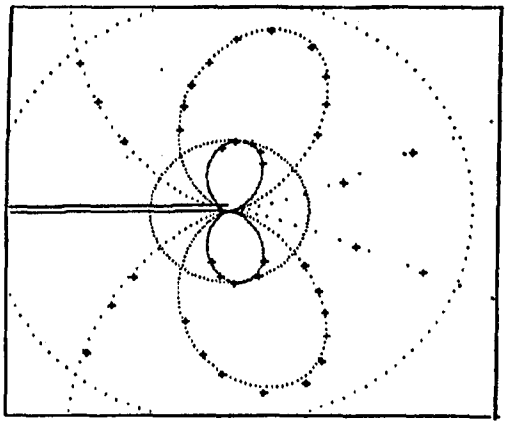

Model No. 3A (β=44.5°)

r_i=0.0185 inch

r_o=0.0925 inch

e2. 5 terms (n=5); SD(%)=2.00

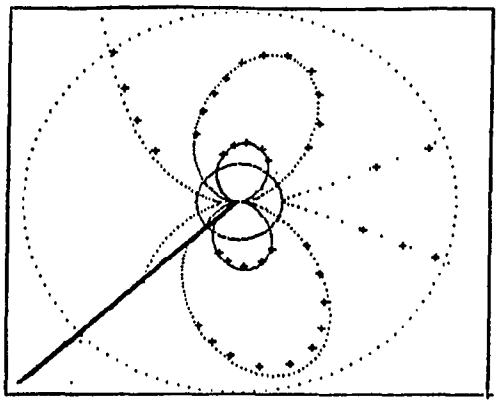

f1. 6 terms (n=6); SD(%)=2.18

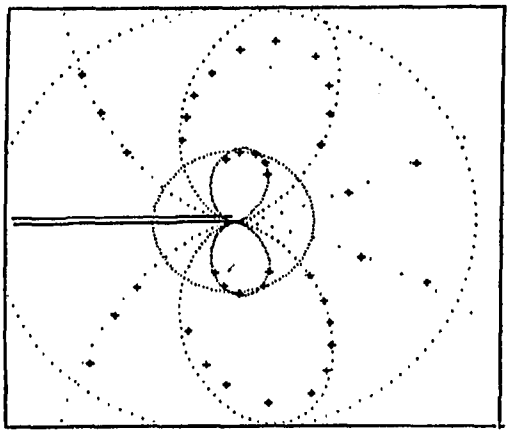

f2. 6 terms (n=6); SD(%)=4.13

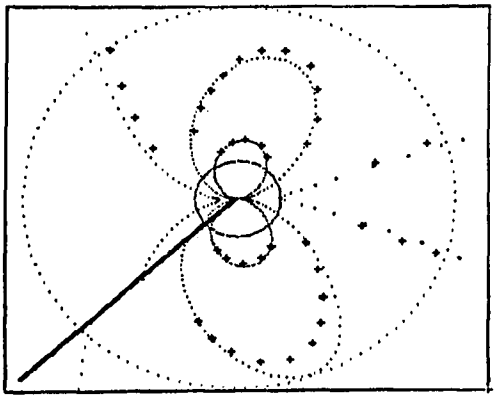

Figure 4-12. Continued

a. Model No. 1A

(β=-0.5°~1.5°)

a =0.3757 inch

r_i=0.0376 inch

r_o=0.1127 inch

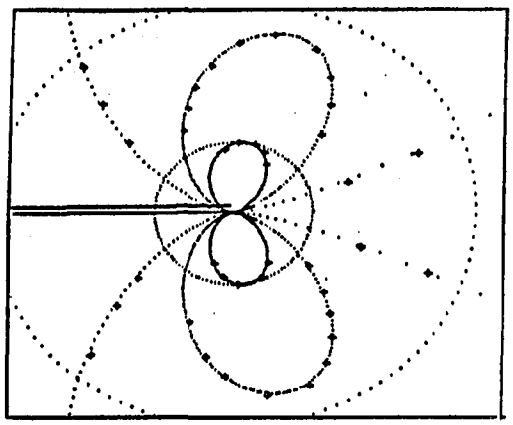

b. Model No. 2A

(β=22.5°)

a =0.3744 inch

r_i=0.0374 inch

r_o=0.1123 inch

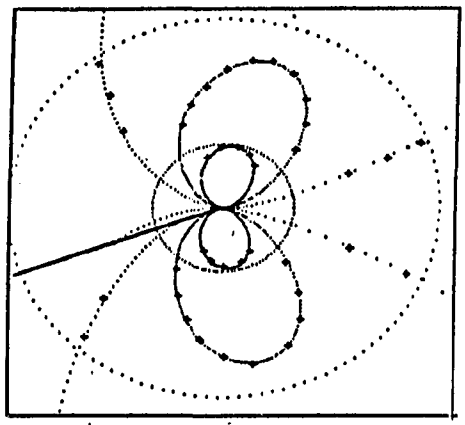

c. Model No. 3A

(β=44.5°)

a =0.3698 inch

r_i=0.0185 inch

r_o=0.0925 inch

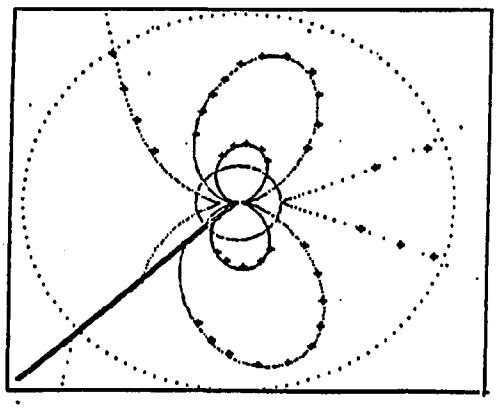

Figure 4-13. Model Nos. 1A, 2A and 3A: Best back-plots drawn by using the results obtained by four terms of Williams equations

3. Load tests on live models

Commonly, the nondimensional normalized Mode I stress intensity factor, K_I/K_{Io} (where $K_{Io}=\sigma\sqrt{\pi a}$), is used to express geometrical or functional relationships of K_I. For example, $K_I=f(a/W)\sigma\sqrt{\pi a}$ so that $K_I/K_{Io}=f(a/W)$.

The purpose of the next set of tests was to find out whether or not the normalizing stress intensity factor, K_{Io}, is a proportional constant, that is, whether the ratio K_{II}/K_I remains constant for the same geometry under different loads. An additional objective was to check the repeatability of data analysis from different data sets produced by different loads.

For this study, another set of models with inclined through-thickness edge cracks were made. The previous model sets (Model Nos. 1A, 2A and 3A) were accidently broken when too much load was applied to them during stress-freezing. The new model geometries were the same as in Figure 4-3, but the slitting saw was now 0.008 inch (0.203 mm) thick rather than 0.006 inch (0.152 mm). This slitting saw cut a straighter slit because it did not warp. The dimensions of the plates after final machining are shown in Table 4-8. The material fringe value (f_σ) in Table 4-8 was measured by the least squares slope method from a disk in compression (Equation (4-2) and Figure 4-5). Since all these three models were machined from the same cast plate, the material fringe value is the same for all of them.

Three different loads were applied to each model, and Figure 4-14 shows the variation of isochromatic fringe loops in the vicinity of the crack tip for three models. The magnitudes of the loads were selected

to produce more than two fringes (N>2) at the crack but low enough not to fracture the model or lead to a large nonlinear zone around the crack tip.

Table 4-8. Dimensions[a] of two-dimensional cracked models for load tests and stress-freeing

Model No.	β^o	a (inch)	W (inch)	t (inch)	2H (inch)	d (inch)	f_σ (lb/in-fringe)
1B	0	0.3716	1.872	0.2049	8.81	0.0085	74.4224
2B	22.5	0.3694	1.880	0.1943	8.78	0.0087	74.4224
3B	45	0.3694	1.870	0.1699	8.75	0.0084	74.4224

[a]See Figure 4-3 for the symbols.

The analysis procedures were the same as in the previous sections. The best results, that is the minimum standard deviations were again obtained when four terms of the Williams equations were used for all cases. Data collection for all three models were within the range $0.07 \leq r/a \leq 0.35$. Fracture parameters, normalized stress intensity factors (K_I/K_{Io}), ratios of K_{II}/K_I, mean of the percentage error ($\bar{E}$) and standard deviation (SD) obtained by four terms of the equations or program WIL4, are tabulated in Table 4-9.

It is evident that the normalized stress intensity factors (K_I/K_{Io}) and ratios of K_{II}/K_I are relatively consistent for the different loads. The maximum variation of K_I/K_{Io} for Model No. 3B is 4.6 percent and that of K_{II}/K_I for the same model is 6.2 percent. These results are included with some other outputs in Table 4-13, and on Figures 4-19 and 4-20 later in this chapter.

Table 4-9. Load test results obtained by program WIL4

Model No.	σ (psi)	K_I (psi$\sqrt{in}$)	K_{II} (psi$\sqrt{in}$)	K_I/K_{Io} [a]	K_{II}/K_I	$\bar{E}$ (%)	SD (%)
	312.229	474.370	1.303	1.406	0.003	0.311	1.244
1B	351.257	533.555	-4.070	1.406	-0.009	0.619	1.899
	390.286	594.143	0.168	1.409	0.000	0.512	2.006
	327.808	453.537	92.975	1.284	0.205	0.463	2.190
2B	368.785	506.032	108.593	1.274	0.215	0.754	2.366
	409.761	547.593	120.733	1.241	0.220	0.346	1.849
	471.013	430.694	221.483	0.849	0.514	-0.094	1.594
3B	518.115	465.036	244.022	0.833	0.525	0.086	1.480
	565.216	494.395	269.795	0.812	0.546	0.071	1.345

[a] $K_{Io} = \sigma\sqrt{\pi a}$, where a=0.3716 inch for Model No. 1B, a=0.3694 inch for Model Nos. 2B and No. 3B

a. Model No. 1B

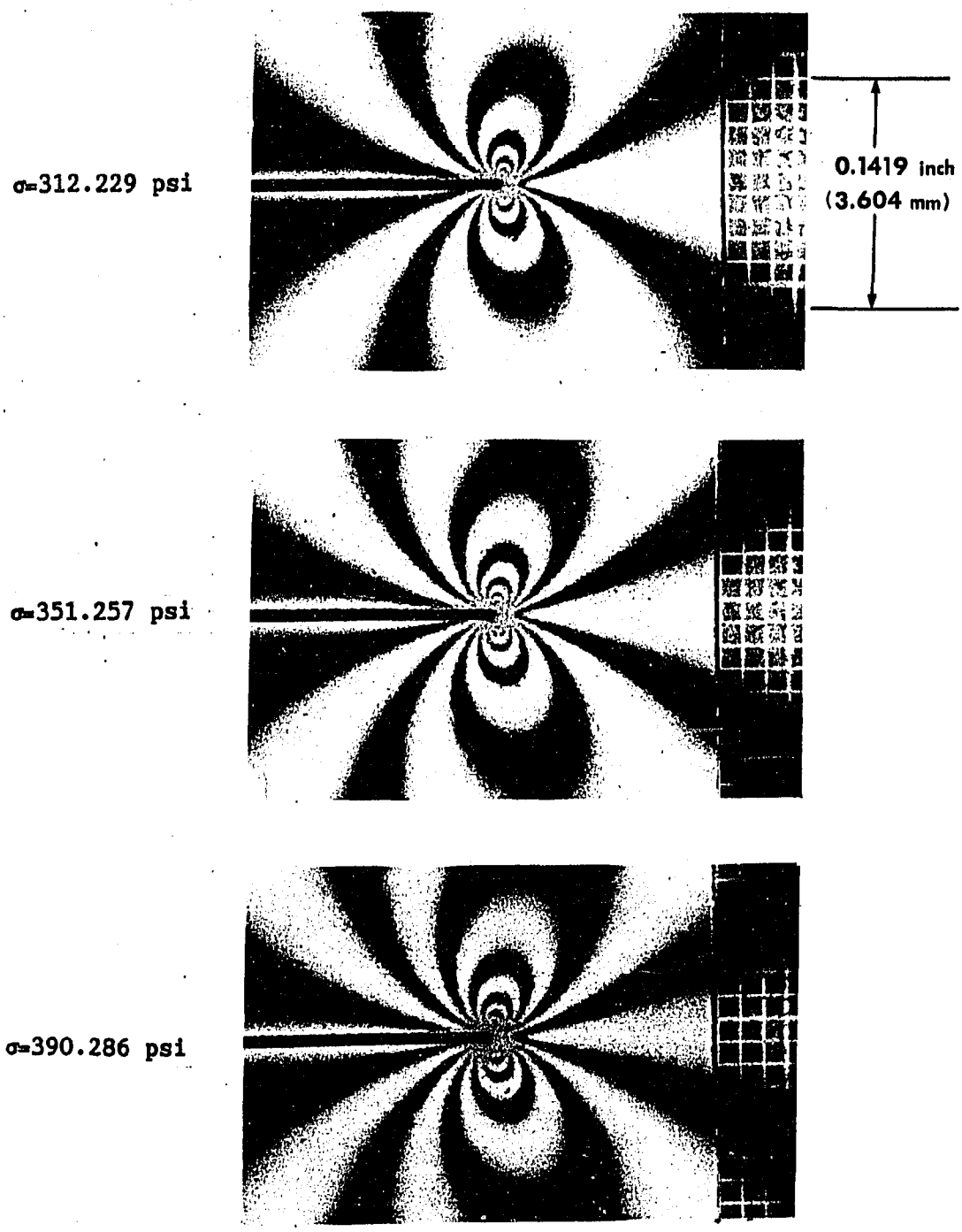

Figure 4-14. Variation of isochromatic fringe loops in the vicinity of the crack tip due to load change

b. Model No. 2B

σ=327.808 psi

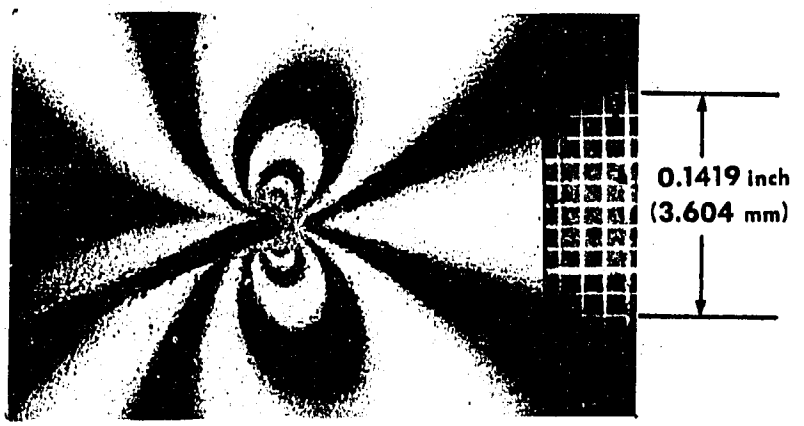

σ=368.785 psi

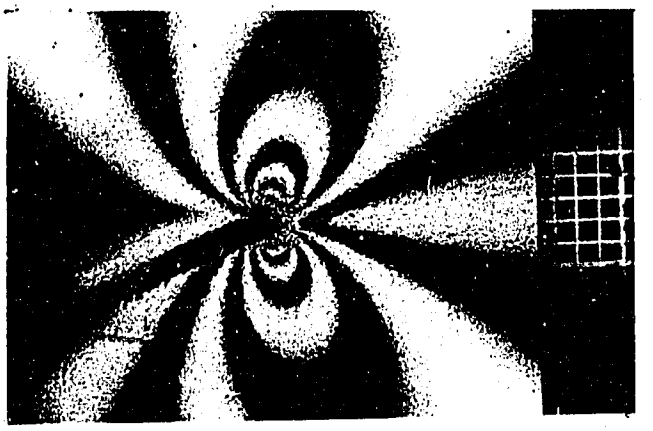

σ=409.761 psi

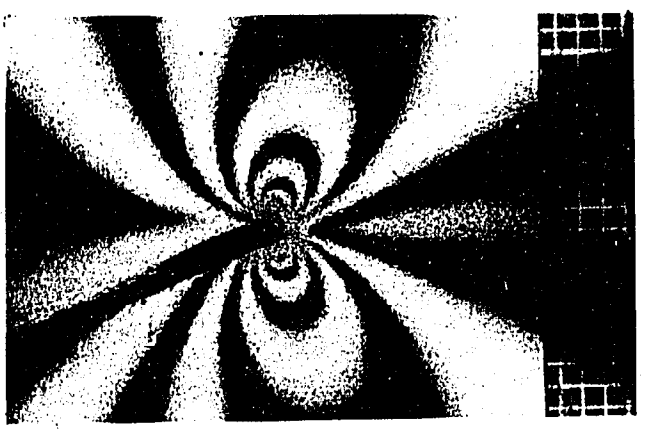

Figure 4-14. Continued

c. Model No. 3B

σ=471.013 psi

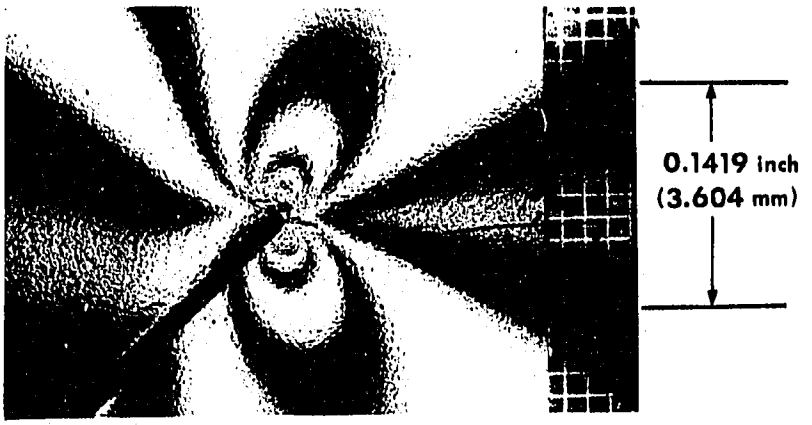

σ=518.115 psi

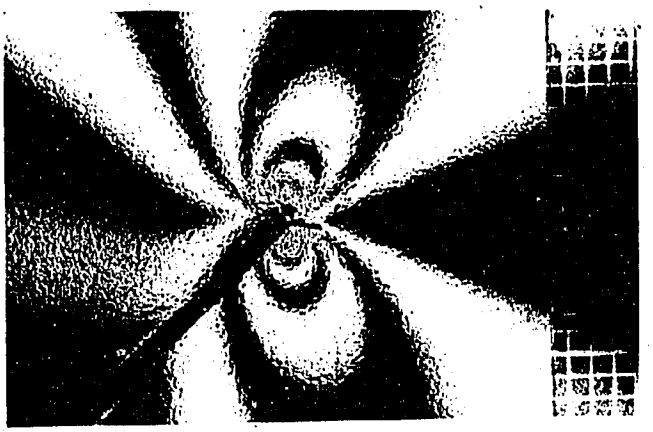

σ=565.216 psi

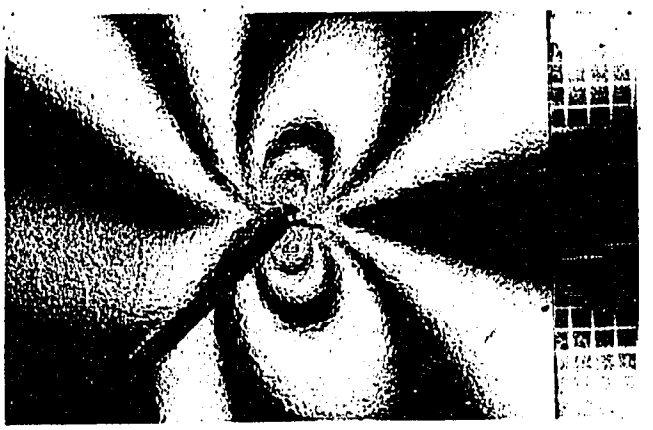

Figure 4-14. Continued

4. Analysis from frozen-stress models

Photoelastic analysis can be done not only from live models but also from frozen-stress models. The main purpose of stress-freezing is for three-dimensional photoelasticity. This technique is possibly the most powerful method in experimental stress analysis because, with it, the stresses at the interior points of a three-dimensional body can be determined by analyzing thin slices cut from the frozen-stress models [100, 101, 102]. However, materials used for three-dimensional photoelasticity by stress-freezing are thermo-setting polymers that experience a sudden change in mechanical and optical properties above their glass transition temperature. Around this temperature, the thermodynamic conformance of the polymer changes from glass-like to rubber-like with a commensurable drop in elastic modulus and an increase in Poisson's ratio. For instance, Table 4-10 shows that the material properties of the 3DMU-050 photoelastic material used in these experiments are very different between those at room temperature and at the critical stress-freezing temperature.

The main objective of using stress-freezing on two-dimensional models is to compare SIFs obtained from live models with those from frozen-stress ones to see if the notable change in material properties will affect the results. For these tests, the same models (Model Nos. 1B, 2B and 3B) in Table 4-8 were used. Stress-freezing of the models and the calibration disk was done in a programmable oven according to the procedures described in Figure 4-2. Figure 4-15 shows the colored fringes of Model No. 1B after stress-freezing, and the frozen-stress circular disk with diametral compression is shown in Figure 4-16.

To calibrate the material fringe value for each model, two methods were used. The first method followed equation (4-1) by reading the fringe order at the center of frozen-stress disk. In order to reduce reading errors in measurement, the fringe order at the center was read five times by Tardy compensation and average value from them was calculated.

Table 4-10. Material properties of 3DMU-050 photoelastic material at room temperature and at critical temperature

Properties	at room temperature[a] (70 ^{o}F)	at critical temperature[b] (275 ^{o}F)
Tensile strength (psi)	10,000	205~220
Young's modulus (psi)	$4.5x10^5$~$5.0x10^5$	2900~3200
Material fringe value (lb/in-fringe)	74 ~76[c]	2.15~2.20
Poisson's ratio	0.33 ~0.37	0.50

[a]Material properties at room temperature are roughly estimated from reference [93].
[b]See Table 4-1 for other properties.
[c]Ranges of material fringe values were obtained from tests conducted for this dissertation.

The second one depended on equation (4-3) by reading fringe values along the cross section in the uniform stress region of the frozen-stress models. Figure 4-17 shows an example of the material fringe value calibration by this method. Note that, from Figure 4-15 and 4-17, uniformity of the applied stress away from the crack tip (far field stress) was achieved.

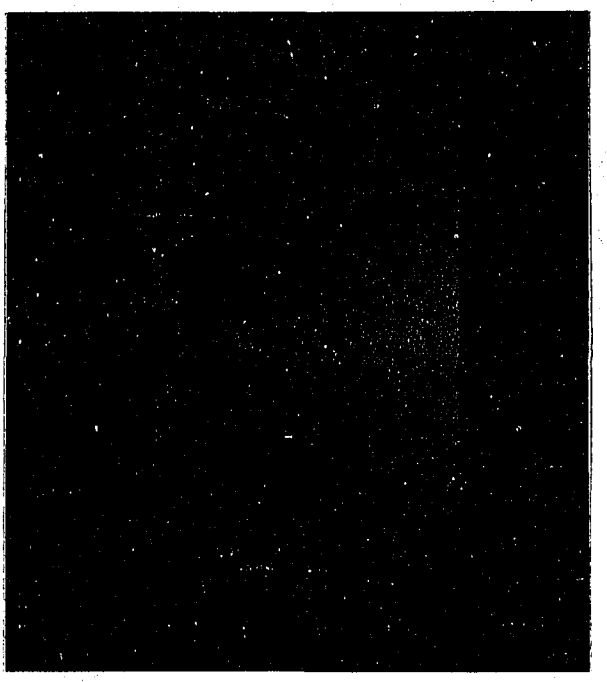

Figure 4-15. Colored fringes of Model No. 1B after stress-freezing (dark field polariscope setup)

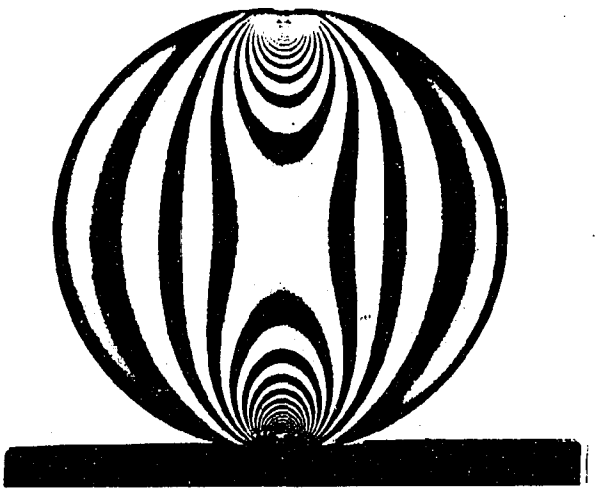

Figure 4-16. Frozen-stress calibration disk (light field polariscope setup)

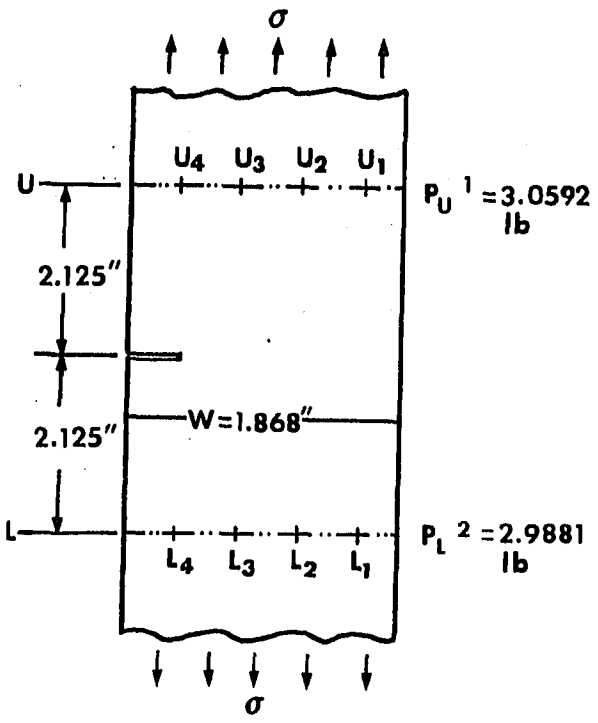

Location	N^3	N_{avg} 4	f_σ 5
U_1	0.7426		
U_2	0.7532		
U_3	0.7556		
U_4	0.7610	0.7531	2.1748
L_1	0.7444		
L_2	0.7315		
L_3	0.7426		
L_4	0.7506	0.7423	2.1550

[1] P_U = Applied load at upper cross section
= P_L + weight of model between L and U.

[2] P_L = Applied load at lower cross section.

[3] N = Fringe order at the designated location.

[4] N_{avg} = Average fringe order along cross section.

[5] f_σ = Material fringe value (lb/in-fringe) calculated by equation (4-3).

Figure 4-17. Model No. 1B: Material fringe value calibration from the uniform stress region

Material fringe value calibrated by above two methods are tabulated in Table 4-11 for the models used in these tests.

As for the frozen-stress models, the SIF analyses were performed by viewing the models in the polariscope directly with the EyeCom II Vidicon camera. Traced images with half- and full-fringe lines can be obtained more easily when the models are viewed on-line than from negatives in which the contrast between dark and light is not even.

Table 4-11. Material fringe values calibrated from circular disk and from uniform stress region in the frozen-stress models

	Material fringe value (f_σ) (lb/in-fringe)			
Model No.	Circular disk	Upper uniform stress region	Lower uniform stress region	Average of f_σ
1B	2.197	2.175	2.155	2.176
2B	2.183	2.185	2.166	2.178
3B	2.188	2.177	2.176	2.180

Figure 4-18 shows a photograph of the isochromatic fringes in the vicinity of the crack tip after stress-freezing as well as the data locations on the traced image and the best back-plot obtained from the analysis for Model No. 1B. The final results obtained from these experiments are tabulated in Table 4-12 and are plotted in Figures 4-19 and 4-20 in the next section. Data collection regions of all three models were limited to $0.07 \leq r/a \leq 0.25$. The values for the Mode I SIF, K_I/K_{Io}, and the ratio K_{II}/K_I, from the stress-frozen models differ very little from those for live models. However, the standard deviations of the frozen-stress models are slightly larger than those of the live

models (see Tables 4-9 and 4-12). This may be due to more severe crack tip blunting at the high temperature. The results from the frozen-stress models are compared with those from the live models in Table 4-13 in the next section.

Table 4-12. Results of SIF values and statistical parameters obtained by program WIL4 after stress-freezing

Model No.	σ (psi)	K_I (psi$\sqrt{in}$)	K_{II} (psi$\sqrt{in}$)	K_I/K_{Io} [a]	K_{II}/K_I	$\bar{E}$ (%)	SD (%)
1B	8.030	12.253	-0.180	1.410	-0.015	0.973	2.276
2B	8.699	11.778	-2.808	1.255	-0.238	0.884	2.373
3B	11.472	10.336	-5.428	0.836	-0.525	0.602	2.127

[a] $K_{Io} = \sigma\sqrt{\pi a}$, where "a" is 0.3728 inch for Model No. 1B, 0.3707 inch for No. 2B, 0.3698 inch for No. 3B, respectively, after stress-freezing.

a. Isochromatic fringes

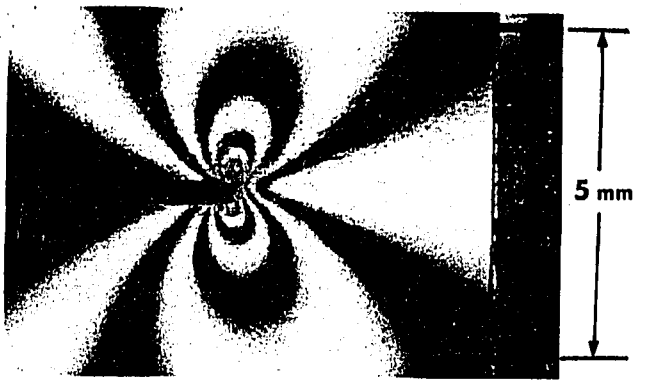

b. Data locations on the traced image

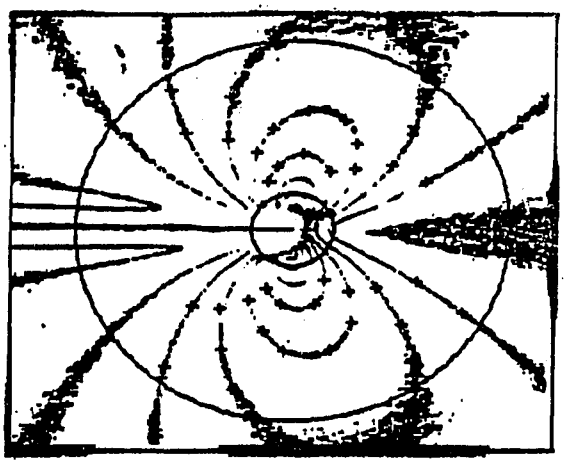

c. Best back-plot

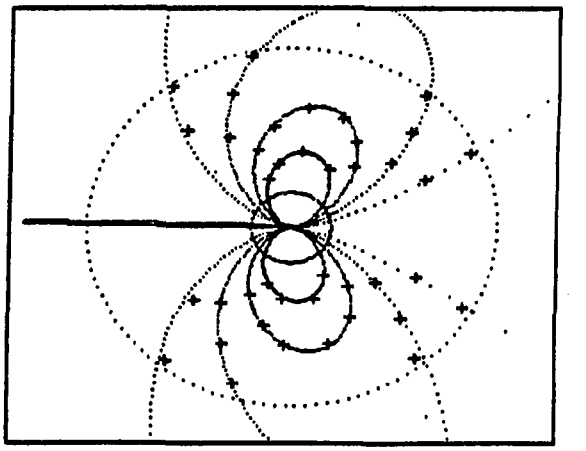

Figure 4-18. Isochromatic fringe loops in the vicinity of the crack tip after stress-freezing, data locations on the traced image and best back-plot fringes of Model No. 1B

D. Results

Table 4-13 summarizes the results from all two-dimensional tests. The results for K_I/K_{Io} and K_{II}/K_I with respect to crack inclination angle (β) are plotted in Figures 4-19 and 4-20. For the same geometries, the numerical results calculated by Zachary [103] and photoelastic experimental results obtained by Smith and Smith [104] are included in the figures.

Table 4-13. Final results obtained from two-dimensional crack analysis

Model No.	β[a] (degree)	a/W[a]	d[a] (inch)	K_I/K_{Io}	K_{II}/K_I	$\bar{E}$ (%)	SD (%)
1A[b]	-0.5~1.5	0.200	0.0068	1.418	0.007	0.246	0.903
1B[c]	0	0.199	0.0085	1.406	0.003	0.311	1.244
				1.406	0.009	0.619	1.899
				1.409	0.000	0.512	2.006
1B[d]	0	0.199	0.0090	1.410	0.015	0.973	2.276
2A[b]	22.5	0.200	0.0064	1.289	0.232	0.111	1.303
2B[c]	22.5	0.196	0.0087	1.284	0.205	0.463	2.190
				1.274	0.215	0.754	2.366
				1.241	0.220	0.346	1.849
2B[d]	22.5	0.196	0.0093	1.255	0.238	0.884	2.373
3A[b]	44.5	0.197	0.0065	0.851	0.494	0.015	1.447
3B[c]	45	0.198	0.0084	0.849	0.514	-0.094	1.594
				0.833	0.525	0.086	1.480
				0.812	0.546	0.071	1.345
3B[d]	45	0.198	0.0088	0.836	0.525	0.602	2.217

[a] See Figure 4-3 for the symbols.
[b] See the results of Table 4-4 for n=4.
[c] Load test results in Table 4-9 for live models.
[d] Results of Table 4-12 obtained from frozen-stress models.

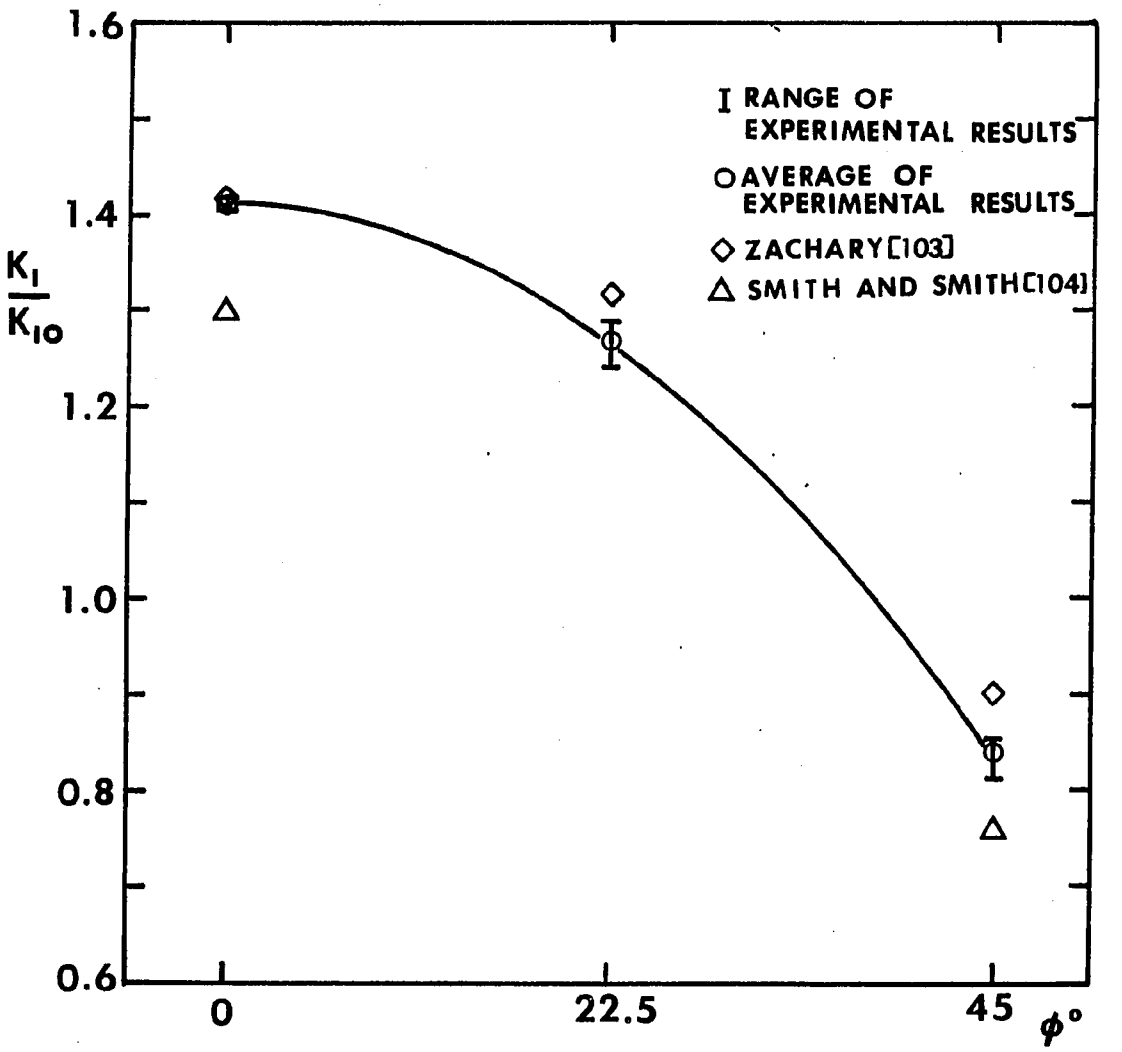

Figure 4-19. K_I/K_{Io} with respect to crack inclination angle (β)

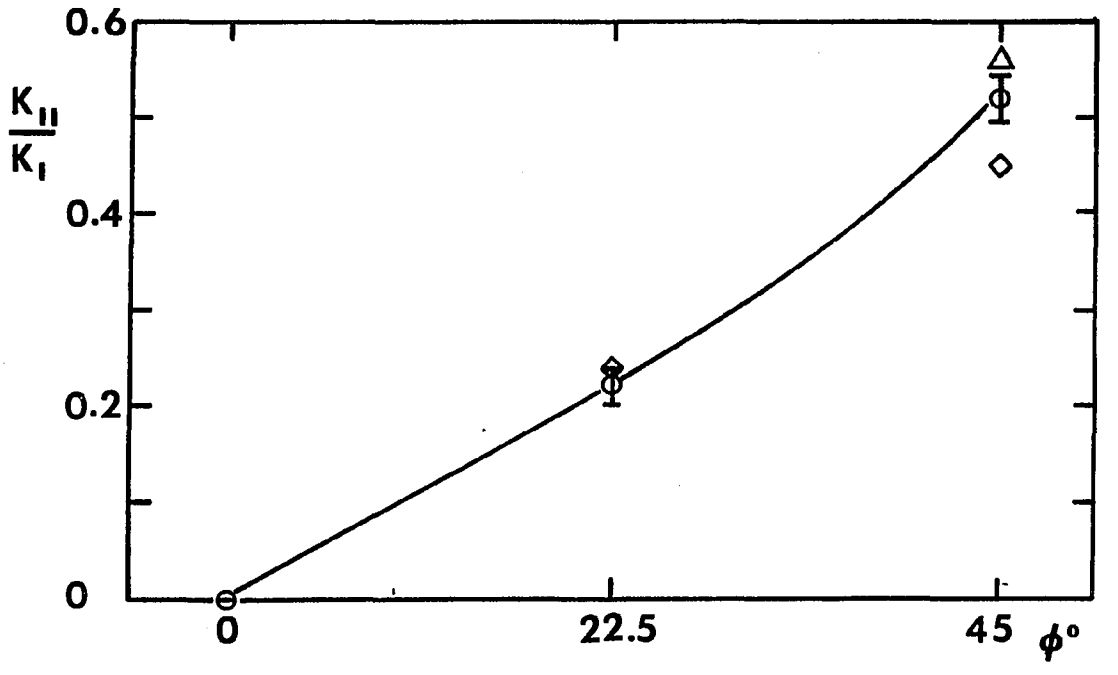

Figure 4-20. K_{II}/K_I with respect to crack inclination angle (β) (See Figure 4-19 for the symbols)

E. Conclusion and Discussion

From the results presented in the preceding sections, the following significant conclusions can be drawn.

1. Correcting the origin of the crack tip by the iterative least squares method can substantially increase the accuracy of data analysis providing that appropriate analytical equations for the stress field in the vicinity of the crack tip are used (see Figure 4-8). The need for this correction is particularly great when the data collection region is small, i.e., $(r/a)_{max}<1$, because a small mislocation of the crack tip location may result in a large percentage error in the coordinate assigned to data points (see Tables 4-4 and 4-5).
2. Statistical parameters such as standard deviation (SD) or correlation coefficient (CC) between measured fringes and regenerated ones are necessary to evaluate the accuracy of the experimental values for SIF. This is particularly important in Mixed Mode tests (see Figures 4-8, 4-9, 4-11 and 4-12).
3. For Mixed Mode cases, two terms of Williams equations (n=1,2 in equations 3-15) or modified Westergaard equations (equations 2-4) may not be sufficient to describe the stress field around a crack tip. This is true even if the data collection region is small. In the tests performed for this dissertation all data points were relatively close to the crack tip, $0.07< r/a<0.30$, yet the effect of using too few terms in the equations were evident. Equations (2-4) can only be used to get an approximate K_I in pure Mode I

(see Figures 4-11 and 4-12). They should not be used for Mixed Mode analyses.

4. Generally, for the relatively close region to the crack tip, r/a=0.07~0.30, used in the experiments refered here, 4 terms or O(r) of Williams power series type expressions appear to be sufficient to describe the stress field around the crack tip for Mode I or Mixed Mode cases. The inclusion of higher order terms in $r\sqrt{r}$ do not improve the accuracy of the SIF results (see Figures 4-11 and 4-12). In fact, the quality of the results deteriorates when n>4.
5. Normalized Mode I stress intensity factors(K_I/K_{Io}) and the ratio K_{II}/K_I remain constant when loads are changed. So, they could be used as parameters to describe geometrical or functional relationships in crack analysis (see Table 4-9).
6. There is no distinct difference between the results of K_I/K_{Io} and K_{II}/K_I analyzed from frozen-stress models and those from the live models. However, the standard deviations of the results from the frozen-stress models are always larger than those from live models (see Tables 4-9, 4-12 and 4-13). The reason for this is not clear but it could be partly due to viscoelastic behavior in the frozen-stress model and/or to increased crack tip blunting and large displacements at the stress freezing temperature. The ratio between the modulus of elasticity at room temperature and at the stress-freezing temperature is ~150:1. The ratio of f_σ is only ~35:1. So, for approximately the same number of fringes, the displacement will be about 4 times as large.

7. Even though there are some scatter bands (maximum 5 percent for K_I/K_{Io}) for the experimental results obtained from different tests in this dissertation (Table 4-13), these bands are significantly smaller than the difference between Zachary's numerical solution [103] and Smith's experimental results [104] as shown in Figures 4-19 and 4-20. Average of the new experimental results presented here (Table 4-13 and Figures 4-19 and 4-20) lies within the range of the results by Zachary and Smith's.
8. In all cases reported in Table 4-13, the standard deviations for Models B, which had wider slits ($d \sim 0.009$ inch), was larger than for Models A, which had slightly narrower slits ($d \sim 0.007$ inch). For wider slits, Figure 3-2 suggests that, for good data, $r/a > 0.08$. Actually a few data points were taken closer than this to the crack tip because $0.07 < r/a < 0.30$. These results tend to support Figure 3-2. The stress fields in a two-dimensional model with a saw cut to simulate a crack is compared to the field for a model with a natural crack in Figures 4-21 and 4-22. The real crack was obtained accidently when a two-dimensional model was momentarily overloaded. The main difference in the fringe pattern is ahead of the crack. Figure 4-21 represents a typical pattern for the fringes ahead of the crack. These photographs support the procedure whereby data is not collected too close to a blunt crack tip.

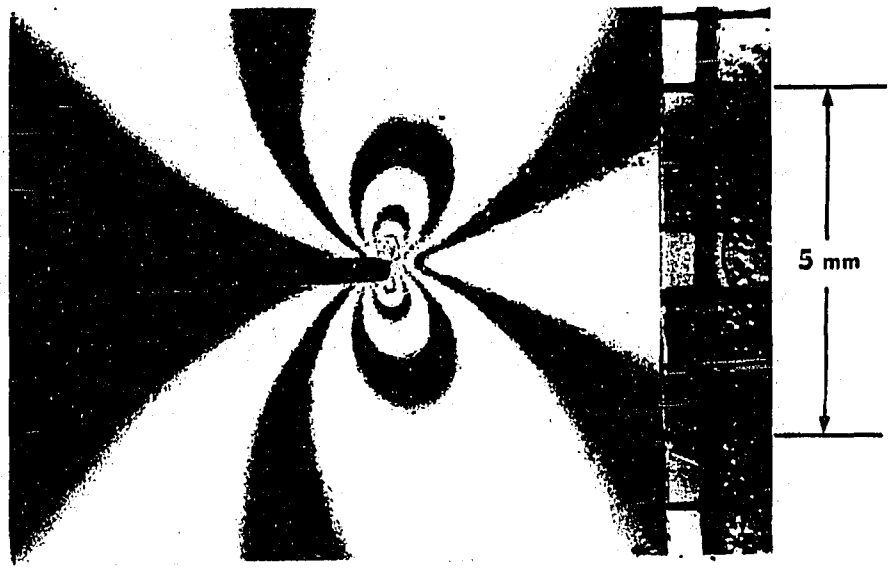

Figure 4-21. Isochromatic fringe loops in the vicinity of the simulated crack tip (Model No. 1B after stress-freezing)

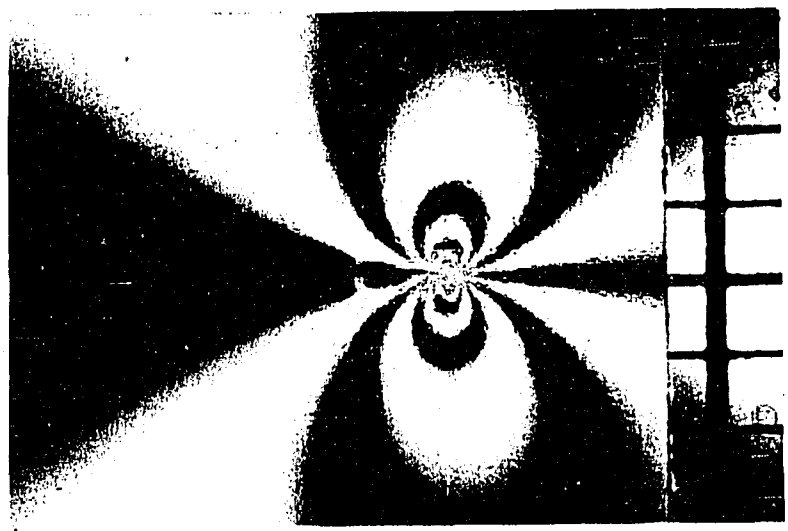

Figure 4-22. Isochromatic fringe loops in the vicinity of a naturally grown crack tip

V. THREE-DIMENSIONAL EXPERIMENTS

This chapter presents the results for pure Mode I loading on a part through semi-circular edge crack in a plate under uniform tension and also the results for Mixed Mode loading on inclined semi-circular edge cracks.

A. Model Geometries

In order to find the SIF variations along the crack front of the semi-circular crack in pure Mode I loading, and to investigate Mixed Mode fracture parameters at the maximum depth of the inclined semi-circular surface cracks, three models which have different crack inclination angles were prepared. The design of the models is shown in Figure 5-1. The ratios of B/a and T/a were both taken as 3.0 to eliminate the extreme boundary effects from the edges of the plate. Plate height (2H) was taken to be over three times the width (2B) to yield a zone of uniform far field stress. These considerations were based on the previous research on boundary effects [97, 98] for two- and three-dimensional crack problem. The dimensions of the oven used determined the dimensions of the mold. The final dimensions after machining are given in Table 5-1.

B. Preparation of Experimental Models

The general procedures for model preparation were the same as for two-dimensional edge crack study described in Chapter IV-A. The differences between them are described below.

1. Crack tip shape and mold box

A major difficulty in making the models was to produce an artificial flaw shape with good tip geometries in the correct location in a test specimen. The simulated cracks were cast to shape in a mold box, whose base plate consisted of separate blocks, so that a "crack tip blade" could be inserted in pre-machined slots of the base blocks. Different base blocks were used for each different crack shape and slant angle. The insert blades for the semi-circular surface flaws were all machined together as a small stack from 0.008 inch thick phosphor bronze shim stock. The semi-circular profile was produced on a milling machine with a concave cutter with the desired radius. After which, both sides of the blade were carefully polished with a fine mesh sand paper to remove all burrs and to shape the crack tip. Figure 5-2 shows the assembled mold box with a crack tip in place. Micrographs of the cast crack and of a naturally grown crack are given in Figure 5-3. The cast tip has a significantly better shape than the machined slit in Figure 4-21.

Table 5-1. Actual geometries and test conditions of the semi-circular surface cracked models (see Figure 5-1 for the symbols)

Model No.	β (degree)	2a (inch)	B_R (inch)	B_L (inch)	H_U (inch)	H_B (inch)	T (inch)	σ^a (psi)
1S	0	0.7470	1.122	1.125	3.790	3.870	1.124	14.527
2S	22.5	0.7499	1.127	1.120	3.885	3.840	1.123	15.841
3S	45	0.7496	1.124	1.127	3.850	3.828	1.121	18.978

[a]Applied tensile stress when stress-freezing.

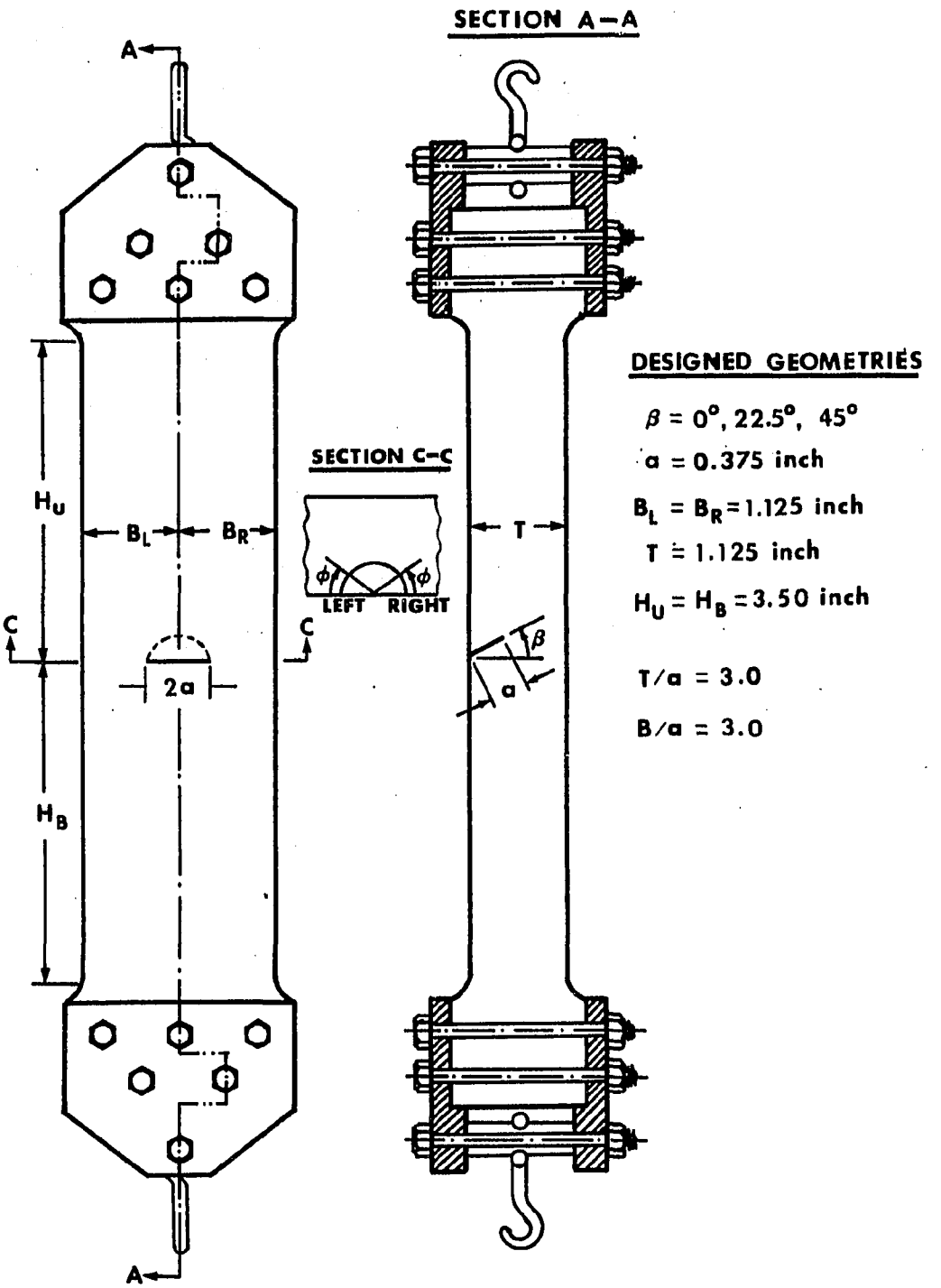

Figure 5-1. Geometries of experimental models for the study of stress intensity factors of the semi-circular surface crack with different crack inclination angle

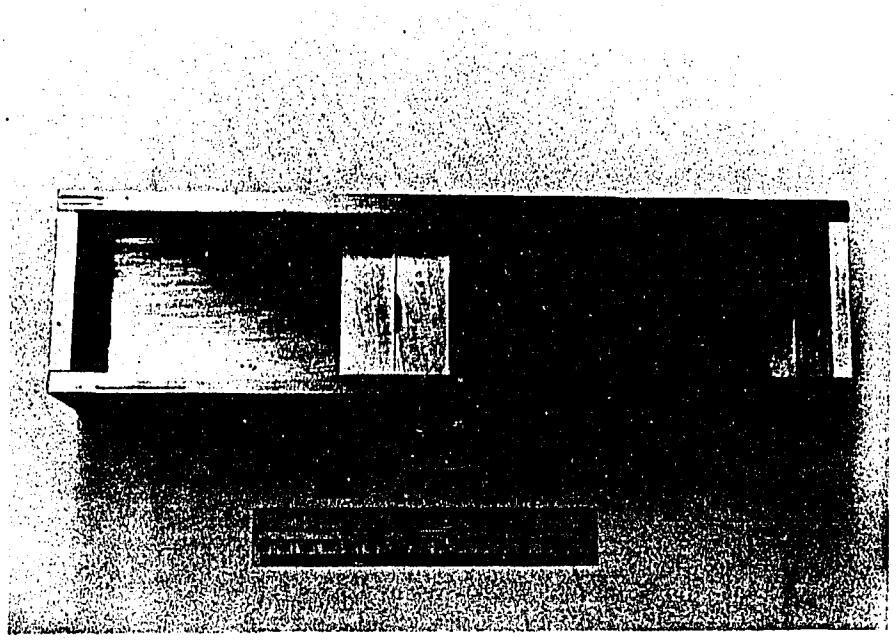

Figure 5-2. Assembled mold box and a crack tip blade for casting a semi-circular surface crack in the experimental model

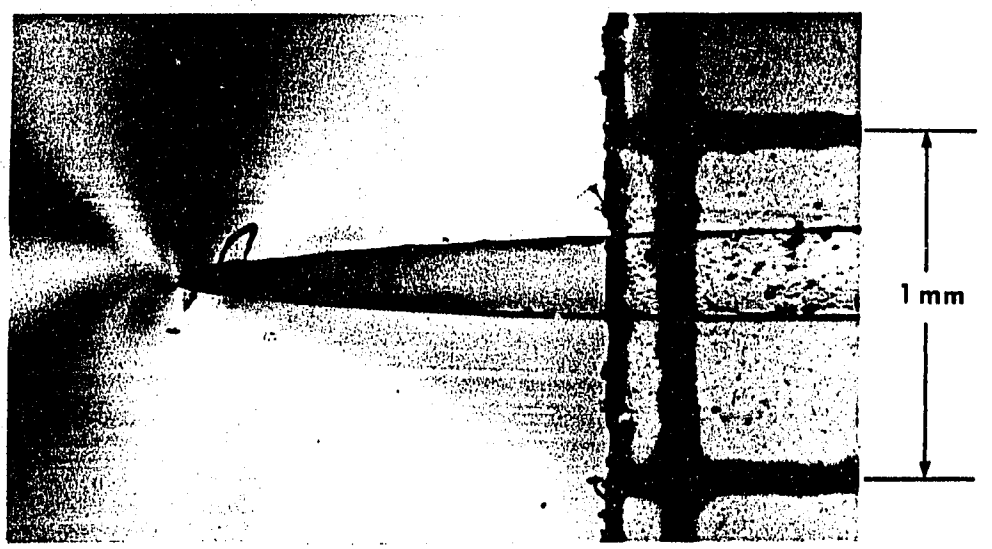

a. a cast crack tip shape

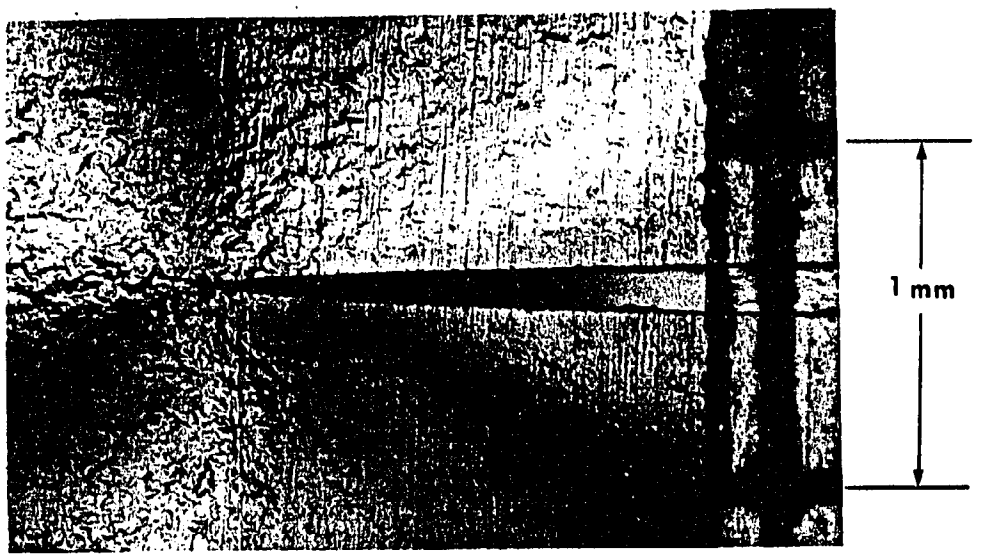

b. a naturally grown crack tip shape

Figure 5-3. Comparison of the detailed crack tip shapes of a cast crack and a naturally grown crack

2. Photoelastic materials and thermal processing

The photoelastic material was "3DMU-050". It is a fast curing epoxy which resists mottling [93]. All the processes, i.e., mixing, preliminary curing, machining and stress-freezing were the same procedures as described in Chapter IV-A. The mold box was coated with silicon RTV rubber[1]. "FREKOTE 44" mold release[2] was applied on the crack tip blade so that the details of the crack tip would not be altered. Figure 5-4 shows the photoelastic material, phthalic anhydride, RTV rubber and mold release used for casting experimental models. The test setup of the model and calibration disk, ready for stress freezing, in the computer controlled oven is shown in Figure 5-5. In Figure 5-6, the front and side views of frozen-stress Model No. 1S through a light field polariscope setup are shown.

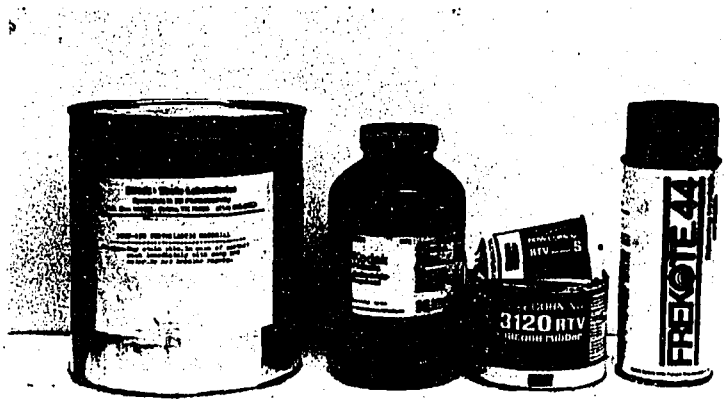

Figure 5-4. Photoelastic materials, RTV rubber and mold release used for casting experimental models

[1]Dow Corning 3120 RTV is a mold making rubber manufactured by Dow Corning Corporation, Midland, Michigan.

[2]FREKOTE 44 is a fluorocarbon mold release and dry lubricant supplied by FREKOTE, Inc., Boca Raton, Florida.

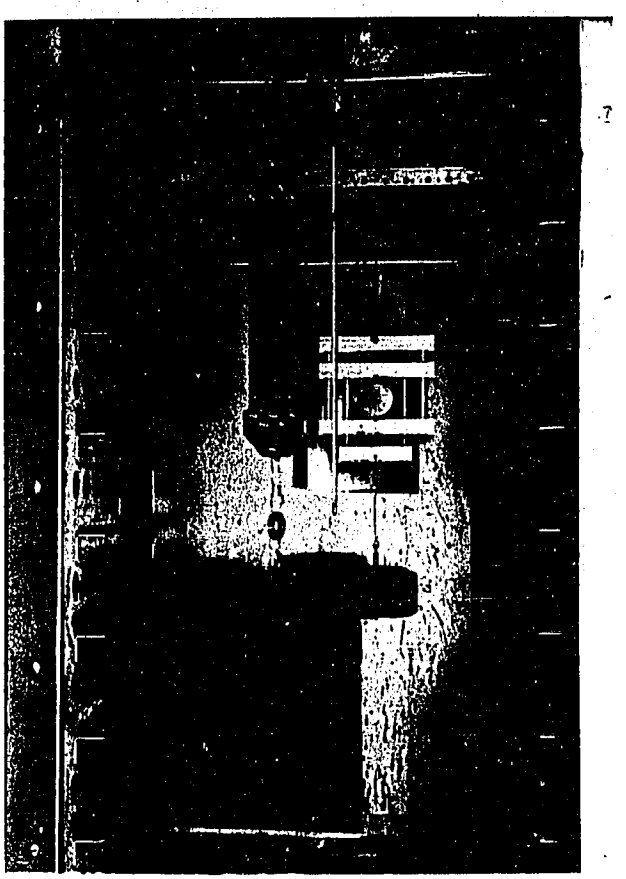

Figure 5-5. Test setup for stress-freezing experimental models for the study of stress intensity factors in a semi-circular surface crack

a. Front view

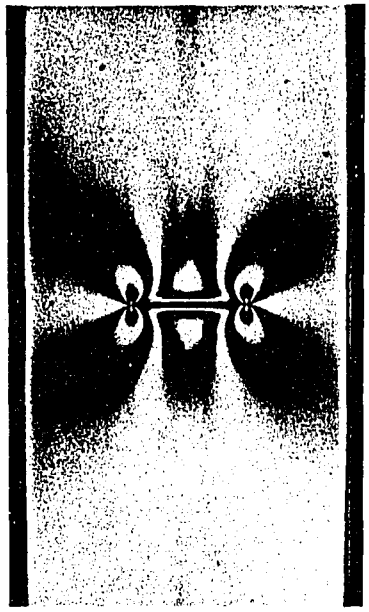

b. Side view

Figure 5-6. Frozen-stress Model No. 1S through the light field polariscope setup

3. Slicing

Slicing may be one of the most difficult procedures for the preparation of three-dimensional photoelastic experimental models since great care should be taken to avoid introducing machining stress. They should, furthermore, be made at the desired positions in the stress frozen body so that data analysis can be in the correct planes. Finally, they should be thin and of even thickness. For Model No. 1S, which is in pure Mode I loading, each slice was taken from a different position along the crack front. For Model Nos. 2S and 3S, a slice was taken at and the maximum depth of the inclined semi-circular surface crack, as shown in Figure 5-7. To avoid introducing machining stresses from heat generated when cutting the slices, the whole frozen-stress model was immersed in a water tank which was specially designed for this purpose. Each slice, whose location could be aligned to the designed position through an angular dividing head, was cut with a 1/64 inch (0.397 mm) thick slitting saw. Figure 5-8 shows the water tank and angular dividing head on the bed of vertical spindle milling machine. After slicing, each slice was separately fly-cut to an even thickness and then carefully polished with micro-polishing aluminum oxide powder (0.3 μmm) mixed with abundant cooling water on a polishing bed. Since epoxy material is sensitive to moisture effects, the slices were kept at 100 $^{\circ}$F in an oven for 24 hours to eliminate stress associated with non uniform moisture content, as recommended by Johnson [96].

Figure 5-9 shows the isochromatic fringes in the slices taken from the different models.

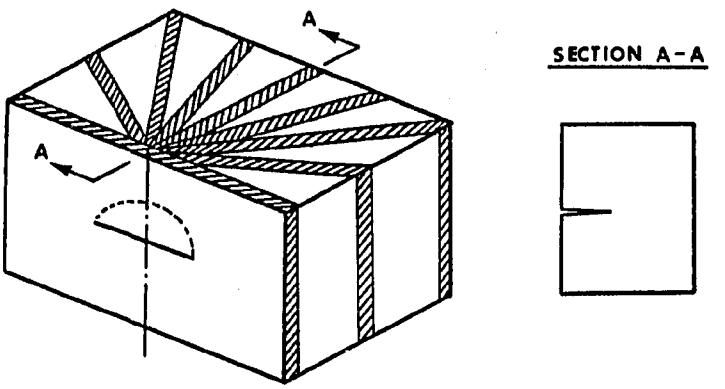

a. Slicing scheme of Model No. 1S

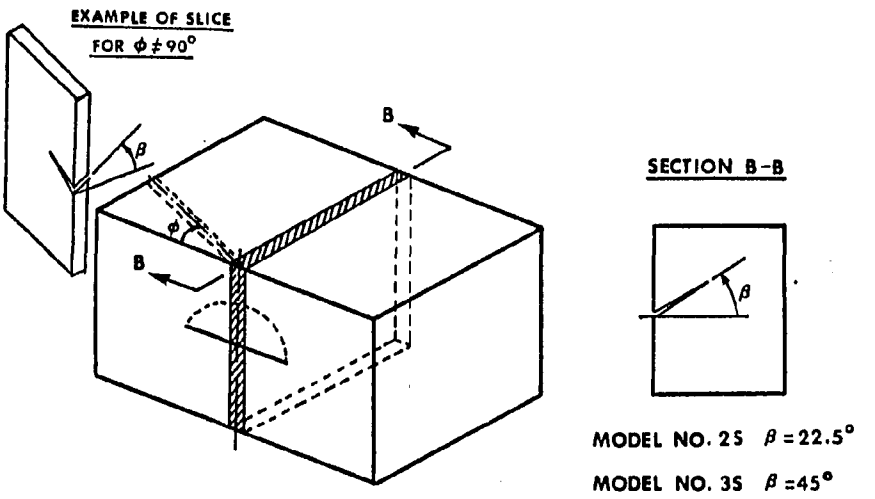

b. Slicing scheme of Model Nos. 2S and 3S

Figure 5-7. Slicing schemes for the SIF study of semi-circular surface cracks in the frozen-stress models

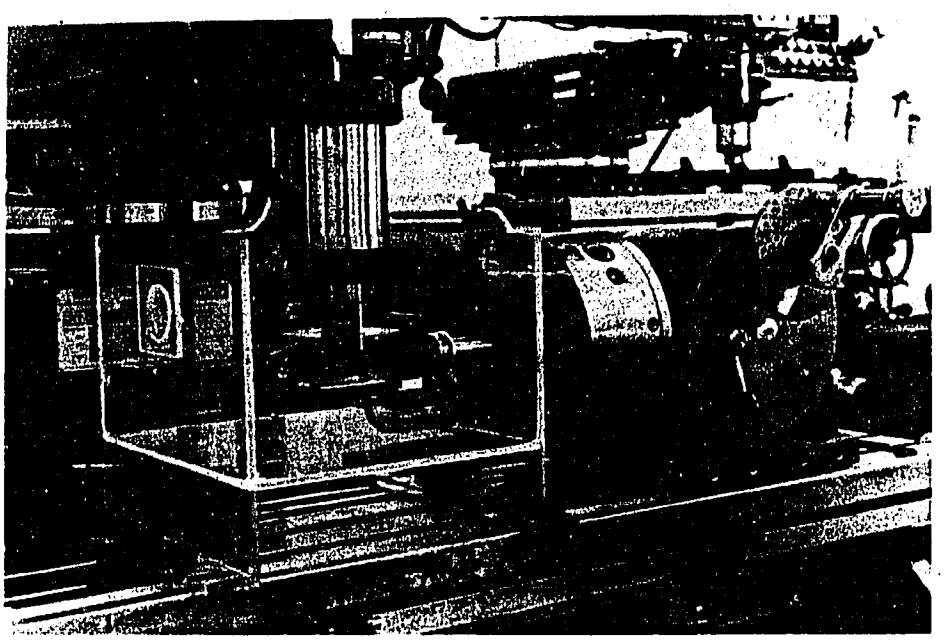

Figure 5-8. Machining setup for slice making

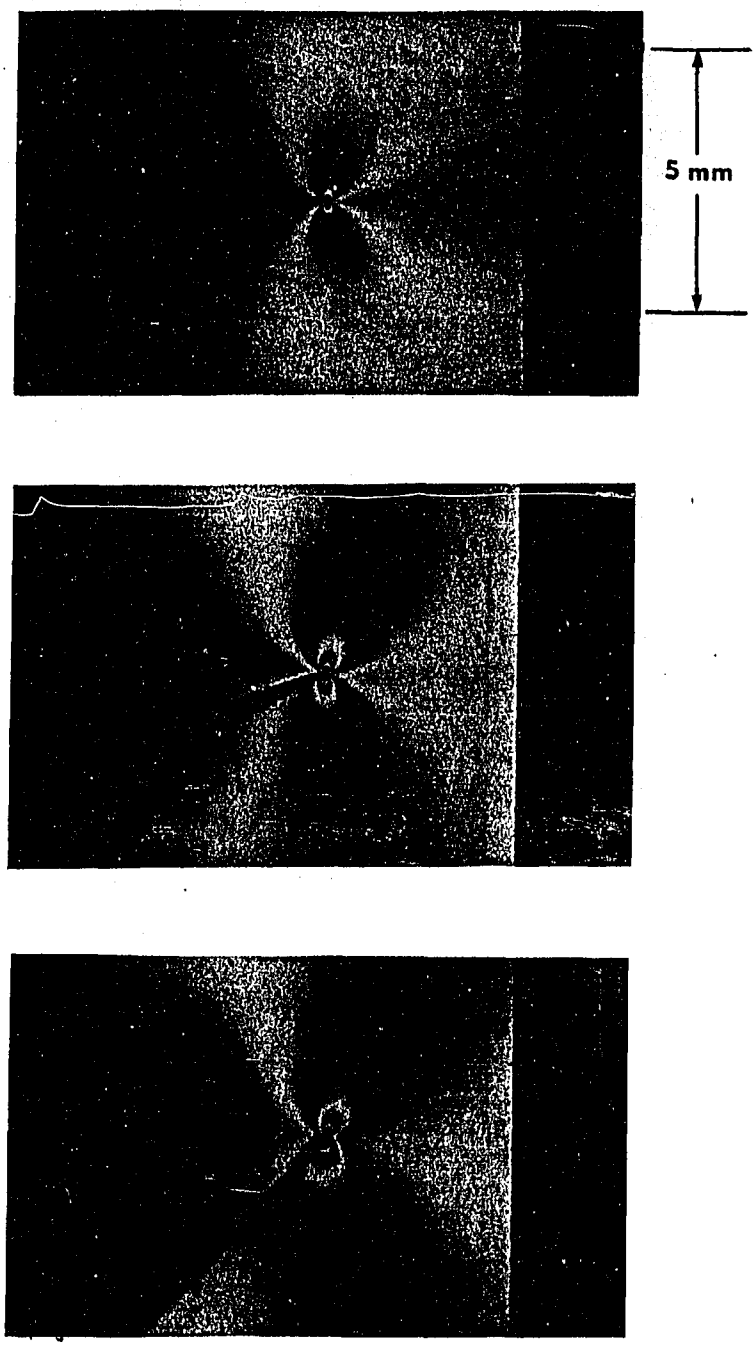

a. Model No. 1S (ϕ=90°)

b. Model No. 2S (ϕ=90°)

c. Model No. 3S (ϕ=90°)

Figure 5-9. Isochromatic fringes in the slice cut from the frozen-stress surface cracked models

C. Preliminary Work for Photoelastic Data Collection from Slices

Accurate data collection is the most important requirement to increase the accuracy of the experimental work. However, from a thin frozen-stress slice, it is difficult to read fringe data accurately by using conventional photoelasticity because the slice does not have enough fringe loops. Fracture of the models during stress-freezing usually limits the largest fringe order in the vicinity of the crack tip to two in a slice with thickness less than 0.10 inch (see Figure 5-9). Post's [105] fringe multiplication technique is often used for photoelastic analysis from thin slices but it needs auxiliary optical equipment and is not readily applicable to the digital imaging hardware used in this research.

For this reason, a new digital technique for fringe multiplication, which does not need auxiliary optic, was developed. The principles for this technique is described below.

In a circular polariscope with dark field setup, the intensity of the transmitted light emerging from the analyzer is given by

$$I_D = A \sin^2(\pi N)$$

$$= \frac{A}{2}\left\{1 - \cos(2\pi N)\right\} \qquad (5\text{-}1)$$

where I_D = light intensity in the dark field;

A = a proportional constant. For uniform fringe intensities, this constant is taken as 255 for the system used.

N = isochromatic fringe order.

While, the light intensity in the light field setup is

$$I_L = A \cos^2(\pi N)$$

$$= \frac{A}{2}\left\{1 + \cos(2\pi N)\right\} \qquad (5\text{-}2)$$

$$= A - I_D$$

where I_L = light intensity in the light field.

Squaring equations (5-1) and (5-2), and adding them gives

$$I_D^2 + I_L^2 = \frac{A^2}{2}\left\{1 + \frac{1}{2}\{1 + \cos(4\pi N)\}\right\} \qquad (5\text{-}3)$$

Rearranging gives

$$I_D^2 + I_L^2 - \frac{A^2}{2} = \frac{A^2}{2}\left\{\frac{1}{2} + \frac{1}{2}\cos(4\pi N)\right\} \qquad (5\text{-}4)$$

But $I_D + I_L = A\{\sin^2(\pi N) + \cos^2(\pi N)\} = A$, therefore,

$$I_L = A - I_D$$

Substituting above equation into (5-4) gives

$$\frac{A}{2}\left\{1 - \cos(4\pi N)\right\} = A - \left\{\frac{I_D^2 + (A - I_D)^2 - A^2/2}{A/2}\right\}$$

$$= \frac{4 I_D I_L}{A}$$

$$= \frac{4I_D(A-I_D)}{A} \qquad (5\text{-}5)$$

When the left side of equation (5-5) is compared with equation (5-1), it can be observed that cos(2πN) term has become cos(4πN). This means that the photoelastic image processing procedure shown in equation (5-5) can be used to double the fringes. Reprocessing equation (5-5) once more yields four times the original fringes, repeating the procedure 8 times, and so on. Figure 5-10 shows original fringe loops in a slice, and the images after 2x and 4x multiplication. The disadvantage of this method is that noise associated with nonuniformity of the light source and inaccurate arrangement of polariscope setup is also magnified by the same order as the fringes. This effect is evident in Figure 5-10 where the dark fringe loops are not evenly dark. When this occurs, program "TRACE" does not yield acceptable results any more. For this reason, the image of two times fringe multiplication was used. It gave enough fringe information for the crack analysis. Data collection was done after sharpening the doubled fringe image with program "TRACE" [89].

Before the analysis, the material fringe value for each model was calibrated from a circular disk, which was cut from the original casting for the specific model (see equation 4-1).

The uniformity of the far-field stress was visually checked from the slices cut from the uniform stress region in the circular polariscope with white light source. Very uniform color from the slice was obtained.

a. Original fringes

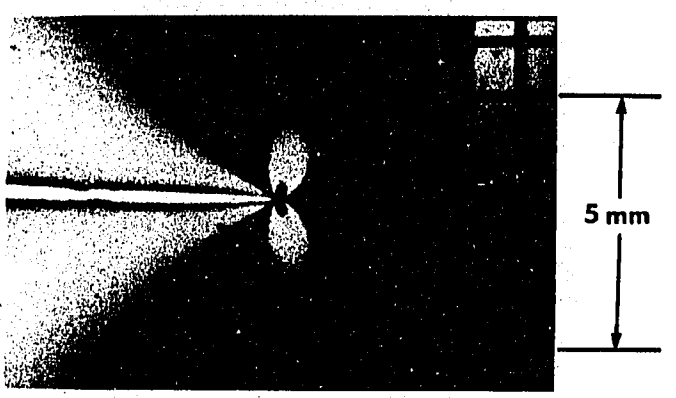

b. Two times fringe multiplication

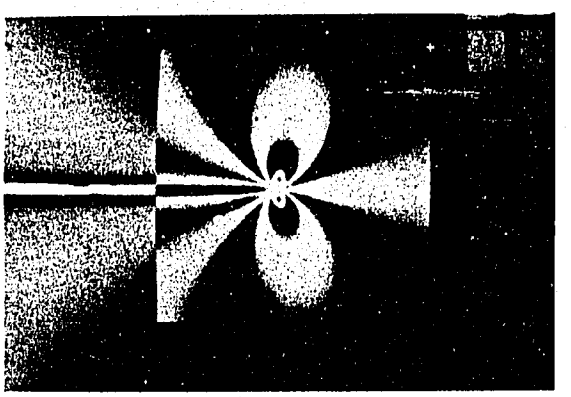

c. Four times fringe multiplication

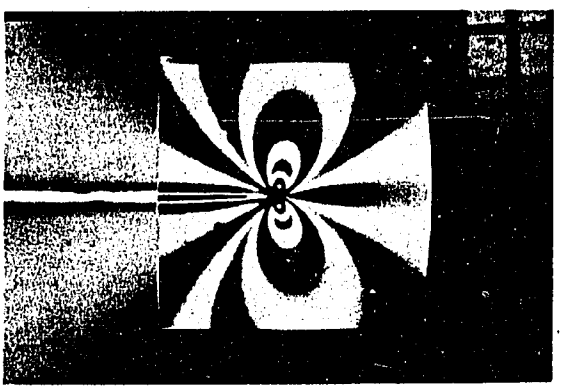

Figure 5-10. Example of fringe multiplication by digital image processing system

D. Data Analysis and Results

Each slice was analyzed with the procedures described in Chapter IV-C. Before analyzing, thickness of the slice in the vicinity of the crack tip was accurately measured with a digital measuring machine[1] to a resolution of 0.0001 inch. Then, the stress intensity factor for portion of the crack contained in the slice was found with programs "WIL4" and "BPOW4" [89]. In Table 5-2, thickness of the slices, material fringe value, stress intensity factors and statistic indices obtained from these experiments are tabulated. Figure 5-11 illustrates the different stages in the analysis of the slices. The figure show, in sequence, the doubled fringes, the sharpened fringes processed from the double fringe and the back-plot results superimposed on the original image.

To compare the experimental results with other solutions, the SIF results were normalized by equation (2-6) which can be simplified to equation (5-6) for an embedded circular crack in an infinite medium.

$$F_m = \frac{K_I}{(2/\pi)\sigma\sqrt{\pi a}} \qquad (5\text{-}6)$$

Experimental results of magnification factor (F_m) are shown in Table 5-3.

For the experimental geometry of the flat semi-circular surface crack (Model No. 1S with $\beta=0^o$ in Table 5-1), two previous known

[1] CORDAX 1000 Measuring Machine, Automatic Measurement Division, Dayton, Ohio.

solutions are available. The first solutions were obtained from empirical equations which were developed on the basis of a finite element analysis [51]. The equations are expressed explicitly so that calculation could be done for this experimental geometry. The other solutions came from photoelastic experiments by Phang and Ruiz [50] with the similar geometrical conditions. For inclined semi-circular surface cracks (Model Nos. 2S and 3S), solutions are not available at present.

In Figure 5-12, the results for the magnification factor (equation 5-6) of Model No. 1S is plotted at selected angle ϕ along the crack front. The values for the right quadrant of the crack are slightly higher than for the left quadrant. The cause for this may be slight nonuniformity of the stress across the model, slight off-center of crack and slight nonsymmetry of cast crack shape. The solutions from reference [50, 51] mentioned above are also plotted in Figure 5-12.

It was possible to cut and analyze 5 slices from Model No. 1S ($\beta=0^{o}$). So the variation of F_m along the crack front could be found (Figure 5-12). However, if slices are cut from the slant-cracked models, Model Nos. 2S and 3S, so that the planes of the slices are in the plane of loading of the model, the crack tip slants through the thickness of the model as shown in Figure 5-7b. It is therefore not possible to extract sensible SIF information from such slices. In these models, only the slices for $\phi=90^{o}$ yield sensible data in stress-freezing photoelasticity. For this reason, Figures 5-13, 5-14 and 5-15 plot data only for the SIF at the point of maximum penetration from the slice at $\phi=90^{o}$. The SIFs at the maximum depth ($\phi=90^{o}$ in Figure 5-1) of semi-circular cracks are compared to those of two-dimensional inclined

edge cracks in Figures 5-13, 5-14 and 5-15 (see Table 5-4). The values of K_I/K_{Io}, K_{II}/K_I, and K_{eff}/K_{Io} are shown in these figures. Here, the effective stress intensity factor, K_{eff}, associated with Mode I and Mode II, is defined by:

$$K_{eff} = \sqrt{K_I^2 + K_{II}^2} \tag{5-7}$$

Table 5-2. Slice thickness (t), material value (f_σ), SIF results and statistical indices analyzed from semi-circular surface cracked models

Model No.		ϕ[b]	t[d]	f_σ[e]	K_I (psi$\sqrt{in}$)	K_{II} (psi$\sqrt{in}$)	$\bar{E}$[f] (%)	SD[g] (%)
1S[a] (β=0°)	R[c]	3	0.0531	2.3065	13.274	0.062	-0.209	1.432
		22.5	0.0564		12.239	0.024	0.103	1.274
		45	0.0591		11.512	0.096	-0.090	1.185
		67.5	0.0546		11.345	0.044	-0.150	1.605
		90	0.0578		11.473	0.065	-0.073	1.171
	L[c]	3	0.0530	2.3065	13.654	0.033	0.025	1.320
		22.5	0.0519		12.838	0.028	0.039	1.095
		45	0.0560		12.139	0.003	0.229	1.146
		67.5	0.0570		11.922	0.011	-0.186	1.186
2S[a] (β=22.5°)		90	0.0772	2.2917	11.023	3.972	-0.440	1.381
3S[a] (β=45°)		90	0.0785	2.2863	8.125	7.110	-0.397	1.477

[a]See Table 5-1 for crack length (2a), applied stress (σ) and other geometries.
[b]ϕ = Circumferential angle of a crack in degrees (Figure 5-1).
[c]R = Right side and L = Left side of a crack as shown in Figure 5-1.
[d]t = Slice thickness in inches.
[e]f_σ = Material fringe value (lb/in-fringe).
[f]$\bar{E}$ = Mean of percentage errors between observed fringes and regenerated ones at data collection points defined by equation (3-36).
[g]SD = Standard deviation of the percentage errors.

Table 5-3. Magnification factor (F_m), and the ratios of K_I/K_{Io}, K_{eff}/K_{Io} and K_{II}/K_I of semi-circular cracked models (see Tables 5-1 and 5-2 for reference data)

Model No.		ϕ	K_{Io}[a]	F_m[b]	K_I/K_{Io}	K_{eff}[c]$/K_{Io}$	K_{II}/K_I
1S	R	0	15.736	1.325	0.844	0.844	0.005
		22.5		1.222	0.778	0.778	0.002
		45		1.149	0.732	0.732	0.008
		67.5		1.132	0.721	0.721	0.004
		90		1.145	0.729	0.729	0.005
	L	0	15.736	1.362	0.867	0.867	0.002
		22.5		1.282	0.816	0.816	0.002
		45		1.212	0.771	0.771	0.000
		67.5		1.190	0.758	0.758	0.001
2S		90	17.194	1.007	0.064	0.681	0.360
3S		90	20.593	0.592	0.395	0.524	0.875

[a] $K_{Io} = \sigma\sqrt{\pi a}$, see Table 5-1 for applied stress (σ) and crack length (2a).

[b] F_m = Magnification factor defined by equation (5-6).

[c] K_{eff} = Effective SIF defined by equation (5-7).

Table 5-4. Comparison of the ratios of K_I/K_{Io}, K_{eff}/K_{Io} and K_{II}/K_I with respect to crack inclination angle (β) between 2-dimensional edge cracks and 3-dimensional semi-circular surface cracks

β[a]	2-dimensional[b]			3-dimensional[c]		
	K_I/K_{Io}	K_{eff}/K_{Io}	K_{II}/K_I	K_I/K_{Io}	K_{eff}/K_{Io}	K_{II}/K_I
0	1.410	1.410	0.015	0.729	0.729	0.005
22.5	1.255	1.290	0.238	0.641	0.681	0.360
45	0.836	0.944	0.525	0.395	0.524	0.875

[a] β = Crack inclination angle in degrees (see Figure 4-4 for 2-dimensional edge crack, and Figure 5-1 for 3-dimensional surface crack).

[b] These values were calculated from the results of stress frozen edge cracked models (see Table 4-12).

[c] These values were obtained from the SIF results at the maximum depth (ϕ=90° in Figure 5-1) of semi-circular surface crack (Table 5-3).

a. Two times fringe multiplied image

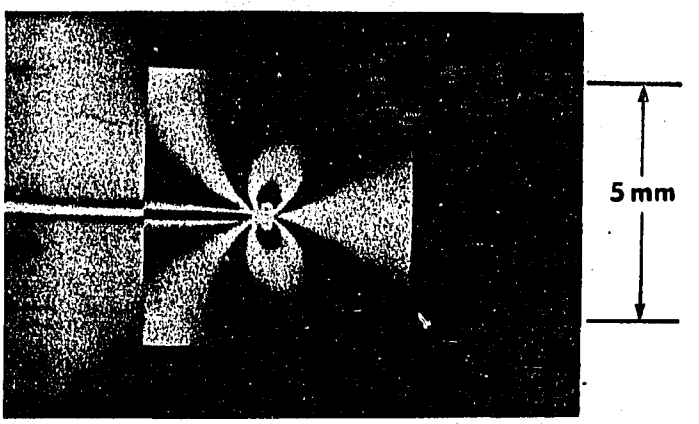

b. Fringe sharpened image from the above image

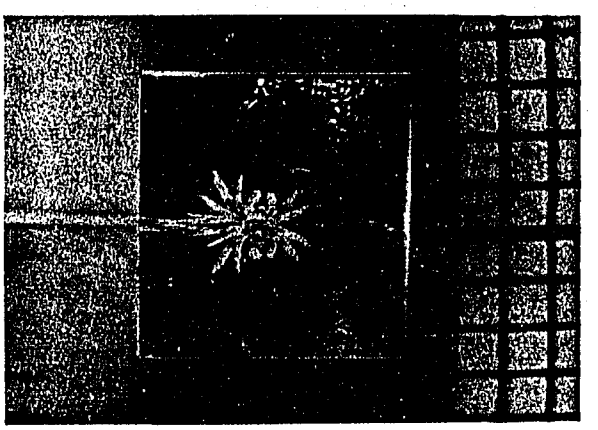

c. Back-plot superimposed on the original image

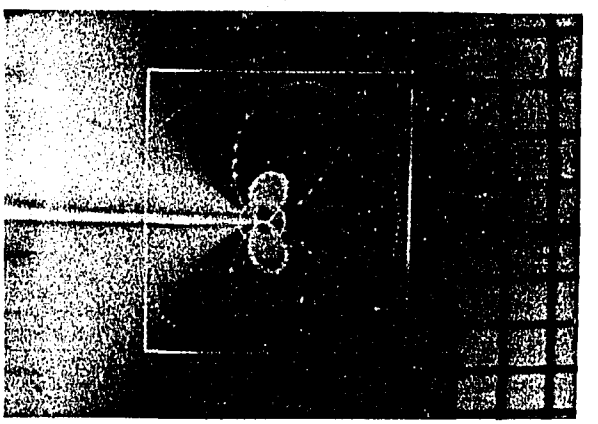

Figure 5-11. Example of data collection and analysis from a thin frozen-stress slice

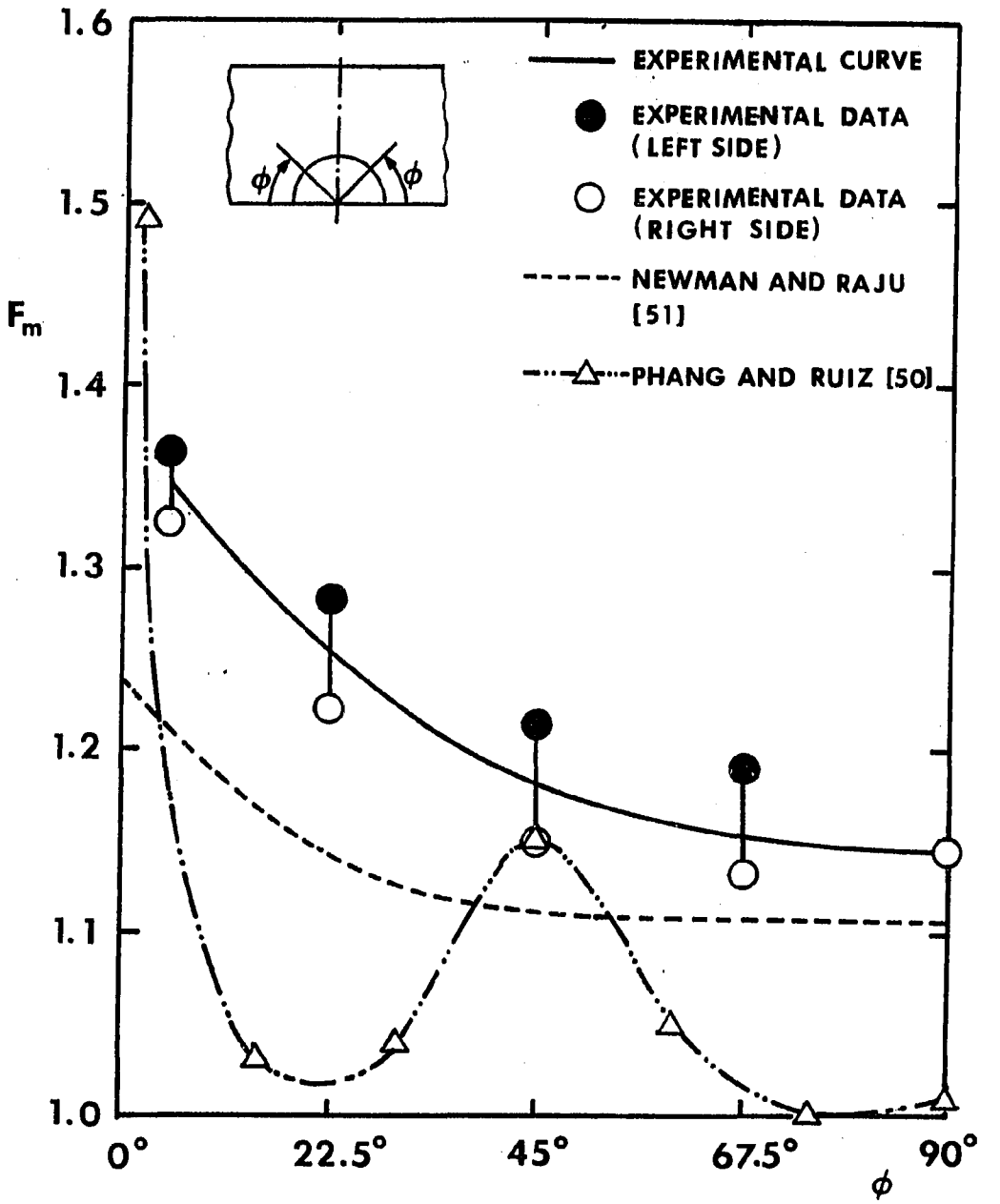

Figure 5-12. Stress intensity magnification factor (F_m) variation along a circumferential angle (ϕ) of the crack front in the flat semi-circular surface crack (Model No. 1S)

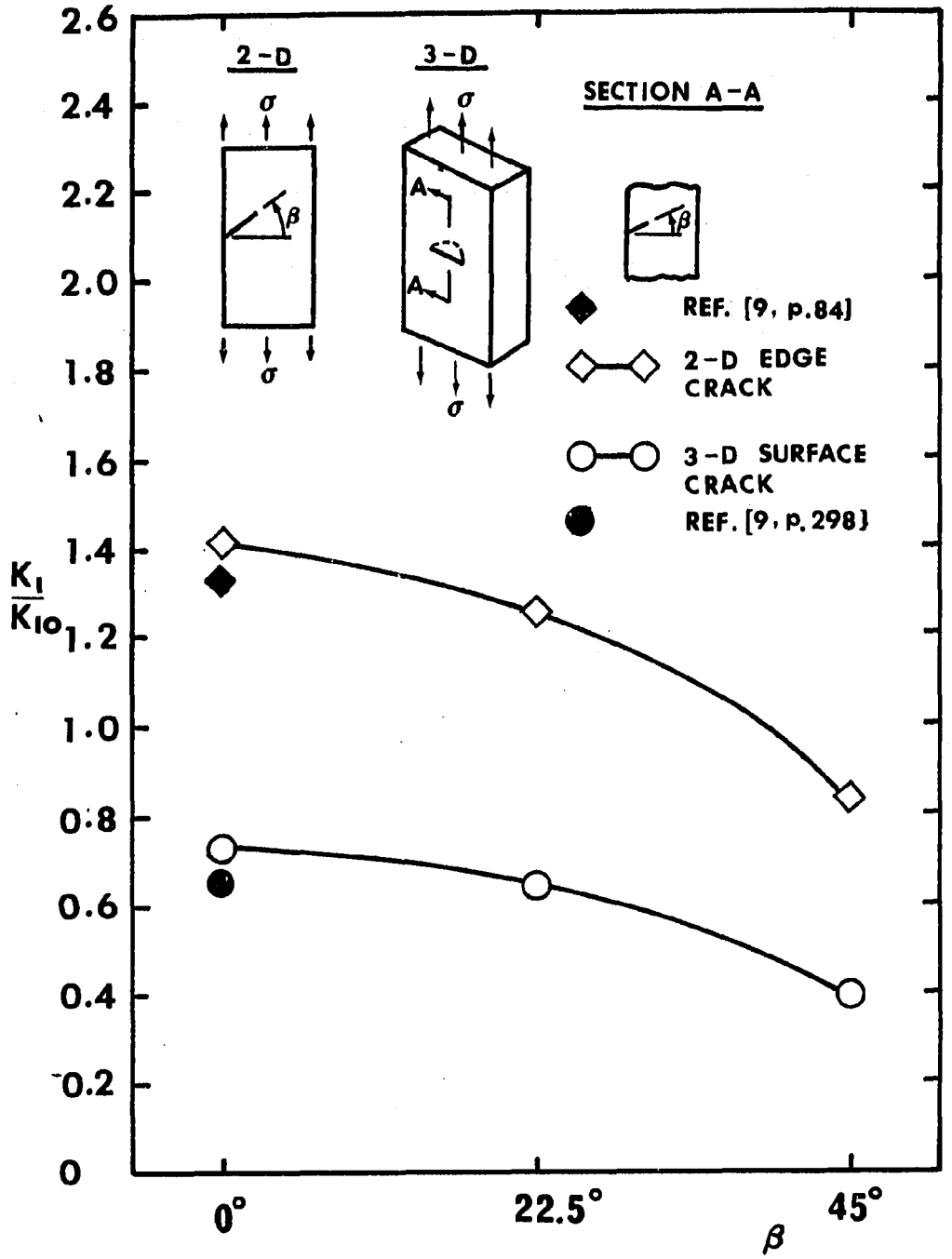

Figure 5-13. Normalized stress intensity factor (K_I/K_{Io}) variation at the maximum depth of the semi-circular surface crack and two-dimensional inclined edge crack with respect to crack inclination angle (β)

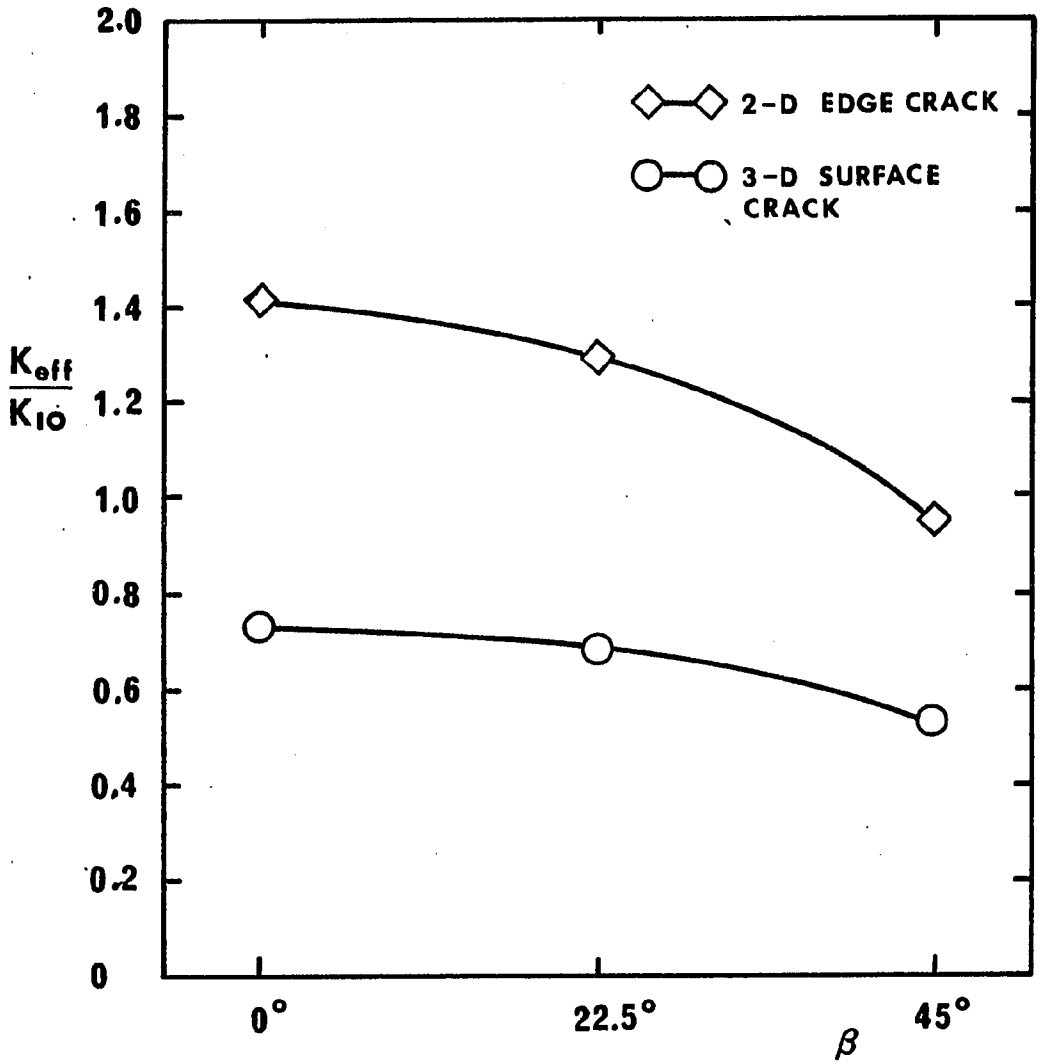

Figure 5-14. Normalized effective stress intensity factor (K_{eff}/K_{Io}) variation at the maximum depth of the semi-circular surface crack and two-dimensional inclined edge crack with respect to crack inclination angle (β)

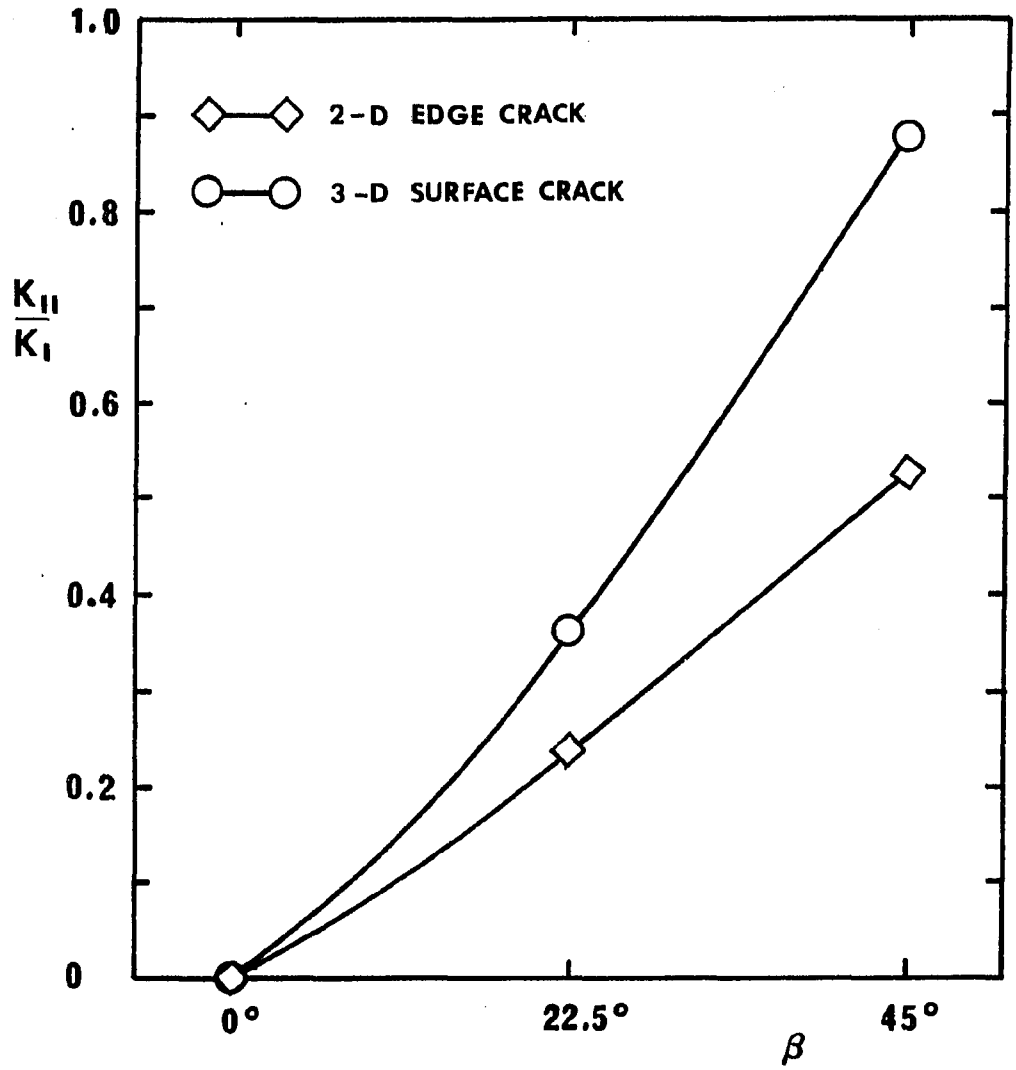

Figure 5-15. Variation of K_{II}/K_I at the maximum depth of the semi-circular surface crack and two-dimensional edge crack with respect to crack inclination angle (β)

E. Conclusion and Discussion

There were two goals for the three-dimensional portion of this research: To find how the stress intensity factor varies along a circumferential crack front in a semi-circular crack in pure Mode I loading, and to obtain Mixed Mode fracture parameters for inclined semi-circular cracks for which solutions are not available.

In the process, a new digital method for fringe multiplication and sharpening were introduced. In photoelastic analysis from thin slices cut from three-dimensional frozen-stress models, it is difficult to get enough fringe information, because increasing the load is likely to fracture the model during stress-freezing.

To obtain reliable experimental data from the desired geometries, a casting method was used to produce a semi-circular crack. It is not possible to machine with a saw a full semi-circular slit. The best that can be achieved is a part circular slit. The casting method has the additional advantage that the tip can be shaped to more accurately simulate a natural crack. The blade tip was sanded and polished to a sharp edge which produced a tip profile as shown in Figure 5-3a. When the standard deviations of two-dimensional edge cracks machined with a 0.008 inch thick slitting saw, and those of a cast three-dimensional semi-circular surface crack are compared, the standard deviation of cast crack is substantially lower (see Figure 4-21 for the machined tip ,and see Figure 5-3a for the cast tip). Tables 4-12 and 5-2 list the values of standard deviation for each of the two cases.

From the results obtained from these experiments, the following

conclusions can be drawn:

1. Variation of stress intensity factor along a circumference of a semi-circular surface crack in pure Mode I loading (Figure 5-12) is similar to that predicted by Newman and Raju in a finite element solution [51]. It is completely differently from the experimental results reported by Phang and Ruiz [50]. The peak in SIF at 45^{o} reported Phang and Ruiz [50] does not appear in the results from the research for this dissertation. This discrepancy may be due to the different schemes for photoelastic data analysis used in the two investigations. For this dissertation, data collection was done from the whole stress field in the vicinity of the crack tip in the region r/a=0.07 to 0.30, and photoelastic data were fitted to the first 4 terms of Williams equations. Finally, fracture parameters were calculated by taking the limit of $r \to 0$ as shown in equations (3-17a) and (3-17b). Phang and Ruiz's experimental results were obtained by the slope method [71] from data along a single selected line, namely $\theta=90^{o}$ in Figure 3-1. The equations they used for the calculations of SIFs were the Westergaard equations which have only singular terms ($1/\sqrt{r}$ terms). Furthermore, their data collection was in the range of $0.05<r/a<0.50$, which is considerably wider than those used in this dissertation and includes data from points further away from the crack tip. It was shown in Chapter IV-C that even for the closer set of data, $(r/a)_{max}=0.30$, higher terms are necessary to yield reliable results (see Figure 5-12 for comparison).

2. Even though the shape of the experimental curve in Figure 5-12 is similar to that for the finite element analysis, the finite element results are lower than those of the experiment by about 10 percent. This may be due to the difference of the Poisson's ratio between the analyses. The Poisson's ratio of the photoelastic material at the stress-freezing temperature is only slightly less than 0.5 while the finite element solution used 0.3. From a study for naturally grown surface crack, Smith and Kirby [48] reported that the influence of the elevated Poisson's ratio in the photoelastic experiment elevates SIF values by about 6 percent.
3. The normalized Mode I SIFs (K_I/K_{Io}) or normalized effective SIFs (K_{eff}/K_{Io}) at the maximum depth of the semi-circular cracks are generally about 50 percent lower than those of two-dimensional edge cracks (see Figures 5-13 and 5-14). Similar conclusion can be drawn from the Compendium of Stress Intensity Factors [9, p. 84 and p. 298]. Their prediction for the Mode I crack ($\beta=0^o$) are included in Figure 5-13.
4. When crack inclination, β, increases to 45^o, the reduction of K_I/K_{Io}, at the maximum depth of three-dimensional semi-circular surface cracks, is about 46 percent compared to that of a flat surface crack ($\beta=0^o$). The reduction of K_{eff}/K_{Io} for $\beta=45^o$ is 28 percent compared to that of the flat surface crack (see Figures 5-13 and 5-14).
5. The ratio of K_{II}/K_I in semi-circular surface cracks increases more rapidly than that of two-dimensional edge cracks when crack

inclination angle (β) increases. This might suggest that, with the increase of crack inclination angle, shear stresses at the crack tip of three-dimensional surface cracks develop more rapidly than for two-dimensional edge cracks (see Figure 5-15).

These conclusions are based on the experimental evidence. For Mixed Mode case, analytical/numerical solutions are not at present available. Since the experimental data provided here are for semi-circular cracks, which is a relatively simple geometry, the results from numerical or analytical solutions will, hopefully, be available soon.

VI. REFERENCES

1. C. P. Burger and A. S. Voloshin. "A new instrument for whole field stress analysis." I.S.A. Transactions, 22, No. 2 (1983), 85-95.

2. A. S. Voloshin and C. P. Burger. "Half-fringe photoelasticity: A new approach to whole field stress analysis." Experimental Mechanics, 23, No. 3 (1983), 304-313.

3. R. N. Kar. "Stress intensity factors in glass plates with edge cracks by half-fringe photoelasticity." M.S. Thesis, Iowa State University, Ames, Iowa, 1982.

4. T. H. Baek. "Analysis of the interacting effect of double surface cracks by three-dimensional photoelastic experiment." M.S. Thesis, Iowa State University, Ames, Iowa, 1984.

5. B. R. Koerner, C. P. Burger and T. H. Baek. "Fringe sharpening method by digital image processing system." Stress Analysis Laboratory, Department of Engineering Science and Mechanics, Iowa State University, Ames, Iowa, 1986. (unpublished paper).

6. R. J. Sanford. "Application of the least squares method to the photoelastic analysis." Experimental Mechanics, 20, No. 6 (1980), 192-197.

7. H. Tada, P. C. Paris and G. R. Irwin. The Stress Analysis of Cracks Handbook. Hellertown, Pennsylvania: Del Research Cooperation, 1973.

8. G. C. Sih. Handbook of Stress Intensity Factors for Researchers and Engineers. Bethlehem, Pennsylvania: Lehigh University, 1973.

9. D. P. Rooke and D. J. Cartwright. Compendium of Stress Intensity Factors. London, England: Her Majesty's Stationery Office, 1976.

10. D. G. Smith and R. B. Mullinix. Fracture Mechanics Design Handbook. Technical Report No. RL-77-5(AD A038457). U.S. Army Missile Command, Redstone Arsenal, Alabama, 1976.

11. C. E. Inglis. "Stress in a plate due to the presence of cracks and sharp corners." Transactions, Institutions of Naval Architects, 60 (March 1913), 219-230.

12. A. A. Griffith. "The phenomena of rupture and flow in solids." Philosophical Transactions, Royal Society of London, Series A, 221, No. 6 (March 1920), 163-198.

13 G. M. Boyd. "From Griffith to COD and beyond." Engineering Fracture Mechanics, 4, No. 3 (1972), 459-482.

14. H. M. Westergaard. "Bearing pressures and cracks." Journal of Applied Mechanics, Series A, 61 (1939), 49-53.

15. G. R. Irwin. "Analysis of stress and strains near the end of a crack traversing a plate." Journal of Applied Mechanics, 24 (September 1957), 361-364.

16. G. R. Irwin. Discussions of reference 17. Proceedings of Society for Experimental Stress Analysis, 16, No. 1 (1958), 93-96.

17. A. Wells and D. Post. "The dynamic stress distribution surrounding a running crack-A photoelastic analysis." Proceedings of Society for Experimental Stress Analysis, 16, No. 1 (1958), 69-92.

18. G. C. Sih. "On the Westergaard method of crack analysis." International Journal of Fracture Mechanics, 2, No. 4 (1966), 628-631.

19. J. Eftis and H. Liebowitz. "On the modified Westergaard equations for certain crack problems." International Journal of Fracture Mechanics, 8, No. 4 (1972), 383-392.

20. W. T. Evans and A. R. Luxmore. "Limitations of the Westergaard equations for experimental evaluations of stress intensity factors." Journal of Strain Analysis, 11, No. 3 (1976), 177-185.

21. R. J. Sanford. "A critical re-examination of the Westergaard method for solving opening-mode crack problem." Mechanics Research Communications, 6, No. 5 (1979), 289-294.

22. H. Liebowitz, J. D. Lee and J. Eftis. "Biaxial load effect in fracture mechanics." Engineering Fracture Mechanics, 10, No. 2 (1978), 315-335.

23. G. R. Irwin, D. B. Barker, R. J. Sanford, W. L. Fourney, J. T. Metcalf, A. Shukla and R. Chona. "Photoelastic studies of damping, crack propagation and crack arrest in polymers and 4340 steel." Technical Report No. NUREG/CR-1455. Division of Reactor Safety Research, Office of Nuclear Regulatory Commission, Washington, D.C., May 1980.

24. M. Cottron and A. Lagarde. "A far field method for the determination of Mixed-Mode stress intensity factors from isochromatic fringe patterns." Solid Mechanics Archives, 7, Issue 1 (March 1982), 1-18.

25. D. R. J. Owen and A. J. Fawkes. Engineering Fracture Mechanics-Numerical Methods and Applications. Swansea, England: Pineridge Press Limited, 1983.

26. M. L. Williams. "Stress singularities resulting from various boundary conditions in angular corners of plates in extension." Transactions of ASME, Journal of Applied Mechanics, 19 (1952), 526-528.

27. F. C. Karal and S. N. Karp. "Stress behavior in the neighborhood of sharp corners." Geophysics, 29, No. 3 (June 1964), 360-369.

28. M. L. Williams. "On the stress distribution at the base of a stationary crack." Journal of Applied Mechanics, 24 (1957), 109-114.

29. M. L. Williams. "The bending stress distribution at the base of a stationary crack." Journal of Applied Mechanics, 28, Series E, No. 1 (March 1961), 78-82.

30. A. E. Green and I. N. Sneddon. "The distribution of stress in the neighborhood of a flat elliptical crack in an elastic solid." Proceedings of the Cambridge Philosophical Society, 46 (1950), 159-163.

31. G. R. Irwin. "Crack-extension force for a part-through crack in a plate." Journal of Applied Mechanics, 29, Series E, No. 4 (1962), 651-654.

32. J. G. Merkle. "A review of some of the existing stress intensity factor solutions for part through surface crack." Technical Report No. ORNL-TM-3983. Oak Ridge National Laboratory, Oak Ridge, Tennessee, January 1973.

33. J. C. Newman, Jr. "A review and assessment of the stress intensity factors for surface cracks." Technical Report No. NASA-TM-78805. National Aeronautics and Space Administration, Langley Research Center, Hampton, Virginia, November 1978.

34. P. C. Paris and G. C. Sih. "Stress analysis of cracks." In Fracture Toughness and its Application, ASTM STP No. 381. Philadelphia, Pennsylvania: American Society for Testing and Materials, 1965, pp. 30-83.

35. F. W. Smith, A. F. Emery and A. S. Kobayashi. "Stress intensity factors for semi-circular cracks: Part 2, Semi-infinite solid." Journal of Applied Mechanics, 34, No. 4 (1967), 953-959.

36. A. S. Kobayashi and M. L. Moss. "Stress intensity magnification factors for surface-flawed tension plate and notched round tension bar." In Fracture 1969, Brighton, England: Chapman and Hall Publishing Company, 1969, pp. 31-35.

37. R. B. Anderson, A. G. Holmes and T. W. Orange. "Stress intensity magnification for deep surface cracks in sheets and plates." Technical Report No. NASA-TND-6504, October 1970.

38. J. C. Newman, Jr. "Fracture analysis of surface- and through-cracked sheets and plates." Engineering Fracture Mechanics, 5, No.3 (1973), 667-689.

39. R. C. Shah and A. S. Kobayashi. "On the surface flaw problem." In The surface crack: Physical problems and computational solutions. Edited by J. L. Swedlow. New York, New York: American Society of Mechanical Engineers, 1972, pp. 79-124.

40. T. K. Hellen and W. S. Blackburn. "Calculation of stress intensity factors in two- and three-dimensions using finite elements." In Computational Fracture Mechanics. Edited by E. F. Rybicki and S. E. Benzley, New York, New York: American Society of Mechanical Engineers, 1972, pp. 103.

41. A. S. Kobayashi. "Crack-opening displacement in a surface-flawed plate subjected to tension or plate bending." Proceedings of the Second International Conference on Mechanical Behavior of Materials, Metals Park, Ohio: American Society for Metals, 1976, pp. 1073-1077.

42. I. S. Raju and J. C. Newman,Jr. "Stress intensity factors for a wide range of semi-elliptical surface cracks in finite thickness plates." Engineering Fracture Mechanics, 11, No. 4 (1979), 817-829.

43. J. R. Rice and N. Revy. "The part through surface crack in an elastic plate." Journal of Applied Mechanics, 39, Series E, No. 1 (March 1972), 185-194.

44. J. Heliot, R. Labbens and A. Pellissier-Tanon. "Benchmark problem No. 1: Semi-elliptical surface crack." International Journal of Fracture, 15, No. 6 (December 1979), R197-R202.

45. T. A. Cruse. "Numerical evaluation of elastic S.I.F. by the boundary integral method." In The Surface Crack: physical problems and computational solutions. Edited by J. L. Swedlow. New York, New York: American Society for Mechanical Engineers, 1972, pp. 153-170.

46. H. Nisitani and Y. Murakami. "Stress intensity factors of an elliptical crack or a semi-elliptical crack subject to tension." International Journal of Fracture, 10, No. 3 (September 1974), 353-368.

47. M. Isida, H. Noguchi and Y. Yoshida. "Tension and bending of finite thickness plates with a semi-elliptical surface crack." International Journal of Fracture, 26, No. 3 (November 1984), 157-188.

48. C. W. Smith and G. C. Kirby. "Stress intensity distributions and width correction factors for natural cracks approaching 'Benchmark' crack depth." In Fracture Mechanics: Fifteenth Symposium, ASTM STP No. 833. Philadelphia, Pennsylvania: American Society for Testing and Materials, 1984, pp. 118-129.

49. C. W. Smith, D. Post and G. Nicoletto. "Experimental stress intensity distributions in three-dimensional cracked-body problems." Experimental Mechanics, 23, No. 4 (December 1983), 378-382.

50. Y. Phang and C. Ruiz. "Photoelastic determination of stress intensity factors for single and interacting cracks and comparison with calculated results, Part II: Three-dimensional problems." Journal of Strain Analysis, 19, No. 1 (1984), 35-41.

51. J. C. Newman, Jr. and I. S. Raju. "An empirical stress intensity factor equation for the surface crack." Engineering Fracture Mechanics, 15, No. 1~2 (1981), 185-192.

52. A. S. Kobayashi, A. F. Emery, N. Polvamah and W. J. Love. "Surface flaw in a thermally shocked hollow cylinder." In The 3rd International Conference on Structural Mechanics in Reactor Technology. Compiled by T. A. Jeager. New York, New York: American Elsevier, 1975, pp. 1-12.

53. K. Hayashi and H. Abe. "Stress intensity factors for a semi-elliptical crack in the surface of a semi-infinite solid." International Journal of Fracture, 16, No. 3 (June 1980), 275-285.

54. R. J. Hartranft and G. C. Sih. "Alternating method applied to edge and surface crack problems." Technical Report No. NASA-CR-112299, 1972.

55. J. J. McGowan, Ed. Benchmark Editorial Committee of the SESA Fracture Committee. "A critical evaluation of numerical solutions to the 'Benchmark' surface flaw problem." Experimental Mechanics, 20, No. 8 (1980), 253-264.

56. F. W. Smith and D. R. Sorensen. "Mixed mode stress intensity factors for semi-elliptical surface cracks." Technical Report No. NASA CR-134684. National Aeronautics and Space Administration, Lewis Research Center, Cleveland, Ohio, June 1974.

57. C. W. Smith, W. H. Peters and A. T. Andonian. "Mixed mode stress intensity distributions for part circular surface flaws." Engineering Fracture Mechanics, 13, No. 3 (1979), 615-629.

58. D. Post. "Photoelastic stress analysis for an edge crack in a tensile field." Proceedings of Society for Experimental Stress Analysis, 12, No. 1 (1954), 99-196.

59. N. S. Murthy and P. R. Rao. "Photoelastic determination of mode I stress intensity factor in tensile strips: Effects of crack length." Engineering Fracture Mechanics, 20, No. 3 (1984), 475-478.

60. W. B. Bradley and A. S. Kobayashi. "An investigation of propagating cracks by dynamic photoelasticity." Experimental Mechanics, 19, No. 3 (1970), 106-113.

61. W. B. Bradley and A. S. Kobayashi. "Fracture dynamics: A photoelastic investigation." Engineering Fracture Mechanics, 3, No. 3 (1971), 317-332.

62. M. A. Schroedl and C. W. Smith. "Local stresses near deep surface flaws under cylindrical fields." In Progress in Flaw Growth and Fracture Toughness Testing, ASTM STP No. 536. Philadelphia, Pennsylvania: American Society for Tesing and Materials, 1973, pp. 45-47.

63. M. A. Schroedl, J. J. McGowan and C. W. Smith. "An assessment factors including data obtained by the photoelastic stress freezing technique for stress fields near crack tips." Engineering Fracture Mechanics, 4, No. 4 (1972), 801-809.

64. C. W. Smith. "Photoelasticity in fracture mechanics." Experimental Mechanics, 20, No. 11 (1980), 390-396.

65. C. W. Smith and J. S. Epstein. "An assessment of far field effects on the photoelastic determination of mixed mode stress intensity factors." Engineering Fracture Mechanics, 16, No. 5 (1982), 605-612.

66. P. S. Theocaris and A. A. Gdoutos. "A photoelastic determination of K_I stress intensity factors." Engineering Fracture Mechanics, 7, No. 2 (1975), 331-339.

67. E. E. Gdoutos and P. S. Theocaris. "A photoelastic determination of mixed mode stress intensity factors." Experimental Mechanics, 18, No. 3 (1978), 87-96.

68. C. W. Smith and O. Olaosebikan. "Use of mixed mode stress intensity algorithms by photoelastic data." Experimental Mechanics, 24, No. 4 (1984), 300-307.

69. A. S. Redner. "Experimental determination of stress intensity factors - A review of photoelastic approaches." In Fracture Mechanics and Technology 1. Edited by G. C. Sih and C. L. Chow. Alphen aan den Rijn, The Netherlands: Sijthoff and Noordhoff International Publishers, 1977, pp. 607-622.

70. C. Ruiz and Y. P. Phang. "Stress intensity for interacting flaws - Part 3: Photoelastic determination of mixed mode stress intensity factors for interacting flaws." Technical Report No. O.U.E.L. No. 1368/81. University of Oxford, Oxford, England, 1981.

71. Y. P. Phang and C. Ruiz. "Photoelastic determination of stress intensity factors for single and interacting cracks and comparison with calculated results. Part 1: 2-dimensional problems." Journal of Strain Analysis, 19, No. 1 (1984), 23-34.

72. J. Morton and C. Ruiz. "Photoelasticity in the assessment of structural integrity." Experimental Mechanics, 22, No. 2 (1982), 210-215.

73. R. J. Sanford and J. W. Dally. "Stress intensity factors in the third-stage fan disk of the TF-30 turbine engines." Technical Report No. NRL-8202. Naval Research Laboratory, Washington, D.C., 1978.

74. R. J. Sanford and J. W. Dally. "A general method for determining mixed mode stress intensity factors from isochromatic fringe patterns." Engineering Fracture Mechanics, 11, No. 4 (1979), 621-633.

75. J. M. Etheridge and J. W. Dally. "A three-parameter method for determining stress intensity factors from isochromatic fringe loops." Journal of Strain Analysis, 13, No. 2 (1978), 91-94.

76. H. P. Rossmanith. "A hybrid technique for improved K determination from photoelastic data." Experimental Mechanics, 23, No. 2 (1983), 152-157.

77. H. P. Rossmanith. "Convergence-aspects of K determination procedures." In Applications of Fracture Mechanics to Materials and Structures. Edited by G. C. Sih, E. Sommer and W. Dahl. Boston, Massachusetts: Martinus Nijhoff Publishers, 1984, pp. 725-737.

78. L. Banks-Sills and M. Arcan. "An edge cracked mode II fracture specimen." Experimental Mechanics, 23, No. 3 (1983), 257-261.

79. M. Ramulu, A. S. Kobayashi and D. B. Barker. "Analysis of dynamic mixed mode isochromatics." Experimental Mechanics, 25, No. 5 (1985), 344-353.

80. R. K. Muller and L. Saackel. "Complete automatic analysis of photoelastic fringes." Presented at the 1978 SESA Spring Meeting, Wichita, Kansas, May 1978.

81. C. P. Burger, T. H. Baek and A. S. Voloshin. "Half Fringe Photoelasticity determines K-factors for double cracks by stress freezing." Presented at SECTAM XII - The Southern Conference on Theoretical and Applied Mechanics, Auburn University, Alabama, 1984.

82. T. H. Baek, C. P. Burger and A. S. Voloshin. "Stress intensity factors for interacting semi-circular surface cracks." In Proceedings of the V International Congress on Experimental Mechanics, Brookfield Center, Connecticut: Society for Experimental Stress Analysis, 1984, pp. 751-757.

83. C. L. Tsai and S. K. Park. "Determination of stress intensity factors of fillet welded T-joints by computer assisted photoelasticity." Experimental Mechanics, 24, No. 3 (1984), 233-242.

84. S. P. Timoshenko and J. N. Goodier. Theory of Elasticity. 3rd edition. New York, New York: McGraw-Hill Book Company, 1970.

85. K. Hellan. Introduction to Fracture Mechanics. New York, New York: McGraw-Hill Book Company, 1984.

86. P. Zhang and C. P. Burger. "Stress intensity factors for edge cracks under transient thermal stresses by photoelasticity." In Proceedings of the 1985 SEM Conference on Experimental Mechanics, Brookfield Center, Connecticut: Society for Experimental Mechanics, 1985, pp. 907-915.

87. C. W. Smith, J. J. McGowan and M. Jolles. "Effects of artificial cracks and Poisson's ratio upon photoelastic stress intensity determination." Experimental Mechanics, 16, No. 5 (1976), 188-193.

88. EyeCom II Handbook. Second edition. Goleta, California: Spatial Data System, Inc., 1980.

89. Program Bank. Stress Analysis Laboratory, Department of Engineering Science and Mechanics, Iowa State University, Ames, Iowa, 1986.

90. R. L. Burden, J. D. Faires and A. C. Reynolds. Numerical Analysis. 2nd edition. Boston, Massachusetts: Prindle, Weber & Schmidt, 1981.

91. L. W. Johnson and D. R. Riess. Numerical Analysis. 2nd edition. Reading, Massachusetts: Addison-Wesley Publishing Company, 1982.

92. J. B. Kennedy and A. M. Neville. Basic Statistical Methods for Engineers and Scientists. 2nd edition. New York, New York: Harper & Row Publishers, Inc., 1976.

93. Preparation manual for 3DMU-050 photoelastic material, Stress Strain Laboratories, Dallas, Texas, 1985.

94. J. Cernosek. "Three dimensional photoelasticity by stress freezing." Experimental Mechanics, 20, No. 12 (1980), 417-426.

95. J. Cernosek. "Fast curing photoelastic materials-processing and properties." In Proceedings of the V International Congress on Experimental Mechanics, Brookfield Center, Connecticut: Society for Experimental Stress Analysis, 1984, pp. 677.

96. R. L. Johnson. "Model making and slicing for three dimensional photoelasticity." Experimental Mechanics, 9, No. 3 (1969), 23N-32N.

97. C. W. Smith and M. Jolles. "Stress intensities in deep surface flaws in plates under mode I loading." In Development in Theoretical and Applied Mechanics. Edited by R. P. McNitt. Blacksburg, Virginia: Virginia Polytechnique Institute and State University, 1976, pp. 151-160.

98. P. S. Theocaris. "Interactions of cracks with other cracks or boundaries." International Journal of Fracture Mechanics, 8, No. 1 (1972), 37-47.

99. J. W. Dally and W. F. Riley. Experimental Stress Analysis. Second edition. New York, New York: McGraw-Hill Book Company, 1978.

100. E. G. Coker and L. N. G. Filon. A Treatise on Photoelasticity. London, England: Cambridge University Press, 1931.

101. A. Kuske and G. Robertson. Photoelastic Stress Analysis. New York, New York: John Wiley and Sons, Inc., 1974.

102. M. M. Frocht. Photoelasticity. Vols. No. 1 and No. 2. New York, New York: John Wiley and Sons, Inc., 1941.

103. L. W. Zachary. "Displacement discontinuity method applied to nondistructive testing related stress problems." International Journal for Numerical Methods in Engineering, 18, No. 8 (1982), 1231-1244.

104. D. G. Smith and C. W. Smith. "Photoelastic determination of mixed-mode stress intensity factors." Engineering Mechanics, 18, No. 3 (1978), 87-96.

105. D. Post. "Isochromatic fringe sharpening and fringe multiplication in photoelasticity." Proceedings of the Society for Experimental Stress Analysis, 12, No. 2 (1955), 143-156.

VII. ACKNOWLEDGEMENTS

It is wonderful to have achieved this final goal. This small miracle was possible only because God's invisible agency helped me pursue this study.

First, I wish to express my sincere gratitude to my major professor, Dr. Christian P. Burger, for his kind guidance and unending encouragement throughout the program of study. Besides providing countless help, Dr. Burger has impressed on my memory his untiring efforts to make my unrefined style of writing worthy of a dissertation regardless of his busy schedule to move to a new place of employment. The valuable experience from this research could not have been gained if not for his supervision.

I would like to thank Dr. Loren W. Zachary, Dr. Thomas J. Rudolphi, Dr. Thomas D. McGee, Dr. Otto Buck and Dr. Ibrahim Miskioglu for their advice and service as my committee members. I am also grateful to Dr. Thomas R. Rogge, Dr. David M. Martin and Dr. Bruce R. Thompson for their agreeing to serve as substitute committee members without any hesitation when some original members were not available during the final examination.

Special thanks are extended to Mr. Thomas J. Elliott for his technical assistance, to Mr. Bruce H. Koerner for his constructive suggestions on programming, to John T. McConnell and technicians in the ERI machine shop for preparing experimental models, and to all my colleagues, including Mr. Krishnaswamy Kumar, Daniel Tarudji and James A. Smith, for their assistance.

The financial support from the Department of Engineering Science and Mechanics and the Engineering Research Institute of Iowa State University is gratefully acknowledged.

Most importantly, I would like to express my appreciation to my wife, Gil-Sung, for her sacrifice and patient effort in caring for my two sons, Seung-Gyou and Seung-Whan, during my course of study. Constant faith in me and encouragement from my mother and sisters also can never be forgotten.

This dissertation is dedicated to my late father, Mr. Do-Sung Baek, who devoted his whole life to his son's education.

VIII. APPENDIX: PROGRAMS

A. Data Collection Program BCOL2

```
      PROGRAM BCOL2
C  ------------------------------------------------------------------------
C
C  DATA COLLECTION PROGRAM
C  ----------------------
C
C  Program BCOL2 collects photoelastic data for the stress analysis of a
C  crack tip. Photoelastic data include Fringe order(Fn), Radial distance(r)
C  from the crack tip and Polar angle(theta) for 40 points. "r" and "theta"
C  are collected from fringe sharpened lines under Joystick control. Fringe
C  order(Fn) at data point should be entered manually. Crack tip data (crack
C  tip location and its direction) and photoelatic data(Fn,r,theta) can be
C  stored on the data files provided by a user.
C  ------------------------------------------------------------------------
C
C  Updated  by Tae Hyun BAEK (20-Dec-1985)
C  Modified by Tae Hyun BAEK (14-Oct-1985)
C  Source : Program CLMN2 written by Ibrahim Miskioglu
C  ------------------------------------------------------------------------
C
C  FORT: BCOL2
C  LINK: BCOL2,SY:(TVLIB,IMLIB,FORLIB)
C
C  BCOL2 calls the following subroutines:
C      From TVLIB.OBJ - OFF, ON, RECKON
C      From IMLIB.OBJ - ROUTE
C      From BCOL2.FOR - COLMAN
C
C  File Locations:
C      TVLIB.OBJ, IMLIB.OBJ, FORLIB.OBJ - DISK "EyeCom II"
C      BCOL2.FOR, BCOL2.SAV -DISK "G Disk"
C  ------------------------------------------------------------------------
C
C  Variables used:
C      DATA(I,1) : Polar angle in radians
C      DATA(I,2) : Radial distance in inches
C      DATA(I,3) : Fringe order
C      JNAME     : File name to store photoelastic data
C      ANS       : Answer by <Y> or <N>
C  ------------------------------------------------------------------------
C
       REAL*4  DATA(40,3)
       LOGICAL*1 JNAME(15)
       LOGICAL*1 ANS
C
C Store image to prepare data collection.
C
       TYPE *,' '
       TYPE *,'  PROGRAM BCOL2'


       TYPE *,' '
       TYPE *,' '
       TYPE *,'   Fringe order and position data is collected manual
      &ly using the'
       TYPE *,'   Joystick cursor.  Data is stored in a file on the
      & users floppy disk .'
801    TYPE *,' '
```

```
      TYPE *,'  Do you want to store the image ? ... <Y> or <N>..'
      TYPE *,' '
      TYPE *,'  CAUTION -- If you have already used the program TRACE
     & do not store'
      TYPE *,'  the image again.'
      READ(5,500)ANS
      IF(ANS.EQ.'N')GO TO 50! to start data collection
      IF(ANS.NE.'Y'.AND.ANS.NE.'N')GO TO 801! to go to the question
      TYPE *,'  '
      TYPE *,'    Position the specimen to show the crack and its'
      TYPE *,'vicinity to store the image on TD:...'
      TYPE *,'  '
C
C Call system subroutines to store the image
C
      CALL OFF('P')
      CALL ON ('S')
      CALL ROUTE
C
C Reset real time processor
C
      CALL RECKON("250)! processed image = image from camera
50    CALL ON ('P')
C
C Start to collect data
C
      TYPE *,'  '
      TYPE *,' Data is collected at 40 points ...'
      TYPE *,'  '
      N=40
      K=0
200   K=K+1
      CALL COLMAN(N,K,DATA)
80    TYPE *,'INPUT the name of the file to store the data.'
      TYPE *,'  '
      READ(5,550,ERR=80)JNAME
      DO 30 I=1,N
         DATA(I,3)=DATA(I,3)-IMIN
30    IF(DATA(I,3).LT.0.0)DATA(I,3)=0.0
C
      OPEN(UNIT=2,NAME=JNAME,TYPE='NEW',ERR=80)
C
      DUMMY=0.0
      WRITE(2,1000)N,DUMMY
1000  FORMAT(I4,F6.1)
      DO 10 I=1,N
10       WRITE(2,2000) (DATA(I,KK),KK=1,3)
2000  FORMAT(3F15.5)
C
      CLOSE(UNIT=2)
C
      WRITE(7,600)JNAME
C
100   TYPE *,' '
      TYPE *,' Do you want to collect data again ?..'
      TYPE *,' ..... Type <Y> or <N> ..............'
      READ(5,500,ERR=100)ANS
      IF(ANS.EQ.'Y')GO TO 200
      IF(ANS.NE.'Y'.AND.ANS.NE.'N')GO TO 100
500   FORMAT(A)
550   FORMAT(15A1)
600   FORMAT(/,5X,'   Data stored in File = ',15A1,//)
      GO TO 999
C
99    STOP '  BAD FILE OPEN'
999   STOP
      END
```

```
      SUBROUTINE COLMAN(N,K,A)
C  ------------------------------------------------------------------------
C
C  This subroutine collects data from TD(EyeCom II) by calling the subroutine
C  RADPOL. 40 data points (fringe order, radial distance, polar angle) are
C  collected at a crack tip manually using the Joystick cursor. Program TRACE
C  can be used prior to using this subroutine to sharpen the isochromatic
C  fringes. Crack tip data and its direction, and scaling factor are setup
C  by this routine.
C  ------------------------------------------------------------------------
C
C  Modified by: Tae Hyun BAEK       26-Nov-85
C  Written by : Ibrahim Miskioglu   26-Jul-85
C  ------------------------------------------------------------------------
C
C  Subroutine calls the following subroutines:
C      From TVLIB.OBJ - COORD, ON, OFF
C      From BCOL2.FOR - CIRCLE, RADPOL
C
C  File Locations:
C      TVLIB.OBJ - DISK "EyeCom II"
C      BCOL2.FOR - DISK "G Disk"
C  ------------------------------------------------------------------------
C
C  Variables used:
C      N = Number of data points (40)
C      K = Index number, i.e., K=1,2,...,40
C      A(N,3) = Output array, i.e.,
C         A(N,1) = Polar angle in radians
C         A(N,2) = Radial distance in inches
C         A(N,3) = Fringe order
C      IXTIP,IYTIP = Crack tip coordinates
C      IXDIR,IYDIR = Coordinates of the points to indicate the crack direction
C  ------------------------------------------------------------------------
C
       COMMON /GIN/IXTIP,IYTIP,IXDIR,IYDIR
       COMMON /GRE/XT,YT,XD,YD,PI
C
       REAL*4  A(N,3)
       LOGICAL*1 INAME(15),ANS
C
       PI=4.*ATAN(1.)
C
C Store the information of crack length, scaling factor, crack tip coodinates
C and its direction.
C
       IF(K.GT.1)GO TO 50
810    TYPE *,' '
       TYPE *,' INPUT the crack length (inches).'
       READ(5,*,ERR=810)CRL
812    TYPE *,' '
       TYPE *,'Length scaling factor (inches).'
       READ(5,*,ERR=812)RDIS! real distance
       CALL OFF('P')! shut off the digitized image temporarily
       CALL ON ('S')! return to the image shown by video camera
       TYPE *,' '
       TYPE *,' ******     Calculate the length scale        ******'
       TYPE *,' '
       TYPE *,' Point to the first known point  and type <RETURN>..'
       PAUSE
       CALL COORD(I1,I2)
       TYPE *,' '
       A11=FLOAT(I1)
       A22=FLOAT(I2)
       TYPE *,' Point to the second known point and type <RETURN>..'
       PAUSE
```

```
      CALL COORD(I1,I2)
      TYPE *,' '
      B11=FLOAT(I1)
      B22=FLOAT(I2)
      PDIS=SQRT((A11-B11)**2+(A22-B22)**2)! distance on the image
      TYPE *,' Distance between the two points for scaling =',PDIS
      FAC=RDIS/PDIS       ! Length scaling factor ( inches/pixel )
C
C Setup the crack tip coordinates and its direction
C
      TYPE *,' '
      TYPE *,'Show crack tip and type <RETURN>..'
      PAUSE
      CALL COORD(IXT,IYT)
        IXTIP=IXT-2! crack tip x coordinate in traced image
        IYTIP=IYT-2! crack tip y coordinate in traced image
      TYPE *,' '
      TYPE *,'Crack tip',IXTIP,IYTIP
      TYPE *,' '
      TYPE *,' Show crack direction and type <RETURN>..'
      PAUSE
      CALL COORD(IXD,IYD)
        IXDIR=IXD-2! x coord. in traced image
        IYDIR=IYD-2! y coord. in traced image
      TYPE *,' '
      TYPE *,'Crack direction',IXDIR,IYDIR
      TYPE *,' '
      CALL ON('P')! return to the digitised image
C
      XT=FLOAT(IXTIP)
      YT=FLOAT(IYTIP)
      XD=FLOAT(IXDIR)

      YD=FLOAT(IYDIR)
C
      DEN=SQRT((XD-XT)**2+(YD-YT)**2)
      COSB=(XD-XT)/DEN
      SINB=(YD-YT)/DEN
      IF(COSB)20,30,20
20    TANB=ATAN2(SINB,COSB)
      BR=TANB
      GO TO 40
30    BR=PI/2.
      IF(YT.GT.YD)BR=-BR
40    BD=BR*180./PI
      TYPE *,'   Angle BETA =',BD
C
804   TYPE *,' '
      TYPE *,' '
      TYPE *,'  Do you want to store the information on the '
      TYPE *,'  coordinate set at the crack tip on a file ?.'
      TYPE *,'  ..... <Y> or <N>.....'
      TYPE *,' '
      READ(5,802)ANS
      IF(ANS.EQ.'N')GO TO 48
      IF(ANS.NE.'Y'.AND.ANS.NE.'N')GO TO 804
802   FORMAT(A1)
803   TYPE *,' '
      TYPE *,' INPUT new file name to store the information'
      TYPE *,'       on the coordinate set at the crack tip.'
      TYPE *,' '
      READ(5,801,ERR=803)INAME
801   FORMAT(15A1)
```

```
C
C Open file to store crack tip coordinates and its direction, crack length
C and scaling factor.
C
      OPEN(UNIT=2,NAME=INAME,TYPE='NEW',ERR=803)
      WRITE(2,100)IXTIP,IYTIP,IXDIR,IYDIR
      WRITE(2,200)XT,YT,XD,YD,CRL,COSB,SINB,BR
      WRITE(2,300)RDIS,PDIS
C
      CLOSE(UNIT=2)
C
      GO TO 50
48    DO 449 I=1,14
449   INAME(I)='-'
C
50    TYPE *,' '
C
C This routine is for establishing the data collection region by entering
C min r/a and indicating max r/a on TD.....
C
      TYPE *,'To establish the data collection region'
      TYPE *,' '
900   TYPE *,'Enter the min of r/a'
      READ(5,*,ERR=900) ROA!ROA=r/a
      CALL ERASER
      CALL ON ('G')
      CALL ON ('P')
C
      CALL CIRCLE(IXTIP,IYTIP,CRL,FAC,ROA)
C
      TYPE *,' '
      TYPE *,' '
      TYPE *,'To draw the circle for max r/a on TD.....'
      TYPE *,' '
      TYPE *,' '
      TYPE *,'Point to the desired point and type <RETURN>...'
      PAUSE
      CALL COORD(IX,IY)
      TYPE *,' '
      X11=FLOAT(IX)
      Y11=FLOAT(IY)
      X1=FLOAT(IXTIP)
      Y1=FLOAT(IYTIP)
      RMS=SQRT((X1-X11)**2+(Y1-Y11)**2)!max radius on TD
      ROA=(RMS*FAC)/CRL
      TYPE *,' '
      TYPE *,'max r/a on TD=',ROA
C
      CALL CIRCLE(IXTIP,IYTIP,CRL,FAC,ROA)
C
C End of drawing inner and outer circles for data collection
C
      TYPE *,' '
C
C Call subroutine RADPOL to collect photoelastic data(N, r, and theta)
C
      CALL RADPOL(N,A,COSB,SINB,FAC,BR)
C
      WRITE(7,800)INAME
800   FORMAT(5X,/,'  File name for the coord. set : ',15A1)
100   FORMAT(4I4)
200   FORMAT(8F10.5)
300   FORMAT(2F15.8)
C
      RETURN
      END
```

```
      SUBROUTINE RADPOL(N,A,COSB,SINB,FAC,BR)
C ---------------------------------------------------------------------
C
C Subroutine RADPOL collects N=40 points of photoelastic data(Fn, r, theta)
C manually for the crack tip stress analysis and returns them to the
C subroutine COLMAN.
C ---------------------------------------------------------------------
C
C Updated by Tae Hyun BAEK      (26-Nov-1985)
C Written by Ibrahim Miskioglu (26-Jul-1985)
C ---------------------------------------------------------------------
C
C Subroutine RADPOL calls the following subroutines:
C     From TVLIB.OBJ - ON, LINE, COORD
C
C File Locations:
C    TVLIB.OBJ - DISK "EyeCom II"
C ---------------------------------------------------------------------
C
      COMMON /GIN/IXT,IYT,IXD,IYD
      COMMON /GRE/XT,YT,XD,YD,PI
C
      LOGICAL*1 ANS
      REAL*4 A(N,3)
C
50    CALL ON ('G')
      CALL LINE(1,IXD,IYD,IXT,IYT)
      TYPE *,' '
      TYPE *,'****    START COLLECTING DATA    ***'
      TYPE *,' '
      DO 200 I=1,N
      IP=I
      TYPE *,' '
      TYPE *,'   Data number :',IP
      TYPE *,'  '
      TYPE *,'   Move the cursor to a point on a fringe and type <RET
     &URN>'
      PAUSE
      CALL COORD(IX1,IY1)
C
C Record the collected data point on the screen
C
      CALL LINE(1,IX1,IY1-3,IX1,IY1+3)
      CALL LINE(1,IX1-3,IY1,IX1+3,IY1)
C
      X1=FLOAT(IX1)
      Y1=FLOAT(IY1)
201   TYPE *,' '
      TYPE *,'  ENTER the fringe order. '
      READ(5,*,ERR=201)A(IP,3)
      XP=(X1-XT)*COS(PI+BR)+(Y1-YT)*SIN(PI+BR)
      YP=-(X1-XT)*SIN(PI+BR)+(Y1-YT)*COS(PI+BR)
      IF(XP.EQ.0)GO TO 58
      TT=ATAN2(YP,XP)
      GO TO 55
58    TT=PI/2.
      IF(YP.LT.0.0)TT=-PI/2.
55    A(IP,1)=TT
      R=SQRT(XP**2+YP**2)    ! Radial distance in pixels
      A(IP,2)=R*FAC          ! Radial distance in inches
200   CONTINUE
      TYPE *,' '
      TYPE *,' '
      TYPE *,'    DATA COLLECTION IS COMPLETED.'
      TYPE *,' '
      TYPE *,' '
```

```
500     TYPE *,' '
        TYPE *,'  Do you want to change the data points ?..'
        TYPE *,'..... Type <Y> or <N> .....'
        READ(5,150)ANS
        IF(ANS.EQ.'Y')GO TO 50
        IF(ANS.NE.'Y'.AND.ANS.NE.'N')GO TO 500
150     FORMAT(A)
C
        RETURN
        END



        SUBROUTINE CIRCLE(IXTIP,IYTIP,CRL,FAC,ROA)
C ---------------------------------------------------------------------------
C
C Subroutine CIRCLE draws a circle from a given crack tip to limit data
C collection region. Crack tip coordinates(IXTIP,IYTIP), crack length(CRL),
C scaling factor(FAC) and r/a(ROA) should be provided.
C ---------------------------------------------------------------------------
C
C Written by Tae Hyun BAEK (26-Nov-1985)
C ---------------------------------------------------------------------------
C
C Subroutine CIRCLE calls the following subroutine:
C     From TVLIB.OBJ - LINE
C
C File Location:
C     TVLIB.OBJ - DISK "EyeCom II"
C ---------------------------------------------------------------------------
C
        PHI=4.*ATAN(1.0)
        RAC=ROA*CRL! actual radius
        RTD=RAC/FAC! radius on TD
        ANG=0.
        X1=FLOAT(IXTIP)
        IX1=INT(X1+RTD+0.5)
        IY1=IYTIP
C
C Draw a circle on the scean
C
        DO 100 I=1,360
          IQ=I
          ALPH=PHI/180.*FLOAT(IQ)
          XB=RTD*COS(ANG+ALPH)+FLOAT(IXTIP)
          YB=RTD*SIN(ANG+ALPH)+FLOAT(IYTIP)
          IX2=INT(XB+0.5)
          IY2=INT(YB+0.5)
          CALL LINE(1,IX1,IY1,IX2,IY2)
          IX1=IX2
          IY1=IY2
100     CONTINUE
C
        RETURN
        END
```

B. Data Analysis Program WIL4

```
      PROGRAM WIL4
C ------------------------------------------------------------------------------
C
C  DATA ANALYSIS PROGRAM
C  ---------------------
C  WIL4(PROGRAM NAME)=Williams equations with 4-terms(n=1,2,3,4). Program WIL4
C  calculates the origin of crack tip (Xo,Yo) and SEVEN coefficients(A1,B1,A2,
C  A3,B3,A4,B4) from the series type stress components expanded by Williams
C  stress function by using a least squares method coupled with Newton-
C  Raphson's iterative technique. This program requires photoelastic data
C  file (fringe order, radial distance from the crack tip and polar angle),
C  for 40 points, generated by data collection program BCOL2. To run this
C  program, model thickness(TH), material fringe value(FC), allowance
C  error(ER), max. number of iterations should be provided. Results of
C  coefficients and crack tip deviation(Xo,Yo) will be stored in the data
C  file(FTN##.DAT) to make back-plot. To estimate reasonable guesses of
C  coefficients, one may need to run program WIL2.
C ------------------------------------------------------------------------------
C
C  Revised by Tae Hyun BAEK (24-DEC-1985)
C  Written by Tae Hyun BAEK (24-NOV-1985)
C ------------------------------------------------------------------------------
C
C  FORT : WIL4
C  LINK : WIL4,SY:(BLIB,FORLIB)
C
C  WIL4 calls the following subroutines:
C      From WIL4.FOR - SIF
C
C  File Locations:
C      BLIB.OBJ, FORLIB.OBJ - DISK "EyeCom II"
C      WIL4.FOR, WIL4.SAV - DISK "Q Disk"
C ------------------------------------------------------------------------------
C
       LOGICAL*1 ANS
       REAL*4 T(40),R(40),SN(40),S(9),SDM(9)
       REAL*4 A1(5),A2(5),A3(5),A4(5)
       REAL*4 B1(5),B3(5),B4(5)
       REAL*4 XO(5),YO(5)
       REAL*4 SK1(5),SK2(5),SOX(5)
       INTEGER*2 IN(5),JJI(5)
C
       PHI=3.141592654
C
       TYPE *,' '
       TYPE *,'....40 data points ...'
       TYPE *,' '
       TYPE *,'INPUT Model thickness & Material fringe constant'
         READ(5,*)TH,FC


       TYPE *,' '
       TYPE *,'INPUT Allowable error & Max. no. of iterations'
         READ(5,*)ER,MA
       TYPE *,' '
       TYPE *,' INPUT estimates of K1,K2,SOX'
         READ(5,*) FK1,FK2,FSO
C
       SDM(1)=FK1/SQRT(2.0*PHI)!  estimate of A1
       SDM(2)=FK2/SQRT(2.0*PHI)!  estimate of B1
       SDM(3)=-FSO/4.0!           estimate of A2
       DO 80 I=4,9
         SDM(I)=0.0!          all other estimates
80     CONTINUE
```

```
C
      DO 90 I=1,9
        S(I)=SDM(I)
90    CONTINUE
C
      TYPE *,' '
      TYPE *,'   INPUT the file number to store SIF results.'
      TYPE *,' '
        READ(5,*) JJK
C
      IFK=0
C
100   TYPE *,'INPUT the data file number -- 2 digits'
        READ(5,*) JJ
C
      OPEN (UNIT=JJ,TYPE='OLD',ERR=100)
C
        IFK=IFK+1
        JJI(IFK)=JJ
C
        READ(JJ,*) N,TINC! N=no. of data, TINC=angle increment
C
        DO 120 I=1,N
          READ(JJ,*) T(I),R(I),SN(I)
120     CONTINUE
C
      CLOSE(UNIT=JJ)
C
C Call subroutine SIF to calculate the coefficients and crack tip deviation
C
      CALL SIF(N,T,R,SN,TH,FC,ER,MA,S,E1,INO)
C
      WRITE(7,10)JJ,TINC
10      FORMAT(//,' FILE NUMBER=',I3,10X,'ANGLE INCREMENT=',F6.1/)
C
      WRITE(7,20) (I,S(I),I=1,9)
20      FORMAT('  S(',I1,')=',F16.8)
C
      A1(IFK)=S(1)
      B1(IFK)=S(2)
      A2(IFK)=S(3)
      A3(IFK)=S(4)
      B3(IFK)=S(5)
      A4(IFK)=S(6)
      B4(IFK)=S(7)
      X0(IFK)=S(8)
      Y0(IFK)=S(9)
C
      SK1(IFK)=S(1)*SQRT(2.0*PHI)
      SK2(IFK)=S(2)*SQRT(2.0*PHI)
      SOX(IFK)=-S(3)*4.0
C
      WRITE(7,25) SK1(IFK),SK2(IFK),SOX(IFK)
25      FORMAT(//,' K1  =',F16.8,/,' K2  =',F16.8,/,' Sox =',F16.8)
C
      IN(IFK)=INO
C
200   TYPE *,'  '
      TYPE *,'  Do you want to run the program again ? '
        READ(5,30)ANS
30        FORMAT(A)
        IF(ANS.EQ.'Y')GO TO 100
        IF(ANS.NE.'Y'.AND.ANS.NE.'N') GO TO 200
C
      IFC=IFK
```

```
C
C Store the results in the file for back-plot and statistical check
C
      OPEN(UNIT=JJK,TYPE='NEW',ERR=99)
C
      DO 300 I=1,IFK
        IF(IN(I).EQ.0)IFC=IFC-1
300   CONTINUE
C
      WRITE(JJK,40)IFC
40      FORMAT(I4)
C
      DO 400 I=1,IFK
        WRITE(JJK,50)JJI(I),A1(I),B1(I),A2(I)
50        FORMAT(I3,3(F13.6,1X))
        WRITE(JJK,55) A3(I),B3(I),A4(I),B4(I)
55        FORMAT(3X,4(F13.6,1X))
        WRITE(JJK,56) XO(I),YO(I)
56        FORMAT(3X,2(F13.6,1X))
        WRITE(JJK,60) SK1(I),SK2(I),SOX(I)


60        FORMAT(3X,3(F13.6,1X))
        WRITE(JJK,65) TH,FC
65        FORMAT(3X,2(F13.6,1X))
400   CONTINUE
C
      CLOSE(UNIT=JJK)
C
      GO TO 999
99    STOP 'BAD OPEN FILE'
999   STOP
      END



      SUBROUTINE SIF(N,T,R,SN,TH,FC,ER,MA,S,E1,INO)
C  ------------------------------------------------------------------------
C
C  From the given data provided by main program WIL4, subroutine SIF
C  calculates the origin of crack tip (XO,YO) and the coefficients(A1,B1,A2,
C  A3,B3,A4,B4) of the stress components expanded from Williams stress
C  function by a least squares method coupled with Newton-Raphson's iterative
C  technique.
C ------------------------------------------------------------------------
C
C  Revised by Tae Hyun BAEK (24-Dec-1985)
C  Written by Tae Hyun BAEK (19-Nov-1985)
C ------------------------------------------------------------------------
C
C  Subroutine SIF calls the following subroutines:
C      From WIL4.FOR - STRESS
C      From BLIB.OBJ - AMPLY, GAUS, RESCOR
C
C  File Locations:
C      WIL4.FOR, WIL4.SAV - DISK "G Disk"
C      BLIB.OBJ - DISK "EyeCom II"
C  ------------------------------------------------------------------------
C
       COMMON /COF/A1,B1,A2,A3,B3,A4,B4,XO,YO
       COMMON /DAT/RM,TM,FN
       COMMON /OUT/GEE,DA1G,DB1G,DA2G,DA3G,DB3G,DA4G,DB4G,DXOG,DYOG
C
```

```
      REAL*4 T(N),R(N),SN(N),S(9)
      REAL*4 SAV(9),G(40),D(9),X(9)
      REAL*4 C(9,9),A(40,9),W(9,40),CS(9,9),DSS(9)
C
C No computation on the material fringe value
C
      INO=1
C
      WRITE(7,10) TH,ER,N,MA
10      FORMAT('  Thick.=',F5.3,' Err.=',F9.7,' N=',I2,' MA=',I4)
C
C << Calculate stress components and partial derivatives of Function>>
C << GEE from subroutine STRESS.....>>
C
      DO 100 I=1,7
        S(I)=S(I)*TH/FC! normalize the coefficients
100   CONTINUE
C
      M=1
160   E1=0
C
      DO 200 I=1,9


        SAV(I)=S(I)
200   CONTINUE
C
      WRITE(7,20) M
20      FORMAT(' ** Iteration No.=',I3)
C
C Substitute variables to call STRESS
C
      A1=S(1)
      B1=S(2)
      A2=S(3)
      A3=S(4)
      B3=S(5)
      A4=S(6)
      B4=S(7)
      XO=S(8)
      YO=S(9)
C
C Generate iterative function GEE and matrix [A] including partial
C derivatives with respect to the coefficients and Xo and Yo by calling
C subroutine STRESS
C
      DO 250 I=1,N
          RM=R(I)!    radial coordinate
          TM=T(I)!    polar angle
          FN=SN(I)!   fringe order
        CALL STRESS
          G(I)=GEE
          A(I,1)=DA1G
          A(I,2)=DB1G
          A(I,3)=DA2G
          A(I,4)=DA3G
          A(I,5)=DB3G
          A(I,6)=DA4G
          A(I,7)=DB4G
          A(I,8)=DXOG
          A(I,9)=DYOG
        E1=E1+G(I)*G(I)
250   CONTINUE
```

```
C
C Generate a transpose of [A], i.e., [W]=transpose of [A]
C
      DO 300 I=1,9
        DO 300 J=1,N
          W(I,J)=A(J,I)
300   CONTINUE
C
C Call subroutine AMPLY to generate square matrix, i.e.,
C [C]=[W]x[A]
C
      CALL AMPLY(W,A,C,9,N)
C
C Calculate for [W]{G}={D}
C
      DO 350 I=1,9
        D(I)=0.0
        DO 350 K=1,N
          D(I)=D(I)+W(I,K)*G(K)
350   CONTINUE
C
C  To change matrices as {D}={DSS}, [C]=-[C] and [CS]=[C]
C
      DO 400 I=1,9
        DSS(I)=D(I)
        DO 400 J=1,9
          C(I,J)=-C(I,J)
          CS(I,J)=C(I,J)
400   CONTINUE
C
C Call subroutine GAUSS to solve the system [C]{X}={D}
C
      CALL GAUS(C,D,X,9,IERROR)
        TYPE *,' IERROR=',IERROR
C
C Call subroutine RESCOR to refine an approximate solution, {X}, to the
C system [CS]{X}={DSS}
C
      CALL RESCOR(CS,DSS,X,9,15)
C
C Add delta quantities, {X}, to the previous estimates, {S}.
C
      DO 500 I=1,9
        S(I)=S(I)+X(I)
500   CONTINUE
C
      WRITE(7,30) (J,S(J),J=1,9)
30      FORMAT('  S(',I1,')=',F16.6)
C
      X1=ABS(X(1))
      X2=ABS(X(2))
      X3=ABS(X(3))
      X4=ABS(X(4))
      X5=ABS(X(5))
      X6=ABS(X(6))
      X7=ABS(X(7))
      X8=ABS(X(8))
      X9=ABS(X(9))
C


C Check the conditions on which the corrections are acceptably small
C
      IF(X1.LE.ER.AND.X2.LE.ER.AND.X3.LE.ER.AND.X4.LE.ER.AND.
     &X5.LE.ER.AND.X6.LE.ER.AND.X7.LE.ER.AND.X8.LE.ER.AND.X9.
     &LE.ER) GO TO 560
```

```
C
      M=M+1
      IF(M.LE.MA)GO TO 160
C
      INO=0
      TYPE *,'    NO CONVERGENCE WITHIN THE SPECIFIED NO OF ITER.'
C
      DO 550 I=1,9
        S(I)=(S(I)+SAV(I))/2.0
550   CONTINUE
C
      WRITE(7,40) (I,X(I),I=1,9)
40      FORMAT('  X(',I1,')=',F16.8)
C
560   DO 600 I=1,7
        S(I)=S(I)*FC/TH
600   CONTINUE
C
      WRITE(7,*) 'RELATIVE ERROR=',E1
C
      RETURN
      END


      SUBROUTINE STRESS
C  ------------------------------------------------------------------------
C
C  Subroutine STRESS expresses the stress components of Williams 4 terms of
C  equations, generates iterative function GEE, and also evaluates partial
C  derivatives of function GEE with respect to A1,B1,A2,A3,B3,A4,B4,XO and
C  YO. All the coefficients are provided by subroutine SIF.
C  ------------------------------------------------------------------------
C
C       Written by Tae Hyun BAEK (25-Nov-1985)
C  ------------------------------------------------------------------------
C
      COMMON /COF/A1,B1,A2,A3,B3,A4,B4,XO,YO
      COMMON /DAT/RM,TM,FN
      COMMON /OUT/GEE,DA1G,DB1G,DA2G,DA3G,DB3G,DA4G,DB4G,DXOG,DYOG
C
      PHI=3.141592654
C
      X=XO+RM*COS(TM)
      Y=YO+RM*SIN(TM)
C
      RE=SQRT(X*X+Y*Y)
C
      IF(X) 100,200,100
100     TE=ATAN2(Y,X)
        GO TO 300
200   TE=PHI/2.0
        IF(Y.LT.0.0) TE=-PHI/2.0
C
300   SQ1=1./SQRT(RE)
      SQ2=SQRT(RE)
C
      C05=COS(0.5*TE)
      C10=COS(1.0*TE)
      C15=COS(1.5*TE)
      C20=COS(2.0*TE)
      C25=COS(2.5*TE)
      C30=COS(3.0*TE)
C
```

```
      S05=SIN(0.5*TE)
      S10=SIN(1.0*TE)
      S15=SIN(1.5*TE)
      S20=SIN(2.0*TE)
      S25=SIN(2.5*TE)
      S30=SIN(3.0*TE)
C
C  Radial stress component calculation
C
        RA1=1.25*C05-0.25*C15


        RB1=-1.25*S05+0.75*S15
        RA2=2.0+2.0*C20
        RA3=2.25*C05+0.75*C25
        RB3=2.25*S05+3.75*S25
        RA4=2.0*C10+8.0*C30
        RB4=2.0*S10+2.0*S30
C
        RS1=A1*RA1+B1*RB1
        RS2=A2*RA2
        RS3=A3*RA3+B3*RB3
        RS4=A4*RA4+B4*RB4
C
      RS=SQ1*RS1+RS2+SQ2*RS3+RE*RS4
C
C Tansential stress component calculation
C
        TA1=0.75*C05+0.25*C15
        TB1=-0.75*S05-0.75*S15
        TA2=2.0-2.0*C20
        TA3=3.75*C05-0.75*C25
        TB3=3.75*S05-3.75*S25
        TA4=6.0*C10-8.0*C30
        TB4=8.0*S10-2.0*S30
C
        TS1=A1*TA1+B1*TB1
        TS2=A2*TA2
        TS3=A3*TA3+B3*TB3
        TS4=A4*TA4+B4*TB4
C
      TS=SQ1*TS1+TS2+SQ2*TS3+RE*TS4
C
C Shear stress component calculation
C
        SA1=0.25*S05+0.25*S15
        SB1=0.25*C05+0.75*C15
        SA2=-2.0*S20
        SA3=0.75*S05-0.75*S25
        SB3=-0.75*C05+3.75*C25
        SA4=2.0*S10-8.0*S30
        SB4=-2.0*C10+2.0*C30
C
        SS1=A1*SA1+B1*SB1
        SS2=A2*SA2
        SS3=A3*SA3+B3*SB3
        SS4=A4*SA4+B4*SB4
C
      SS=SQ1*SS1+SS2+SQ2*SS3+RE*SS4
C
C  Partial differentiation loop
C
      DXOR=X/RE
      DYOR=Y/RE
      DXOT=-Y/(RE*RE)
      DYOT=X/(RE*RE)
```

```
C
      DXOSG1=(-0.5/RE**1.5)*DXOR
      DYOSG1=(-0.5/RE**1.5)*DYOR
C
      DXOSG2=(0.5/SQRT(RE))*DXOR
      DYOSG2=(0.5/SQRT(RE))*DYOR
C
C  Partial differentiation of the stresses with respect to XO
C
        DRA1=-0.625*S05+0.375*S15
        DRB1=-0.625*C05+1.125*C15
        DRA2=-4.0*S20
        DRA3=-1.125*S05-1.875*S25
        DRB3=1.125*C05+9.375*C25
        DRA4=-2.0*S10-18.0*S30
        DRB4=2.0*C10+6.0*C30
C
        DXORA1=DRA1*DXOT
        DXORB1=DRB1*DXOT
        DXORA2=DRA2*DXOT
        DXORA3=DRA3*DXOT
        DXORB3=DRB3*DXOT
        DXORA4=DRA4*DXOT
        DXORB4=DRB4*DXOT
C
        RX1=DXOSG1*(A1*RA1+B1*RB1)
        RX2=SG1*(A1*DXORA1+B1*DXORB1)
        RX3=A2*DXORA2
        RX4=DXOSG2*(A3*RA3+B3*RB3)
        RX5=SG2*(A3*DXORA3+B3*DXORB3)
        RX6=DXOR*(A4*RA4+B4*RB4)
        RX7=RE*(A4*DXORA4+B4*DXORB4)
C
      DXORS=RX1+RX2+RX3+RX4+RX5+RX6+RX7
C
        DTA1=-0.375*S05-0.375*S15
        DTB1=-0.375*C05-1.125*C15
        DTA2=4.0*S20
        DTA3=-1.875*S05+1.875*S25
        DTB3=1.875*C05-9.375*C25
        DTA4=-6.0*S10+18.0*S30
        DTB4=6.0*C10-6.0*C30
C
        DXOTA1=DTA1*DXOT


        DXOTB1=DTB1*DXOT
        DXOTA2=DTA2*DXOT
        DXOTA3=DTA3*DXOT
        DXOTB3=DTB3*DXOT
        DXOTA4=DTA4*DXOT
        DXOTB4=DTB4*DXOT
C
        TX1=DXOSG1*(A1*TA1+B1*TB1)
        TX2=SG1*(A1*DXOTA1+B1*DXOTB1)
        TX3=A2*DXOTA2
        TX4=DXOSG2*(A3*TA3+B3*TB3)
        TX5=SG2*(A3*DXOTA3+B3*DXOTB3)
        TX6=DXOR*(A4*TA4+B4*TB4)
        TX7=RE*(A4*DXOTA4+B4*DXOTB4)
C
      DXOTS=TX1+TX2+TX3+TX4+TX5+TX6+TX7
C
```

```
            DSA1=0.125*C05+0.375*C15
            DSB1=-0.125*S05-1.125*S15
            DSA2=-4.0*C20
            DSA3=0.375*C05-1.875*C25
            DSB3=0.375*S05-9.375*S25
            DSA4=2.0*C10-18.0*C30
            DSB4=2.0*S10-8.0*S30
C
            DXOSA1=DSA1*DXOT
            DXOSB1=DSB1*DXOT
            DXOSA2=DSA2*DXOT
            DXOSA3=DSA3*DXOT
            DXOSB3=DSB3*DXOT
            DXOSA4=DSA4*DXOT
            DXOSB4=DSB4*DXOT
C
            SX1=DXOSG1*(A1*SA1+B1*SB1)
            SX2=SG1*(A1*DXOSA1+B1*DXOSB1)
            SX3=A2*DXOSA2
            SX4=DXOSG2*(A3*SA3+B3*SB3)
            SX5=SG2*(A3*DXOSA3+B3*DXOSB3)
            SX6=DXOR*(A4*SA4+B4*SB4)
            SX7=RE*(A4*DXOSA4+B4*DXOSB4)
C
          DXOSS=SX1+SX2+SX3+SX4+SX5+SX6+SX7
C
C  Partial differentiation of the stresses with respect to YO
C
            DYORA1=DRA1*DYOT
            DYORB1=DRB1*DYOT
            DYORA2=DRA2*DYOT
            DYORA3=DRA3*DYOT
            DYORB3=DRB3*DYOT
            DYORA4=DRA4*DYOT
            DYORB4=DRB4*DYOT
C
            RY1=DYOSG1*(A1*RA1+B1*RB1)
            RY2=SG1*(A1*DYORA1+B1*DYORB1)
            RY3=A2*DYORA2
            RY4=DYOSG2*(A3*RA3+B3*RB3)
            RY5=SG2*(A3*DYORA3+B3*DYORB3)
            RY6=DYOR*(A4*RA4+B4*RB4)
            RY7=RE*(A4*DYORA4+B4*DYORB4)
C
          DYORS=RY1+RY2+RY3+RY4+RY5+RY6+RY7
C
            DYOTA1=DTA1*DYOT
            DYOTB1=DTB1*DYOT
            DYOTA2=DTA2*DYOT
            DYOTA3=DTA3*DYOT
            DYOTB3=DTB3*DYOT
            DYOTA4=DTA4*DYOT
            DYOTB4=DTB4*DYOT
C
            TY1=DYOSG1*(A1*TA1+B1*TB1)
            TY2=SG1*(A1*DYOTA1+B1*DYOTB1)
            TY3=A2*DYOTA2
            TY4=DYOSG2*(A3*TA3+B3*TB3)
            TY5=SG2*(A3*DYOTA3+B3*DYOTB3)
            TY6=DYOR*(A4*TA4+B4*TB4)
            TY7=RE*(A4*DYOTA4+B4*DYOTB4)
C
          DYOTS=TY1+TY2+TY3+TY4+TY5+TY6+TY7
C
```

```
            DYOSA1=DSA1*DYOT
            DYOSB1=DSB1*DYOT
            DYOSA2=DSA2*DYOT
            DYOSA3=DSA3*DYOT
            DYOSB3=DSB3*DYOT
            DYOSA4=DSA4*DYOT
            DYOSB4=DSB4*DYOT
C
            SY1=DYOSQ1*(A1*SA1+B1*SB1)
            SY2=SQ1*(A1*DYOSA1+B1*DYOSB1)
            SY3=A2*DYOSA2
            SY4=DYOSQ2*(A3*SA3+B3*SB3)
            SY5=SQ2*(A3*DYOSA3+B3*DYOSB3)
            SY6=DYOR*(A4*SA4+B4*SB4)
            SY7=RE*(A4*DYOSA4+B4*DYOSB4)
C
          DYOSS=SY1+SY2+SY3+SY4+SY5+SY6+SY7


C
C  Iterative function, GEE, and partial derivatives of GEE with respect to
C  A1,B1,A2,A3,B3,A4,B4,XO,YO
C
          DS=RS-TS
          GEE=DS*DS+4.0*SS*SS-FN*FN
C
          DS2=2.0*DS
          SS8=8.0*SS
C
          DA1G=DS2*SQ1*(RA1-TA1)+SS8*SQ1*SA1
          DB1G=DS2*SQ1*(RB1-TB1)+SS8*SQ1*SB1
          DA2G=DS2*(RA2-TA2)+SS8*SA2
          DA3G=DS2*SQ2*(RA3-TA3)+SS8*SQ2*SA3
          DB3G=DS2*SQ2*(RB3-TB3)+SS8*SQ2*SB3
          DA4G=DS2*RE*(RA4-TA4)+SS8*RE*SA4
          DB4G=DS2*RE*(RB4-TB4)+SS8*RE*SB4
          DXOG=DS2*(DXORS-DXOTS)+SS8*DXOSS
          DYOG=DS2*(DYORS-DYOTS)+SS8*DYOSS
C
          RETURN
          END
```

C. Back-plot Program BPOW4

```
      PROGRAM BPOW4
C  ------------------------------------------------------------------------
C
C  BACK-PLOT PRGRAM
C  ----------------
C  Program BPOW4 is the back-plot program which uses four terms of Williams
C  stress function, i.e.,n=1,2,3,4, or seven coefficients (A1,B1,A2,A3,B3,
C  A4,B4) produced by program WIL4. The crack tip location is corrected by Xo
C  and Yo from the original estimated one. To make a back plot, the followins
C  data files should be provided.
C
C       Data collection file: FTN**.DAT (senerated by program BCOL2)
C                             ** should be specified by 2-digits
C       Crack tip data file : Complete file name (senerated by program BCOL2)
C       SIF data file       : FTN**.DAT (senerated by program WIL4)
C                             ** should be specified by 2-digits
C
C  Program BPOW4 can make a back-plot for qualitative comparison between the
C  data points and resenerated frinses. For quantitative comparison, this
C  program can also yield statistical parameters, such as percentase error
C  at each data point, standard deviation of the percentase errors and
C  correlation coefficient between the data points and resenerated frinses
C  at those points.
C  ------------------------------------------------------------------------
C
C  Updated  by Tae Hyun BAEK (29-Dec-1985)
C  Modified by Tae Hyun BAEK (28-Dec-1985)
C  Revised  by Tae Hyun BAEK (21-Dec-1985)
C  Written  by Tae Hyun BAEK (30-Nov-1985)
C  ------------------------------------------------------------------------
C
C  FORT : BPOW4
C  LINK : BPOW4,SY:(FORLIB,TVLIB,BLIB)
C
C  BPOW4 calls the following subroutines:
C      From BPOW4.FOR - TRFORM, FPLOT
C      From TVLIB.OBJ - ERASER, ON, LINE
C
C  File Locations:
C      TVLIB.OBJ, FORLIB.OBJ, BLIB.OBJ - DISK "EyeCom II"
C      BPOW4.FOR, BPOW4.SAV - DISK "Q Disk"
C  ------------------------------------------------------------------------
C
       COMMON /GIN/NXT,NYT,NXD,NYD
       COMMON /ASF/BR,RDIS,PDIS,PHI,RFAC,CRL
       COMMON /DAT/FS,H,A1,B1,A2,A3,B3,A4,B4
C
       LOGICAL*1 INAME(15)
       REAL*4 T(40),R(40),FN(40)


C
       CALL ERASER
       CALL ON ('G')
C
       PHI=3.141592654
C
C To restore crack tip coordinates and its direction, and scaling factor
C
10     TYPE *,' '
       TYPE *,'Enter the file name to restore the crack tip data'
       TYPE *,' '
```

```
          READ(5,100,ERR=10) INAME
100       FORMAT(15A1)
C
         OPEN(UNIT=2,NAME=INAME,TYPE='OLD',ERR=10)
           READ(2,*) IXT,IYT,IXD,IYD
           READ(2,*) XT,YT,XD,YD,CRL,COSB,SINB,BR
           READ(2,*) RDIS,PDIS
         CLOSE(UNIT=2)
C
         RFAC=PDIS/RDIS! magnification factor
C
C To restore data file of coefficients, SIF values, crack tip deviation,
C model thickness and material fringe value
C
20       TYPE *,' '
         TYPE *,' Enter the FILE NO which has SIF results <2 digit>'
         TYPE *,' '
           READ(5,*) JJ
C
         OPEN(UNIT=JJ,TYPE='OLD',ERR=20)
           READ(JJ,*) NS ! no. of data set
           READ(JJ,*) NF,A1,B1,A2! NF:data file no.(n,r,t)
           READ(JJ,*) A3,B3,A4,B4
           READ(JJ,*) XO,YO
           READ(JJ,*) SK1,SK2,SOX
           READ(JJ,*) H,FS
         CLOSE(UNIT=JJ)
C
C To account for the deviation of crack tip origin from the originally
C estimated one.
C
        IXO=INT(XO*RFAC+0.5)! X dev. of crack tip in PD
        IYO=INT(YO*RFAC+0.5)! Y dev. of crack tip in PD
        NXT=IXT-IXO
        NYT=IYT-IYO
        NXD=IXD-IXO
        NYD=IYD-IYO
C
        CALL LINE(1,IXT,IYT,IXD,IYD)!  measured crack line
        CALL LINE(1,NXT,NYT,NXD,NYD)!  corrected crack line
C
C To restore the data file of fringe data (theta,radius, fringe order)
C
30       TYPE *,' '
         TYPE *,' To restore the data(theta,radius,fr.order) file '
         TYPE *,' '
         TYPE *,' Please the FILE NO--2 DIGITS--------------------'
         TYPE *,' '
           READ(5,*) IFD
C
        OPEN(UNIT=IFD,TYPE='OLD',ERR=30)
          READ(IFD,*) N,DUMMY
          DO 200 I=1,N
            READ(IFD,*) TM,RM,FN(I)
            XM=RM*COS(TM)
            YM=RM*SIN(TM)
C
C To set data point from the crack tip on the screen
C
             CALL TRFORM(XM,YM,XE,YE)
C
               IXP=IXT+INT(XE*RFAC+0.5)
               IYP=IYT+INT(YE*RFAC+0.5)
C
```

```
C To recover the data points on the screen
C
            CALL LINE(1,IXP-3,IYP,IXP+3,IYP)
            CALL LINE(1,IXP,IYP-3,IXP,IYP+3)
C
C Calculation of corrected radius R(I) and theta T(I)
C
            X=XM+XO
            Y=YM+YO
            R(I)=SQRT(X*X+Y*Y)
            IF(X) 210,220,210
210         T(I)=ATAN2(Y,X)
              GO TO 200
220         T(I)=PHI/2.0
              IF(Y.LT.0.0) T(I)=-PHI/2.0
200       CONTINUE
        CLOSE(UNIT=IFD)
C
C Print all the information produced by program WIL4
C
        WRITE(5,300) H,FS,CRL,A1,B1,A2,A3,B3,A4,B4,SK1,SK2,SOX,XO,YO
        WRITE(6,300) H,FS,CRL,A1,B1,A2,A3,B3,A4,B4,SK1,SK2,SOX,XO,YO
300     FORMAT(/,

     &' SIF ANALYSIS PROGRAM : WIL4',/,
     &' ----------------------------',///,
     &' [ MODEL SPECIFICATION      ]',//,
     &'   THICKNESS OF MODEL(inch)----------------------',F13.4,/,
     &'   MATERIAL FRINGE VALUE(lb/fr-in)---------------',F13.4,/,
     &'   CRACK LENGTH(inch)----------------------------',F13.4,//,
     &' [ CALCULATED COEFFICIENTS  ]',//,
     &'   A( 1) =',F13.4,/,
     &'   B( 1) =',F13.4,/,
     &'   A( 2) =',F13.4,/,
     &'   A( 3) =',F13.4,/,
     &'   B( 3) =',F13.4,/,
     &'   A( 4) =',F13.4,/,
     &'   B( 4) =',F13.4,//,
     &' [ STRESS INTENSITY FACTORS ]',//,
     &'   K 1    =',F13.4,/,
     &'   K 2    =',F13.4,/,
     &'   Sox    =',F13.4,//,
     &' [ DEVIATION OF CRACK TIP   ]',//,
     &'   X o    =',F13.5,/,
     &'   Y o    =',F13.5)
C
C To make a back-plot and statistical check
C
        CALL FPLOT(N,T,R,FN)
C
        STOP
        END


        SUBROUTINE FPLOT(N,T,R,FN)
C  ------------------------------------------------------------------------
C
C  Subroutine FPLOT makes a back-plot and statistical check between the data
C  points and resenerated fringes at data points. The callins program should
C  provide the followins informations:
C
C      N         : Number of data points
C      T(I)      : Polar anale of data point
C      R(I)      : Radial distance of data point from the crack tip
```

```
C       FN(I)     : Fringe order at data point
C       BR        : Crack inclination angle on the screen
C       RDIS      : Real distance, i.e., inch, between two points indicated
C       PDIS      : Distance on the screen by pixels between two points
C                   indicated
C       PHI       : 3.141592654
C       RFAC      : Scaling factor (RFAC=PDIS/RDIS)
C       CRL       : Crack length
C       IX1,IY1,IX2,IY2 : Crack tip coordinates and its direction
C  ------------------------------------------------------------------------------
C
C  Updated by Tae Hyun BAEK (28-Dec-1985)
C  Written by Tae Hyun BAEK (30-Nov-1985)
C  ------------------------------------------------------------------------------
C
C  Subroutine FrLOT calls the following subroutines:
C       TVLIB.OBJ - CURSOR, LINE, ERASER, ON
C       BPOW4.FOR - CIRCLE, TRIGO, CONST, TRFORM, ECORD
C       BLIB.OBJ  - PLROOT, CHECK
C
C  File Locations:
C       TVLIB.OBJ, BLIB.OBJ - DISK "EyeCom II"
C       BPOW4.FOR, BPOW4.SAV - DISK "G Disk"
C  ------------------------------------------------------------------------------
C
        COMMON /ASF/BR,RDIS,PDIS,PHI,RFAC,CRL
        COMMON /WIN/IX1,IY1,IX2,IY2
C
        LOGICAL*1 ANS
        REAL*4 A(7),RT(6)
        REAL*4 T(40),R(40),FN(40)
C
C Selection of routine for back plot or deviation check
C
30      TYPE *,' '
        TYPE *,'Please enter 1 if you want to make a back plot      '
        TYPE *,'--------------'
        TYPE *,'Or      enter 0 if you want to check the deviation  '
        TYPE *,'--------------'


        TYPE *,'between REGENERATED & EXPERIMENTAL fringes !        '
        TYPE *,' '
          READ(5,*,ERR=30) IANS
C
        IF(IANS.EQ.0) GO TO 190
        IF(IANS.NE.0.AND.IANS.NE.1) GO TO 30
C
C       Generate the window to limit the region for back-plotting
C
        TYPE *,'Locate the Joystick to the left upper corner of the'
        TYPE *,' '
        TYPE *,'window you want to make and type <BS>.............'
          CALL CURSOR(IX1,IY1)
        TYPE *,' '
        TYPE *,'Locate the Joystick to the right below corner of the'
        TYPE *,' '
        TYPE *,'window you want to make and type <BS>.............'
          CALL CURSOR(IX2,IY2)
C
        CALL LINE(1,IX1,IY1,IX2,IY1)
        CALL LINE(1,IX1,IY1,IX1,IY2)
        CALL LINE(1,IX1,IY2,IX2,IY2)
        CALL LINE(1,IX2,IY1,IX2,IY2)
```

```
C
C This routine makes two circles of min. and max. of r/a to see the collected
C data location by scale. These two circles do not indicate data collection
C region.
C
40      TYPE *,' '
        TYPE *,'Please enter the min. & max. of r/a to see the data'
        TYPE *,' '
        TYPE *,'collection region.
        TYPE *,' '
          READ(5,*) RAMIN,RAMAX
C
        RMIN=RAMIN*CRL
        CALL CIRCLE(RMIN)
C
        RMAX=RAMAX*CRL
        CALL CIRCLE(RMAX)
C
C Routine for back-plotting of fringe loops
C
50      TYPE *,' '
        TYPE *,'Enter the fringe order you want to plot'
        TYPE *,' '
        READ(5,*) FON
C
        ALPA=0.0
60      RDN=(PHI/180.0)*ALPA
        IF(ALPA.GE.0.0.AND.ALPA.LE.180.0) GO TO 150
70      TYPE *,' '
        TYPE *,'Do you want to plot for another fr order <Y> or <N>?'
        TYPE *,' '
        READ(5,100) ANS
100     FORMAT(A)
        IF(ANS.EQ.'Y') GO TO 50
        IF(ANS.NE.'Y'.AND.ANS.NE.'N') GO TO 70
          GO TO 180
C
150     AP=RDN
        CALL TRIGO(AP,P1,Q1,P2,Q2,P3,Q3,P4,Q4)
        CALL CONST(FON,P1,Q1,P2,Q2,P3,Q3,P4,Q4,A)
C
          NP=6
          ERROR=0.00001
          MITER=500
        CALL PLROOT(NP,A,ERROR,MITER,NR,RT)
          IF(NR.EQ.0) GO TO 160
          CALL CHECK(NR,RT,ERDP,IFLAG)
C
        IF(IFLAG.EQ.0) GO TO 160
          XP=ERDP*COS(AP)
          YP=ERDP*SIN(AP)
        CALL TRFORM(XP,YP,X2P,Y2P)
        CALL ECORD(X2P,Y2P,IX2P,IY2P,JFLAG)
        IF(JFLAG.EQ.0) GO TO 160
        CALL LINE(1,IX2P,IY2P)
C
160     AM=-RDN
        CALL TRIGO(AM,P1,Q1,P2,Q2,P3,Q3,P4,Q4)
        CALL CONST(FON,P1,Q1,P2,Q2,P3,Q3,P4,Q4,A)
C
          NP=6
          ERROR=0.00001
          MITER=500
        CALL PLROOT(NP,A,ERROR,MITER,NR,RT)
          IF(NR.EQ.0) GO TO 170
          CALL CHECK(NR,RT,ERDM,IFLAG)
```

```
C
        IF(IFLAG.EQ.0) GO TO 170
          XM=ERDM*COS(AM)
          YM=ERDM*SIN(AM)
        CALL TRFORM(XM,YM,X2M,Y2M)
        CALL ECORD(X2M,Y2M,IX2M,IY2M,JFLAG)
        IF(JFLAG.EQ.0) GO TO 170
        CALL LINE(1,IX2M,IY2M)
C


170     ALPA=ALPA+1.0
        GO TO 60
C
C Statistical check between data points and regenerated fringes at data
C points
C
180     TYPE *,' '
        TYPE *,'Do you want to get the differences between the  '
        TYPE *,' '
        TYPE *,'regenerated and experimental fringes ?          '
        TYPE *,' '
        TYPE *,'Please type <Y> or <N>..................... '
        TYPE *,' '
          READ(5,80) ANS
80        FORMAT(A)
C
        IF(ANS.EQ.'Y') GO TO 190
        IF(ANS.NE.'Y'.AND.ANS.NE.'N')GO TO 180
          GO TO 999
C
C  Generation of window for plot of deviation between regenerated and
C  experimental fringes at data points
C
190     CALL ERASER
        CALL ON('G')
C
        CALL LINE(1,60,60,552,60)
        CALL LINE(1,60,60,60,360)
        CALL LINE(1,60,360,552,360)
        CALL LINE(1,552,60,552,360)
C
        CALL LINE(1,60,210,552,210)
C
C  Generation of scale plot at the window lines
C
        DO 500 I=60,540,12
          IX=I
          CALL LINE(1,IX,60,IX,63)
          CALL LINE(1,IX,360,IX,357)
500     CONTINUE
C
        DO 600 I=60,360,30
          IY=I
          CALL LINE(1,60,IY,63,IY)
          CALL LINE(1,549,IY,552,IY)
600     CONTINUE
C
C Print statistical table
C
        WRITE(6,84) "14! start to print on the new page
84      FORMAT('0',A1)
C
```

```
      WRITE(5,85)
      WRITE(6,85)
85    FORMAT(/,
     &' BACK PLOT PROGRAM : BPOW4',/,
     &' ---------------------------',/,
     &' [ INPUT DATA TABLE ]',//,
     &' NO      R-DIST      THETA     N(exp)     N(rea)    % ERROR')
C
      SX=0.0
      SY=0.0
      SXY=0.0
      SSX=0.0
      SSY=0.0
C
      SUM=0.0
      SSUM=0.0
C
      DO 700 I=1,N
        REX=R(I)
        ANG=T(I)
        FON=FN(I)
        CALL TRIGO(ANG,P1,Q1,P2,Q2,P3,Q3,P4,Q4)
        CALL FRINGE(REX,P1,Q1,P2,Q2,P3,Q3,P4,Q4,RFN)
C
        SX=SX+FON
        SSX=SSX+FON*FON
        SY=SY+RFN
        SSY=SSY+RFN*RFN
        SXY=SXY+FON*RFN
C
        DIFR=RFN-FON
        PERR=(DIFR/FON)*100.0
C
        SUM=SUM+PERR
        SSUM=SSUM+PERR*PERR
C
        Y=3.0*PERR
        IY=210-INT(Y+0.5)
        IX=60+I*12
C
        ID=I
C
        CALL LINE(1,IX-3,IY,IX+3,IY)
        CALL LINE(1,IX,IY-3,IX,IY+3)
C
        THETA=(180.0/PHI)*ANG


C
        WRITE(5,95) ID,REX,THETA,FON,RFN,PERR
        WRITE(6,95) ID,REX,THETA,FON,RFN,PERR
95      FORMAT(1X,I2,3X,F8.5,3X,F7.2,3X,F7.4,3X,F7.4,3X,F7.2)
C
700   CONTINUE
C
      DN=FLOAT(N)
      AVR=SUM/DN
      VAR=(SSUM-(SUM*SUM)/DN)/(DN-1.0)!Variance
      SDV=SQRT(VAR)!standard deviation
C
      WRITE(6,770) '14
770   FORMAT('$',A1)
C
```

```
      WRITE(5,800) DN,AVR,VAR,SDV
      WRITE(6,800) DN,AVR,VAR,SDV
800   FORMAT(//,' [ DEVIATION TABLE ]',//,
     &' Number of Data Point--------------------------------',F10.4,/,
     &' Average Deviation between Nexp & Nres in Percent--',F10.4,/,
     &' Variance between Nexp & Nres in Percent-----------',F10.4,/,
     &' Standard Deviation of Percentage error------------',F10.4)
C
      C1=DN*SXY-SX*SY
      C2=SQRT((DN*SSX-SX*SX)*(DN*SSY-SY*SY))
C
      IF(C2.EQ.0.0) GO TO 999
        COR=C1/C2
        WRITE(5,850) COR
        WRITE(6,850) COR
850     FORMAT(/,
     &' Correlation between Nexp & Nres-------------------',F10.4)
C
999   RETURN
      END


      SUBROUTINE TRIGO(G,P1,Q1,P2,Q2,P3,Q3,P4,Q4)
C  ------------------------------------------------------------------------
C
C  Subroutine TRIGO calculates the constant terms of radial, tangential and
C  shear stress components for a given angle(G). The calling program should
C  provide the following variables:
C
C      G                      : Polar angle
C      A1,B1,A2,A3,B3,A4,B4 : Coefficients of Williams equations with 4 terms
C
C  TRIGO returns the followings:
C
C      P1,Q1 : Constants of 1/sqrt(r) terms
C      P2,Q2 : Constants of constant terms
C      P3,Q3 : Constants of sqrt(r) terms
C      P4,Q4 : Constants of (r) terms
C  ------------------------------------------------------------------------
C
C  Written by Tae Hyun BAEK (30-Nov-1985)
C  ------------------------------------------------------------------------
C
      COMMON /DAT/FS,H,A1,B1,A2,A3,B3,A4,B4
C
      C05=COS(0.5*G)
      C10=COS(1.0*G)
      C15=COS(1.5*G)
      C20=COS(2.0*G)
      C25=COS(2.5*G)
      C30=COS(3.0*G)
C
      S05=SIN(0.5*G)
      S10=SIN(1.0*G)
      S15=SIN(1.5*G)
      S20=SIN(2.0*G)
      S25=SIN(2.5*G)
      S30=SIN(3.0*G)
C
C Constants of radial stress component for a given angle
C
      RA1=1.25*C05-0.25*C15
      RB1=-1.25*S05+0.75*S15
      RA2=2.0+2.0*C20
```

```
      RA3=2.25*C05+0.75*C25
      RB3=2.25*S05+3.75*S25
      RA4=2.0*C10+6.0*C30
      RB4=2.0*S10+2.0*S30
C
C Constants of tangential stress component for a given angle
C
      TA1=0.75*C05+0.25*C15
      TB1=-0.75*S05-0.75*S15
      TA2=2.0-2.0*C20
      TA3=3.75*C05-0.75*C25
      TB3=3.75*S05-3.75*S25
      TA4=6.0*C10-6.0*C30
      TB4=6.0*S10-2.0*S30
C
C Constants of shear stress component for a given angle
C
      SA1=0.25*S05+0.25*S15
      SB1=0.25*C05+0.75*C15
      SA2=-2.0*S20
      SA3=0.75*S05-0.75*S25
      SB3=-0.75*C05+3.75*C25
      SA4=2.0*S10-6.0*S30
      SB4=-2.0*C10+2.0*C30
C
C Calculate constants for (radial stress-tangential stress) and shear stress
C for 1/sqrt(r), constant, sqrt(r) and (r) terms
C
      P1=A1*(RA1-TA1)+B1*(RB1-TB1)
      P2=A2*(RA2-TA2)
      P3=A3*(RA3-TA3)+B3*(RB3-TB3)
      P4=A4*(RA4-TA4)+B4*(RB4-TB4)
C
      Q1=A1*SA1+B1*SB1
      Q2=A2*SA2
      Q3=A3*SA3+B3*SB3
      Q4=A4*SA4+B4*SB4
C
      RETURN
      END


      SUBROUTINE CONST(FN,P1,Q1,P2,Q2,P3,Q3,P4,Q4,C)
C  ---------------------------------------------------------------------
C
C  Subroutine CONST calculates the constants of polynomial equation of
C  sqrt(r). The calling program must provide the following variables:
C
C      FN, FS, H : Fringe order, material fringe value and thickness of the
C                  model respectively
C      P1,Q1     : Constants of 1/sqrt(r)  terms for a given angle
C      P2,Q2     : Constants of constant terms for a given angle
C      P3,Q3     : Constants of sqrt(r) terms for a given angle
C      P4,Q4     : Constants of (r) terms for a given angle
C
C  CONST returns the following constants:
C
C      C(1)      : Constant of 6 powers of sqrt(r)
C      C(2)      : Constant of 5 powers of sqrt(r)
C      C(3)      : Constant of 4 powers of sqrt(r)
C      C(4)      : Constant of 3 powers of sqrt(r)
C      C(5)      : Constant of 2 powers of sqrt(r)
```

```
C       C(8)       : Constant of sqrt(r)
C       C(7)       : Constant
C  ------------------------------------------------------------------------
C
C  Written by Tae Hyun BAEK (30-Nov-1985)
C  ------------------------------------------------------------------------
C
        COMMON /DAT/FS,H
C
        REAL*4 C(7)
C
        R=FN*FS/H
C
C Calculation of each constant of polynomial equation of sqrt(r)
C
        C(1)=P4*P4+4.0*Q4*Q4
        C(2)=2.0*P3*P4+8.0*Q3*Q4
        C(3)=2.0*P2*P4+P3*P3+8.0*Q2*Q4+4.0*Q3*Q3
        C(4)=2.0*P1*P4+2.0*P2*P3+8.0*Q1*Q4+8.0*Q2*Q3
        C(5)=2.0*P1*P3+P2*P2+8.0*Q1*Q3+4.0*Q2*Q2-R*R
        C(6)=2.0*P1*P2+8.0*Q1*Q2
        C(7)=P1*P1+4.0*Q1*Q1
C
        RETURN
        END


        SUBROUTINE FRINGE(R,P1,Q1,P2,Q2,P3,Q3,P4,Q4,RN)
C  ------------------------------------------------------------------------
C
C  Subroutine FRINGE regenerates the fringe orders for a given data points
C  (a fixed polar angle and radial coordinate). The calling program should
C  provide the following variables:
C
C      R      : Radial distance from the crack tip
C      P1,Q1  : Constants of sqrt(r) terms for a given angle
C      P2,Q2  : Constants of constant terms for a given angle
C      P3,Q3  : Constants of sqrt(r) terms for a given angle
C      P4,Q4  : Constants of (r) terms for a given angle
C      FS, H  : Material fringe value and model thickness
C
C  FRINGE returns the regenerated value (RN)
C  ------------------------------------------------------------------------
C
C  Written by Tae Hyun BAEK (30-Nov-1985)
C  ------------------------------------------------------------------------
C
        COMMON /DAT/FS,H
C
        SQR1=1.0/SQRT(R)
        SQR2=SQRT(R)
C
C  Calculation of PR=(Radial stress - Tansential stress) and QR=Shear stress
C
        PR=SQR1*P1+P2+SQR2*P3+R*P4
        QR=SQR1*Q1+Q2+SQR2*Q3+R*Q4
C
C  Calculation of regenerated fringe order (RN)
C
        RN=SQRT(PR*PR+4.0*QR*QR)*(H/FS)
C
        RETURN
        END
```

```
      SUBROUTINE TRFORM(X,Y,XE,YE)
C  ------------------------------------------------------------------------
C
C  Subroutine TRFORM transforms the coordinate system with respec to crack
C  line on the screen. The callins program should provide the followins
C  variables:
C
C      X, Y : Coordinates of data point
C      PHI  : 3.141592654
C      BR   : Crack inclination ansle
C
C  TRFORM returns the coordinates on the screen (XE, YE).
C  ------------------------------------------------------------------------
C
C  Written by Tae Hyun BAEK (30-Nov-1985)
C  ------------------------------------------------------------------------
C
      COMMON /ASF/BR,RDIS,PDIS,PHI,RFAC
C
      XE=X*COS(PHI+BR)-Y*SIN(PHI+BR)
      YE=X*SIN(PHI+BR)+Y*COS(PHI+BR)
C
      RETURN
      END


      SUBROUTINE ECORD(X,Y,IXP,IYP,JFLAG)
C  ------------------------------------------------------------------------
C
C  Subroutine ECORD calculates the location of data points on the screen by
C  considerins scalins factor. This routine limits the resion of data points
C  only within the window specified by a user. ECORD returns the coordinates
C  (IXP,IYP) for a siven point (X,Y). IF JFLAG=0, this routine passes, and
C  JFLAG=1, the routine performs the calculation.
C  ------------------------------------------------------------------------
C
C  Updated by Tae Hyun BAEK (26-Dec-1985)
C  Written by Tae Hyun BAEK (30-Nov-1985)
C  ------------------------------------------------------------------------
C
      COMMON /GIN/NXT,NYT
      COMMON /ASF/BR,RDIS,PDIS,PHI,RFAC
      COMMON /WIN/IX1,IY1,IX2,IY2
C
      XRF=X*RFAC
      YRF=Y*RFAC
C
      IF(ABS(XRF).LT.1000.0.OR.ABS(YRF).LT.1000.0) GO TO 100
        JFLAG=0
        RETURN
C
100   JFLAG=1
      IXX=INT(XRF+0.5)
      IYY=INT(YRF+0.5)
      IXP=NXT+IXX
      IYP=NYT+IYY
C
      IF(IXP.LE.IX1) IXP=IX1
      IF(IXP.GE.IX2) IXP=IX2
      IF(IYP.LE.IY1) IYP=IY1
      IF(IYP.GE.IY2) IYP=IY2
C
      RETURN
      END
```

```
      SUBROUTINE CIRCLE(R)
C  ------------------------------------------------------------------------
C
C  Subroutine CIRCLE draws a circle whose radius is (R) from the crack tip.
C
C  CIRCLE calls the following subroutines:
C      From TVLIB.OBJ - LINE
C      From BPOW4.FOR - ECORD
C  ------------------------------------------------------------------------
C
C  Written by Tae Hyun BAEK (30-Nov-1985)
C  ------------------------------------------------------------------------
C
      COMMON /ASF/BR,RDIS,PDIS,PHI
C
      ANG=0.0
      DO 100 I=1,360,3
        IG=I
        ALPA=(PHI/180.0)*FLOAT(IG)
        X=R*COS(ANG+ALPA)
        Y=R*SIN(ANG+ALPA)
        CALL ECORD(X,Y,IXP,IYP)
        CALL LINE(1,IXP,IYP)
100   CONTINUE
C
      RETURN
      END
```

D. Library Subroutines BLIB

```
      SUBROUTINE PLROOT(N,A,ERROR,MITER,NROOT,ROOT)
C  ------------------------------------------------------------------------
C
C  Subroutine PLROOT uses Newton's method and deflation to find the real
C  roots of a polynomial. The calling program must supply the following
C  values:
C
C      N      : Degree of polynomial
C      A(I)   : Coefficients of X**(N+1-I)
C      ERROR  : Allowable error limit
C      MITER  : Maximum iteration number
C
C  The subroutine returns :
C
C      NROOT  : Number of real roots found
C      ROOT(I): The roots (in an array root)
C
C  At each stage of the deflation, Newton's method terminates when MITER
C  iterations have been executed or when two successive iterates are less
C  than ERROR in absolute value. N must be .GE.2
C  ------------------------------------------------------------------------
C
C  Updated by: Tae Hyun BAEK (01-Jan-1986)
C  Updated by: Tae Hyun BAEK (29-Dec-1985)
C  Edited  by: Tae Hyun BAEK (15-Nov-1985)
C  Source    : NUMERICAL ANALYSIS,(L.W. Johnson & R.D.Riess)
C  ------------------------------------------------------------------------
C
      REAL*4 A(21),B(21),C(21),ROOT(20)
C
      NROOT=0
C
      IF(N.EQ.2) GO TO 550
      NP1=N+1
C
100   ITR=0
      X=1.0
C
C    Synthetic devision algorithm to evaluate polynomial and its
C    derivative
C
200   B(1)=A(1)
      C(1)=B(1)
C
      DO 300 I=2,N
        B(I)=X*B(I-1)+A(I)
        C(I)=X*C(I-1)+B(I)
300   CONTINUE
C


      B(NP1)=X*B(N)+A(NP1)
C
C    Newton's method update to old estimate of root
C
      ACN=ABS(C(N))
      IF(ACN.LE.0.1E-15) RETURN! To prevent overflow
C
      XCORR=B(NP1)/C(N)
C
      IF(ABS(XCORR).GT.1000.0) RETURN
      X=X-XCORR
```

```
C
      IF(ABS(X).GT.1000.0) RETURN!To prevent overflow
C
      IF(ABS(XCORR).LT.ERROR) GO TO 400
        ITR=ITR+1
        IF(ITR.LT.MITER) GO TO 200
          RETURN
C
400   NROOT=NROOT+1
      ROOT(NROOT)=X
C
C     Setup coefficients of deflated polynomial
C
      NP1=N
      N=N-1
C
      DO 500 I=1,NP1
        A(I)=B(I)
500   CONTINUE
C
C     Use Quadratic formula when deflated polynomial has degree 2
C
550   IF(N.GT.2) GO TO 100
        DISCRM=A(2)*A(2)-4.*A(1)*A(3)
        IF(DISCRM.GE.0.) GO TO 600
          RETURN
C
600   ROOT(NROOT+1)=(-A(2)+SQRT(DISCRM))/(2.*A(1))
      ROOT(NROOT+2)=(-A(2)-SQRT(DISCRM))/(2.*A(1))
C
      NROOT=NROOT+2
C
700   RETURN
      END


      SUBROUTINE CHECK(NR,RT,ERD,IFLAG)
C  ------------------------------------------------------------------------
C  Subroutine CHECK chooses the smallest positive root from the real roots.
C  The calling program must supply NR and RT(NR), then the subroutine returns:
C
C     ERD    ;  Effective radius
C     IFLAG=1;  Signal represents positive real root exist
C           =0;  Signal represents non positive root
C  ------------------------------------------------------------------------
C
C  Written by Tae Hyun BAEK (29-DEC-1985)
C  ------------------------------------------------------------------------
C
      REAL*4 RT(20)
C
      J=0
      DO 100 I=1,NR
        IF(RT(I).LT.0.0) GO TO 100
        J=J+1
        RT(J)=RT(I)
100   CONTINUE
C
      IF(J.EQ.0) GO TO 300
      IF(J.EQ.1) GO TO 400
C
      JM=J-1
      DO 200 I=1,JM
        IF(RT(I).LT.RT(I+1)) GO TO 200
```

```
            TEMP=RT(I)
            RT(I)=RT(I+1)
            RT(I+1)=TEMP
200       CONTINUE
          GO TO 400
C
300       IFLAG=0
          GO TO 500
C
400       IFLAG=1
          ERD=RT(1)*RT(1)
C
500       RETURN
          END


          SUBROUTINE AMPLY(W,A,C,NI,NJ)
C  ------------------------------------------------------------------------
C
C  Subroutine AMPLY performs matrix multiplication to make square matrix as
C  [W]x[A]=[C], where [C] is a square matrix. The calling program must supply
C  matrices, [W] and [A], and element numbers, NI and NJ. This subroutine
C  returns [C].
C  ------------------------------------------------------------------------
C
C  Source: IMLIB.FOR (written by Ibrahim Miskioglu)
C  ------------------------------------------------------------------------
C
          REAL*4 W(NI,NJ),A(NJ,NI),C(NI,NI)
C
          DO 100 I=1,NI
            DO 100 J=1,NI
              C(I,J)=0.0
              DO 100 K=1,NJ
                C(I,J)=C(I,J)+W(I,K)*A(K,J)
100       CONTINUE
C
          RETURN
          END


          SUBROUTINE GAUS(A,B,X,N,IERROR)
C  ------------------------------------------------------------------------
C
C  Subroutine GAUS uses Gassian elimination (without pivoting) to solve the
C  system [A]{X}={B}. The calling program must supply the matrix [A], the
C  vector {B} and an integer N, where [A] is NxN. Arrays [A] and {B} are
C  destroyed in GAUS. The subroutine returns {X} and a flag, IERROR, set
C  to 1 if [A] is non-singular, and set to 2 if [A] is singular.
C  ------------------------------------------------------------------------
C
C  Source: IMLIB.FOR (written by Ibrahim Miskioglu)
C  ------------------------------------------------------------------------
C
          REAL*4 A(N,N),B(N),X(N)
C
          NM1=N-1
C
          DO 500 I=1,NM1
C
C Search for non-singular pivot element and interchange rows if necessary.
C If no non-zero pivot element is found, set IERROR=2 and return.
C
```

```
          DO 300 J=I,N
            IF(A(J,I).EQ.0.0) GO TO 300
            DO 200 K=I,N
              TEMP=A(I,K)
              A(I,K)=A(J,K)
200           A(J,K)=TEMP
            TEMP=B(I)
            B(I)=B(J)
            B(J)=TEMP
            GO TO 400
300       CONTINUE
          GO TO 800
C
C Eliminate the coefficients of X(I) in rows I+1,.....,N
C
400       IP1=I+1
          DO 500 K=IP1,N
            Q=-A(K,I)/A(I,I)
            A(K,I)=0.0
            B(K)=Q*B(I)+B(K)
            DO 500 J=IP1,N
              A(K,J)=Q*A(I,J)+A(K,J)
500       CONTINUE
C
          IF(A(N,N).EQ.0.0) GO TO 800
C
C Backsolve the equivalent triangularized system, set IERROR=1


C and return
C
          X(N)=B(N)/A(N,N)
          NP1=N+1
C
          DO 700 K=1,NM1
            Q=0.0
            NMK=N-1
            DO 600 J=1,K
              Q=Q+A(NMK,NP1-J)*X(NP1-J)
600         CONTINUE
            X(NMK)=(B(NMK)-Q)/A(NMK,NMK)
700       CONTINUE
          IERROR=1
          RETURN
C
800       IERROR=2
          RETURN
          END


          SUBROUTINE RESCOR(A,B,XC,N,M)
C  ---------------------------------------------------------------------
C
C  Subroutine RESCOR uses iterative improvement to refine an approximate
C  solution, XC, to the system [A]{X}={B}. The calling program must supply
C  the matrix [A], the approximate solution vector {XC}, the vector {B}, an
C  integer N, where [A] is NxN, and an integer M=number of times. {XC} is to
C  be refined.
C  ---------------------------------------------------------------------
C
C  Source: IMLIB.FOR (written by Ibrahim Miskioglu)
C  ---------------------------------------------------------------------
C
          REAL*4 RES(20)
          REAL*4 A(N,N),SA(20,20),B(N),XC(N),SRES(20),E(20)
```

```
C
      DO 100 I=1,N
        DO 100 J=1,N
          SA(I,J)=A(I,J)
100   CONTINUE
C
200   CONTINUE
C
      DO 300 I=1,N
        DO 300 J=1,N
          A(I,J)=SA(I,J)
300   CONTINUE
C
C Compute residual, {RES}=[A]{XC}-{B}
C
      DO 400 I=1,N
        RES(I)=-B(I)
        DO 400 J=1,N
          RES(I)=RES(I)+A(I,J)*XC(J)
400   CONTINUE
C
      DO 500 I=1,N
        SRES(I)=RES(I)
500   CONTINUE
C
C Solve [A]{E}={RES} and update {XC} to {XC}={XC}-{E}
C
      CALL GAUS(A,SRES,E,N,IERROR)
C
      DO 600 I=1,N
        XC(I)=XC(I)-E(I)
600   CONTINUE
C
C Test to see if residual correction should be applied to the updated


C approximation, XC.
C
      M=M-1
C
      IF(M.GT.0) GO TO 200
C
      RETURN
      END
```

E. Fringe Multiplication Program FTWICE

```
      PROGRAM FTWICE
C  ------------------------------------------------------------------------------
C
C  FRINGE DOUBLING PROGRAM
C  -----------------------
C
C  This program is to double fringes from a given photoelastic image by
C  the EyeCom II digital image processing system. To run this program,
C  a photoelastic image should be stored in the memory.
C  ------------------------------------------------------------------------------
C
C  Written by Tae Hyun BAEK (July 1, 1986)
C  Source  : provided by Bruce H. Koerner
C  ------------------------------------------------------------------------------
C
C  FORT: FTWICE
C  LINK: FTWICE,SY:(FORLIB,TVLIB)
C
C  FORLIB = Fortran function library
C  TVLIB  = Subroutine package of EyeCom II
C
C  FTWICE calls the following subroutines:
C      From TVLIB.OBJ - GRAFIN, GRAFOT, CURSOR, ERASER, ON, LINE
C
C  File Locations:
C      FORLIB.OBJ, TVLIB.OBJ - DISK "EyeCom II"
C      FTWICE.FOR, FTWICE.OBJ - DISK "G Disk"
C  ------------------------------------------------------------------------------
C
       INTEGER*2 GRAFIN,GRAFOT
C
C To make a window to limit image processing region
C
       TYPE *,' '
       TYPE *,'Please locate the Joystick to the LEFT UPPER CORNER'
       TYPE *,' '
       TYPE *,'to make a window for fringe doubling and TYPE <BS> '
       TYPE *,' '
       CALL CURSOR(IXL,IYL)! to read Joystic X, Y coordinates
C
       TYPE *,' '
       TYPE *,'Please locate the Joystick to the RIGHT LOWER CORNER'
       TYPE *,' '
       TYPE *,'to make a window for fringe doubling and TYPE <BS> '
       TYPE *,' '
       CALL CURSOR(IXR,IYR)
C
       CALL ERASER! to erase grahic memory
       CALL ON ('G')! to activate graphic memory


C
C To make lines for window to limit image processing region
C
       CALL LINE(1,IXL,IYL,IXR,IYL)
       CALL LINE(1,IXL,IYL,IXL,IYR)
       CALL LINE(1,IXL,IYR,IXR,IYR)
       CALL LINE(1,IXR,IYL,IXR,IYR)
```

```
C
C Main routine for Prinse doublins
C
      DO 100 IX=IXL,IXR! Ster throush window area
        DO 100 IY=IYL,IYR
          IZA=0
          DO 90 IP1=-1,1! 3x3 averase of lisht intensities
            DO 90 IP2=-1,1
              CALL GRAFIN(IX+IP1,IY+IP2,IZ)! to load IZ at coordinates
              IZA=IZA+IZ
90        CONTINUE
          D=FLOAT(IZA)/9.0! averase IZA on 9 pixels
          DZ=4.0*D*(255.0-D)/255.0! Prinse double transformation
          IDZ=INT(0.5+DZ)
        CALL GRAFOT(IX-1,IY-1,IDZ)! to store IDZ at coordinates
100   CONTINUE
C
      STOP
      END
```

F. Fringe Sharpening Program TRACE

```
      PROGRAM TRACE
C
C     This program is for sharpening low noise fringe images (such as
C     photoelastic images) to precisely determine the locations of the
C     full and half order fringes.  It runs on the EYECOM II and operates
C     on an area within an already stored image.  TRACE does not accumulate
C     any images. It requests four points to be chosen by the user to
C     determine the area to be enhanced, then procedes with the enhancement.
C     TRACE marks those points where the light intensity gradient changes
C     direction abruptly; these include half and full order fringes, extrema
C     in fringe order, and noise.  If the resulting image is not satisfatory
C     defocusing the camera slightly, immersing or polishing the specimen,
C     or digitally filtering the image may help.
C
C     TRACE calls the following subroutines:
C           From BORDER.OBJ - PIXBND and BORDER
C           From TVLIB.OBJ - COORD and DISOT
C           From FORLIB.OBJ - EXIT
C
C     TRACE.FOR, TRACE.SAV, and all of the above may be found on
C     BK Disk 1, or any EYECOM II System disk.
C
C     Collect four points for area of interest.
C
      TYPE 10, "33, "33
10    FORMAT('$',A1,'[H',A1,'[J'//////,
     +       ' ',20X,'Indicate, with the joystick, four points'/
     +       ' ',17X,'on the outside of the section to be shapened.'////)
      IXMIN = 640
      IXMAX = 0                          ! Ensure initial values won't be kept.
      IYMIN = 480
      IYMAX = 0
      DO 30 I = 1,4                      ! Collect the four points.
21       J = ITTINR()
         IF (J.GE.0) GOTO 21
         TYPE 20, "33, I
20       FORMAT ('$',A1,'M',
     +        23X,'Indicate point',I2,' and press <RETURN>')
         IXMIN = 640
22       J = ITTINR()
         IF (J.LE.0) GOTO 22
         CALL COORD (IX,IY)
         IF (IX.GT.IXMAX) IXMAX = IX  ! Adjust limits to include point.
         IF (IX.LT.IXMIN) IXMIN = IX
         IF (IY.GT.IYMAX) IYMAX = IY
         IF (IY.LT.IYMIN) IYMIN = IY
30       CONTINUE
C
C     Enhance area of interest.
C
      CALL DISOT ("40)                   !Set display to refresh only.
      CALL PIXBND (IXMIN,IXMAX,IYMIN,IYMAX)
      CALL BORDER                        !Perform enhancement.
      CALL DISOT ("43)                   !Restore alphanumerics.
C
      CALL EXIT
C
C                                              Written by Bruce Koerner,
C                                              with the skills God gave me.
C                                              Last Update: Aug. 7, 1984
      END
```

```
;
   PIXBND::
;
;       This routine is a FORTRAN callable service routine. It establishes
;       the area of the EYECOM II screen that will be used in subsequent
;       pixel by pixel processing.
;
;       The FORTRAN call for PIXBND is:
;
;               CALL PIXBND (IXMIN,IXMAX,IYMIN,IYMAX)
;
;       Where IXMIN and IXMAX are the limits in the X-direction, IYMIN and
;       IYMAX are the limits in the Y-direction, and all parameters are
;       INTEGER*2 values given in EYECOM II co-ordinates.  PIXBND assumes
;       that the numbers given are valid EYECOM II co-ordinates.  The routine
;       draws a box about the area selected, and adjusts the screen limits
;       to the edges of the box.
;
;       PIXBND is on BK Disk 1, filename: BORDER.MAC
;
;       PIXBND places the screen limit values in a common PSECT that is not
;       listed within this subroutine.  The PSECT contains the locations
;       XMIN, XMAX, YMIN, and YMAX. These locations recieve the parameters
;       in order of appearance.
;
;       Set the screen limits.
;
        MOV     @2(R5),XMIN             ; Move values into PSECT.
        MOV     @4(R5),XMAX
        MOV     @6(R5),YMIN
        MOV     @10(R5),YMAX
        BIC     #2,POINT                ; Ensure access to image memory.
;
;       Draw the box.
;
        MOV     XMIN,X          ; Start with the upper left corner.
        MOV     YMIN,Y
        DEC     Y
        MOV     XMAX,R0
        INC     R0
TOPLIN: BIS     #377,DATA       ; Draw the line across the top.
        INC     X
        CMP     X,R0
        BLT     TOPLIN
        MOV     YMAX,R0         ; Draw the right edge.
        INC     YMAX
RTLIN:  BIS     #377,DATA
        INC     Y
        CMP     Y,R0
        BLT     RTLIN
        MOV     XMIN,R0         ; Draw the bottom edge.
        DEC     R0
BTMLIN: BIS     #377,DATA
        DEC     X
        CMP     X,R0
        BGT     BTMLIN
        MOV     YMIN,R0         ; Draw the left edge.
        DEC     R0
LFTLIN: BIS     #377,DATA
        DEC     Y
        CMP     Y,YMIN
        BGE     LFTLIN
        RTS     PC              ; All done!
;
;                                       Writen by: Bruce Koerner,
;                                       with skills God gave me.
;                                       Last Update: Aug. 7, 1986
```

```
;
BORDER::
;
;       This routine is the heart of the TRACE image enhancement program.
;       It locates "light intensity ridges" and "light intensity valleys"
;       by generating a measure of the similarity in direction of the light
;       intensity gradient vectors over a 5 x 5 pixel area.  The measure
;       is then inverted, and substituted into the upper left corner of
;       the 5x5 area (this produces a 2 pixel shift diagonally left and up
;       in the enhanced image).
;
;       The FORTRAN call for BORDER is:
;
;               CALL BORDER
;
;       BORDER assumes a previous call to PIXBND, and may give unpredictable
;       results if PIXBND isn't called.
;
;       BORDER is on BK Disk 1, filename: BORDER.MAC
;
;       BORDER includes references to a common PSECT that determines the
;       area of the screen that it deals with. The identifiers XMIN, XMAX,
;       YMIN, and YMAX are part of that PSECT.
;
;       Throughout the routine, R0 will be used to hold the X-Component
;       sum, R1 will be used for the magnitude sum, R2 for the Y-Component
;       sum, and R3 for calculating gradient components.
;
;       This routine represents an efficiency improvement over the
;       published version. By taking a different set of component vectors,
;       this routine requires fewer location changes to acheive the same
;       result.
;
        MOV     XMIN,X          ; Start at upper left hand corner.
        MOV     YMIN,Y
        SUB     #4,XMAX         ; Limit range to avoid outside data.
        SUB     #4,YMAX
        BIC     #2,POINT        ; Ensure acess to image memory.
;
;       Enhancement loop.
;
BLOOP:  INC     Y               ; Collect vector component.
        MOV     DATA,R3
        ADD     #2,X
        SUB     DATA,R3
        MOV     R3,R0
        BGE     ABS0            ; Absolute value.
        NEG     R3
ABS0:   MOV     R3,R1
        MOV     DATA,R3         ; Collect vector component
        ADD     #2,X
        SUB     DATA,R3
        ADD     R3,R0
        TST     R3              ; Absolute value.
        BGE     ABS1
        NEG     R3
ABS1:   ADD     R3,R1
        DEC     X               ; Collect vector componenet
        DEC     Y
        MOV     DATA,R3
        ADD     #2,Y
        SUB     DATA,R3
        MOV     R3,R2
        BGE     ABS2            ; Absolute value.
        NEG     R3
```

```
ABS2:   ADD     R3,R1
        MOV     DATA,R3         ; Collect vector componenet
        ADD     #2,Y
        SUB     DATA,R3
        ADD     R3,R2
        TST     R3              ; Absolute value.
        BGE     ABS3
        NEG     R3
ABS3:   ADD     R3,R1
        INC     X               ; Collect vector componenet
        DEC     Y
        MOV     DATA,R3
        SUB     #2,X
        SUB     DATA,R3
        SUB     R3,R0
        TST     R3              ; Absolute value.
        BGE     ABS4
        NEG     R3
ABS4:   ADD     R3,R1
        MOV     DATA,R3         ; Collect vector componenet
        SUB     #2,X
        SUB     DATA,R3
        SUB     R3,R0
        BGE     ABS5            ; Absolute value of X-Component Sum
        NEG     R0
ABS5:   TST     R3
        BGE     ABS6            ; Absolute value.
        NEG     R3
ABS6:   ADD     R3,R1
        INC     X               ; Collect vector componenet
        INC     Y
        MOV     DATA,R3
        SUB     #2,Y
        SUB     DATA,R3
        SUB     R3,R2
        TST     R3              ; Absolute value.
        BGE     ABS7
        NEG     R3
ABS7:   ADD     R3,R1
        MOV     DATA,R3         ; Collect vector componenet
        SUB     #2,Y
        SUB     DATA,R3
        SUB     R3,R2
        BGE     ABS8            ; Absolute value of Y-Component Sum
        NEG     R2
ABS8:   ADD     R2,R0           ; Chessboard Magnitude of Sum.
        TST     R3              ; Absolute value.
        BGE     ABS9
        NEG     R3
ABS9:   ADD     R3,R1           ; Complete Chessboard Sum of Magnitudes.
        BNE     MAXM            ; Avoid divide by zero.
        CLR     R2
        BR      NXTPT
MAXM:   CLR     R2              ; Fixed point divide.
        MOV     #200,R3
FLOOP:  ASL     R0
        CMP     R1,R0
        BHI     FSR
        SUB     R1,R0
        ADD     R3,R2
FSR:    ASR     R3
        BCC     FLOOP
```

```
NXTPT:  DEC     X               ; Place Result in upper left corner.
        SUB     #377,R2
        NEG     R2
        MOVB    R2,DATA
        INC     Y               ; Move on to next point.
        CMP     Y,YMAX
        BLT     LOOPER
        MOV     YMIN,Y          ; End of column.
        INC     X
        CMP     X,XMAX
        BLT     LOOPER
        ADD     #4,YMAX         ; End of window, restore PSECT.
        ADD     #4,XMAX
        RTS     PC              ; All done.
;
LOOPER: JMP     BLOOP           ; Extra statement because loop is too long.
;
;                                       Written by: Bruce Koerner,
;                                       with the skills God gave me.
;                                       Last Update: Aug. 7, 1986
```